Evaluation of Two Monitoring Systems for Significant Bridges in Texas

by

Chris T. Bilich, B.S.C.E.

Thesis

Presented to the Faculty of the Graduate School of

The University of Texas at Austin

in Partial Fulfillment

of the Requirements

for the Degree of

Master of Science in Engineering

The University of Texas at Austin

August, 2003

Evaluation of Two Monitoring Systems for

Significant Bridges in Texas

Approved by
Supervising Committee:

Sharon L. Wood, Supervisor

Karl H. Frank

Dedication

This thesis is dedicated with love to my car, "The 'mans." Without this wonderful and capable machine, I may have never made it to the lab. ☺

Acknowledgements

This research project began in August 2000 with the formation of a research team at the University of Texas at Austin, led by Dr. Sharon L. Wood. I would like to thank Professor Wood for her kind, careful, and diligent direction of my development as a graduate student, as well as her never-ending encouraging remarks made during my time on this project. I will always remember how, no matter how horrible a chapter initially appeared, she always had something positive to say. That's a hell of a boss!

I would also like to thank Dr. Karl H. Frank for providing his expertise on this project, for being a reader of this thesis, and for putting up with me in his classes and his office while I pursued this degree. Anyone who can do all of that with a smile deserves at least a sentence or two! ☺

Alan Kowalik, P.E, provided TxDOT oversight and supervision. I would like to thank him for his guidance during this project and not pushing me off the top of the south tower of the Veterans Memorial Bridge. It would have hurt when I hit the water.

I wish to give thanks to what has to be the greatest family in the entire world – mom, dad, Andria, and Stacey. Their love and support has never wavered, through all of my crazy ideas, college degrees, and the possession of more cars and car parts than a sane man should ever have. I love you all so much – thanks for being there for me.

To all of my wonderful friends, here's to you. Many have come. Some have gone. A few have been nuts enough to stay. I have been honored to have you all in my life and have welcomed the joys (and sometimes the pains) that each of you has brought into my life. We have shared so much, and I am eternally grateful.

To all the Civil Engineering professors who have touched my life during my six years at the University of Texas at Austin, I thank you all. Each of you has left special memories in my heart and mind that I will carry forever. It's been a wild ride, to be sure, but a special one that I will never forget.

Finally, special thanks go out to the staff of the Ferguson Structural Engineering Laboratory - Blake, Dennis, Mike, Hortensia, Regina, and the rest of the wonderful crew who has come and gone during my time at "The Lab." I have to say this is the best lab a kid could ever hope to work in. I will be forever thankful that I worked with such special and interesting people…and that I finally got to "break really big stuff."

August 15, 2003

Abstract

Evaluation of Two Monitoring Systems
for Significant Bridges in Texas

Christopher Thomas Bilich, M.S.E.

The University of Texas at Austin, 2003

Supervisor: Sharon L. Wood

Two monitoring systems for bridges were evaluated for the Texas Department of Transportation. TxDOT prefers to use monitoring systems that can be installed and maintained by independent organizations. It is important that the acquired data be interpreted by the independent organization, and that only the important engineering data be relayed to TxDOT. The systems examined were the *NetForce* global positioning system by Mezure, Inc. and the *MicroSAFE* autonomous data acquisition system for strain by Invocon, Inc. Each system was tested extensively in the laboratory and in the field. Both technologies were found to be viable for use by TxDOT. Each system is user-friendly, providing immediate return of meaningful engineering data with minimal effort on the part of TxDOT.

Table of Contents

List of Tables

List of Figures

CHAPTER 1

Introduction

The Texas Department of Transportation (TxDOT) has a few important bridges that utilize new and relatively uncommon structural systems. These include cable-stayed and post-tensioned box girder bridges. Because of their unique designs, the structural response and behavior of these bridges may be different than the vast majority of bridges in Texas. Therefore, the monitoring and evaluation of the structural health of these structures presents unique challenges for TxDOT inspection personnel. TxDOT Project 4096, *Structural Health Evaluation and Monitoring of Major and Unique Bridges in Texas*, was created to identify and evaluate monitoring systems that would provide response information that is not available during routine inspections of these major and unique bridges in Texas.

1.1   RECENT EXPERIENCES BY TxDOT

The research team is aware of two monitoring efforts by TxDOT within the last several years: acoustic monitoring of the stay cables on the Fred Hartman Bridge and scour morning of the bridge piers on FM 1157 over Mustang Creek. Monitoring of the Fred Hartman Bridge by Pure Technologies, Inc. is considered to be a success. Staff from Pure Technologies installed three accelerometers on each of the 192 stay cables and monitors the response of each instrument for indications of damage. To date, the system has detected a number of events. Weld fractures of the guide pipes have been confirmed and possible wire breaks have been identified. Pure Technologies is responsible for maintaining the

monitoring system and evaluating all data. All information is available to TxDOT personnel via a secure web site.

The scour monitoring system was not as successful. The system was developed during a research project, and was not ruggedized for field use. In addition, TxDOT district personnel were responsible for maintaining the system and interpreting the data. Therefore, training of field personnel became an important concern and data were often not available for evaluation by engineers in the design division. As a result of these technical and administrative problems, TxDOT currently relies on underwater inspection, rather than a scour monitoring system, to identify possible structural problems.

Based on these experiences, TxDOT prefers to use monitoring systems that can be installed and maintained by an independent organization. It is also important that the information be interpreted by the independent organization, and that only the important engineering data be relayed to TxDOT.

1.2   SURVEY OF CURRENT PRACTICES IN THE US

To evaluate current practices in the US related to structural health monitoring of bridges, the research team surveyed all state Departments of Transportation. The results of this survey are summarized in this section.

The Florida Department of Transportation uses global positioning (GPS) technology to monitor structural displacements on the Dames Point Bridge, a 1300-ft concrete, cable-stayed span over the St. John's River in Jacksonville. Five points on the structure are monitored using GPS hardware and services provided by Mezure, Inc. This GPS technology provides an automated system that facilitates the full-time, long-term monitoring of structural displacements without regular attention or maintenance (Angus, 2001).

The Alabama DOT has tested developed and two systems that monitor bridge scour. The first system, installed on two bridges, uses a modified depth finder. This system sends alerts via cellular signal when a scour problem is detected. The second system uses tilt meters on the bridge to monitor pier movement due to scour. Both of these systems operate autonomously during data acquisition. However, the systems were developed by researchers and require regular attention by AlDOT personnel for maintenance and upkeep (Conner and Conway, 2001).

The Connecticut DOT, in conjunction with the University of Connecticut, has developed extensive systems to monitor various aspects of structural performance on almost any bridge. These systems use tilt meters, accelerometers, displacement gages, and strain gages. These systems are also complicated, bulky, and are not durable in a long-term outdoor environment. Data can be acquired autonomously, but complex data reduction algorithms are required to obtain meaningful engineering data (Sime and D'Attilio, 2001).

The Delaware DOT has installed permanent monitoring systems on three bridges, each acquiring a variety of data (strains, loads, deflections, tilt angles, accelerations). DelDOT is experimenting with compact, battery powered, rapidly deployable data acquisition systems for strain measurement of bridges girders and decks. The current generation of hardware requires the data to be downloaded each month. Future generations will have the ability to send strain data over the Internet. All DelDOT systems acquire raw data that must then be analyzed by DelDOT personnel before meaningful engineering values are obtained (O'Shea, 2001).

The Kentucky DOT performs short-term monitoring on problem bridges only. This involves the use of strain gages, acoustic emission, and occasional

video setups. These systems are complex, bulky, and not durable in a long-term environment (Givan, 2001).

The New York DOT has not implemented any systems that monitor a bridge as a whole, but has funded research to establish long-term monitoring systems. According to the NYDOT, baseline information must include data from complete environmental cycles because measurements vary considerably with temperature, solar radiation, and vehicular traffic (Alampalli, 1999). Also, changes in modal frequencies and mode shapes have been used to evaluate bridge damage (Alampalli, 1995). However, these techniques still rely on researchers for implementation and evaluation of data.

Other states described activities with goals and objectives similar to those for this project, but had not implemented real-time monitoring to date. Most states continue to use visual inspections as the only indicator of overall structural health. Inspectors visually examine key structural components for signs of damage. If damage is detected, repairs are performed and the bridge remains in service.

1.3   SCOPE OF PROJECT

Based on recent experiences at TxDOT, the research team decided to investigate two types of monitoring systems.

A GPS-based system for monitoring structural deformations was selected because the conceptual design of the system is similar to the monitoring system that has been installed on the Fred Hartman Bridge. The GPS units are purchased from the company that will install the units. For an annual fee, this company is responsible for interpreting the data and maintaining the units. The GPS system developed by Mezure was selected for investigation because of the experiences

working with the Florida DOT and because the web-based interface provided an easy way to obtain and interpret the data.

The second system selected for evaluation was designed to enhance the amount of quantitative information that is available during routine inspections of bridges. This battery powered, self-contained, miniature data acquisition system, developed by Invocon, Inc., can be easily installed in the field and provides the inspection team with rainflow counting data, in addition to raw strain data. The ability to acquire actual strain data would be especially important for inspection of fracture-critical bridges.

The experiments used to evaluate the GPS system by Mezure and strain-recording system by Invocon are presented in this thesis. Chapter 2 presents a brief history of satellite navigation systems and discusses the Mezure system used for monitoring structural deformations. Chapter 3 discusses the collection and evaluation of data from the Mezure system. Chapter 4 discusses the strain-recording system by Invocon, as well as the collection and evaluation of data from this system. Chapter 5 presents conclusions and recommendations for future research.

CHAPTER 2

Introduction to Satellite Navigation and GPS

This chapter presents a brief history of satellite navigation systems and discusses a commercially available Global Positioning System (GPS) used for monitoring structural deformations. Global Positioning Systems (GPS) are a relatively new method of locating points on and navigating the Earth. These systems use satellites in orbit high above the Earth that send radio signals to receivers on the surface. In their simplest description, modern GPS receivers gauge the distance from an individual satellite to a point. Four or more distance measurements are then used to determine a single position in four-dimensional space.

2.1 TRANSIT

The United States Navy developed the first satellite navigation system in the late 1950's for use in guiding nuclear powered submarines and launching Polaris intercontinental ballistic missiles. The missiles themselves were not guided by this system, but rather the launch point position was estimated for proper programming of the missile's on-board navigation systems. This first satellite navigation system, called *Transit*, comprised four to seven satellites in low-altitude, almost perfectly circular polar orbits.

With so few satellites, only one was in view at a given moment. Precise clocks onboard each satellite relayed time data to receivers on the ships. *Transit* used the Doppler effect, along with the transmitted time data, to determine the position of an object in the two-dimensional space of the Earth's surface. The Doppler effect is most simply explained using the example of a moving object

emitting a sound (a car blowing its horn) and a fixed object receiving that sound (a bystander on a street corner). The observed pitch of the sound (frequency) changes as the distance between the observer and car change. This frequency shift can be measured and correlated to extract a distance measurement.

If the location (the orbit) of the moving satellite was known, the distance to a relatively fixed object (a ship or submarine on the ocean surface) could be computed. Velocity of the "fixed" object could be incorporated into the calculations to increase the accuracy of the location of an object. However, a 1 km/h error in the velocity estimate could create as much as a 200 m error in the reported position. Even with these errors, a nuclear warhead could still be launched at a target. However, because of these errors, other use of the *Transit* system was limited until more accurate positions could be obtained.

The passing of radio signals through the Earth's ionosphere and troposphere generated other problems. The Navy explored and adopted the use of dual-frequency transmitters (150 and 400 MHz) to aide in the removal of these errors. Modern GPS systems have retained this feature.

Two-dimensional positioning accuracy using the *Transit* system was approximately 25 m for a stationary object. Beginning in 1967, *Transit* was in limited use by other maritime organizations. If a stationary receiver collected continuous data for several days (hundreds of consecutive satellites passes), positioning data could be averaged to generate a three-dimensional position accurate to within 5 m. In 1967, this was a considerable achievement. Better accuracy was realized when measuring relative distances from other fixed points. Accuracies of one meter were obtained over a distance of hundreds of kilometers when measuring satellite data concurrently at both points (Hoffman-Wellenhoff et al. 1997).

By the late 1960's, the benefits of satellite navigation were becoming clearer. Accurate three-dimensional positions could be measured anywhere on the globe without physical reference to a fixed point. All that was needed to increase accuracy was additional measurement time. As computing power and technology advanced, satellite navigation systems became even more accurate (Mirsa and Enge 2001).

2.2 GPS

What eventually became the Global Positioning System (GPS) is use today began in the early 1970's with a joint venture of the United States Navy and Air Force, under the direction of the Department of Defense. Technology had advanced far enough to create a more accurate system than *Transit*. This new system would generate a more accurate three-dimensional position in far less time.

By the late 1970's, clock technology had improved to the point where the internal clocks on each satellite could be perfectly synchronized. A more accurate position could be computed with increased speed, providing that more satellites were in view of a single receiver and that each satellite could output its position and time more accurately than before. A medium Earth orbit of 5,000 – 20,000 km was chosen to allow a relatively small constellation of 24 satellites to blanket the Earth with coverage. With this system, any single receiver would have between four and twelve satellites in view at any given moment. Each satellite had the potential to stay in view of a stationary receiver for a few hours, allowing significantly longer data acquisition than the 10 - 20 min viewing times for *Transit* satellites.

Choosing the satellites' orbital distance from Earth required some compromise for designers. Satellites with increased orbital distance from Earth

are more expensive to launch and require more signal power to transmit their signals back to Earth. However, as orbital distance is reduced, each satellite would have a shorter viewing window for a given receiver, requiring more satellites. For these reasons, the medium Earth orbit and constellation of 24 satellites was chosen.

The choice of a transmitter frequency band took into account a number of factors. Higher frequencies lessen ionospheric and tropospheric frequency refraction, but increase signal strength loss. The L-band of frequencies (1-2 GHz, fairly low in the spectrum and relatively uncluttered at the time) was chosen to combat these effects.

Designers also faced the decision of whether GPS would be a passive or an active system. Passive satellites transmit data to ground receivers but do not receive any data in return. Active satellites would have two-way data transmission capabilities. The main military advantage of the passive system is that it allows anonymity of position for the GPS user. Military personnel could generate accurate positions without giving away their own. In addition, it would allow an unlimited number of receivers to operate at a single time. The choice of a passive system was obvious.

A minimum of three satellites must be in view at all times for dual-frequency GPS to produce the most accurate three-dimensional position,. Clocks onboard each satellite must maintain perfect synchronization with each other to produce the best ranging calculations. Clocks within the GPS receiver must also remain perfectly synchronized with the satellite clocks. This presented a dilemma that would be very expensive to solve. The simplest solution, however, was to employ inexpensive quartz clocks in each GPS receiver. These clocks would keep accurate time, but would not be synchronized with those onboard the satellites. The timing error between the receiver clock and each synchronized

satellite time would be identical (called *receiver clock bias*). The use of data from a fourth satellite would remove this time bias and allow for the most accurate of measurements in four-dimensional space (3 space dimensions, one time dimension) without the expense of synchronizing receiver clocks.

A final caveat to GPS measurement is that vertical positioning values will be less accurate than horizontal positioning values for any GPS receiver. This phenomenon can be explained by understanding the geometric relationship between a single ground-based GPS receiver and the constellation of orbiting satellites. The majority of satellites in view of a ground-based GPS receiver will be closer to the horizontal plane tangent to the Earth at the point of GPS reception than to the vertical axis running directly through the GPS receiver. There may be a few satellites located "above" the GPS receiver, but not nearly as many as "to the sides" of the receiver. A GPS station moving horizontally will move farther from the satellites "to the side" of it than those "above" it. The opposite is true for GPS stations moving vertically. These stations will move farther from the satellites above the station than those to the sides. Larger changes in distance will generate more accurate results, since the distance changes will be greater than the background noise level. For these reasons, horizontal movements will be easier to resolve than vertical movements.

With all apparent problems solved, system architecture was approved by the Department of Defense in 1973. The first satellite was launched in 1978, but the system was not deemed operational until 1995. Over $10 billion was invested in the system, and $500 million per year is spent for its upkeep (Mirsa and Enge 2001).

The military's goals with GPS were to obtain velocity, distance, and time measurements quickly and accurately for use against its enemies in a variety of

ways. Like any weapon, it would be most useful if the enemy were not allowed access to it. Upon verification of the accuracy and usability of the system, plans were devised to allow only the government access to the most accurate GPS positioning data.

In the early 1990's, GPS signals were encrypted and could only be decoded by those with the appropriate key – the federal government. By the mid 1990's, civilian objection to signal encryption had grown strong enough to cause a change in GPS signaling. A new plan was instituted, called Selective Availability, where non-encrypted signals were distributed, free for use by anyone. Errors were pre-programmed into these signals, changing horizontal positioning accuracy from approximately 10 m to 500 m. Only the military would have prior knowledge of these randomly generated errors and be able to remove them to obtain the best accuracy. Selective availability allowed civilian use of GPS, but not with enough accuracy to do any significant military damage (National Academy of Sciences, 1995).

Unfortunately for the United States government, other nations began to experience acceptable accuracies using their own GPS satellites and hardware. The need for selective availability was rapidly diminishing. On May 2, 2000, a Presidential Order decommissioned Selective Availability. The most accurate GPS signals were now available to everyone.

2.3 PRESENT DAY GPS

Since the Presidential Order canceling Selective Availability, very accurate global positioning data have been available to the entire world. Civilians can now spend about $100 and purchase a pocket-sized GPS receiver that can calculate a variety of variables with the push of a button. Horizontal positioning accuracy on these units is as low as 5 m. Vertical positioning accuracy, as with

any GPS receiver, may be double this value or more. These personal GPS receivers can calculate distance traveled, velocity, bearing, heading, elevation, latitude, longitude, time-zone changes, and even draw a scalable map as you travel. As long as a clear view of the sky is maintained, positioning errors remain small, even for these very basic and inexpensive systems.

Upon the removal of Selective Availability, the commercial market for GPS boomed. Many companies now offer survey-grade equipment that can be purchased for $10,000-50,000 per receiver. This level of equipment can generate accuracies of approximately 10 mm in a relatively short amount of time. Automobile manufacturers have begun to adapt GPS receivers into their cars as navigation aides. Personal watercraft manufacturers have followed to aid in open-water navigation. These interactive systems can integrate destination information and position information to guide the user with great accuracy and speed. Consumers now have the ability to purchase vehicles of nearly any sort, and arrive at almost any destination without the use of a conventional map.

2.3.1 Differential GPS

For the majority of users, positioning values within a few meters of the actual location are sufficient for navigation. However, for surveying the location of a structural component, more accurate measurements are required. Differential dual-frequency GPS equipment is often employed to obtain the best possible GPS measurements.

Differential GPS employs two or more GPS receivers working together, communicating with each other via radio. One receiver is fixed over a known position, while the other "rover" unit is stationed on the object to be monitored. The rover unit takes positioning data relative to the known location of the fixed unit. The fixed unit must be within proximity (a few kilometers) of the rover at

all times, so that the same satellite signals are being received and processed by both units. Since the location of the fixed point is known and each unit is processing the same satellite signals, most errors caused by atmospheric effects can be considered and neglected. This method of GPS measurement can result in very accurate positioning values, usually within 10 mm of the actual position in the horizontal plane.

2.3.2   Striving for Better Accuracy

Two types of errors exist when acquiring data in any situation: random errors and systematic errors. One possible systematic error in GPS is frequency shift. As the satellite signal passes through different atmospheric layers its frequency can change, changing the apparent position of the receiver. Each signal passing through a given layer at the same time will encounter the same frequency shift. However, random errors may result from the constantly changing thickness of these layers, from random satellite transmission interruption, or a variety of other causes. Using more than one GPS receiver for a given position calculation allows the removal of systematic errors. One receiver acts as the control to the GPS experiment, while the other receiver(s) act as variables. This scientific method of problem solving greatly aids in improving positioning accuracy due to the removal of systematic errors.

Unfortunately, a GPS user must still consider random errors. Random errors cannot be completely removed, but averaging can diminish their experimental effects. When data are collected at a fixed point and averaged, effects from randomly occurring errors can be dramatically reduced. As more data are averaged over a longer period, the likelihood of encountering the both positive and negative random errors increases. As more errors of varying signs are encountered, they begin to balance out, improving positioning accuracy. The

data presented in Chapter 3 will show that experimental accuracy generally improves with averaging time, but does have some exceptions.

Dual-frequency differential global positioning systems provide the most accurate satellite positioning information currently available. When data from these units are averaged over time, positioning should become increasingly more accurate.

2.4   NETFORCE GLOBAL POSITIONING SYSTEM

This section will review the testing and evaluation of a commercially available, dual-frequency, differential global positioning system. Mezure, Inc., located in Bend, Oregon, developed this system, called NetForce. NetForce was developed to measure very small displacements of an object over a long period of time (weeks, months, years, etc). This thesis will examine the NetForce system as it would be used to observe long-term structural deformations of various bridge components. Examples of these components may include, but are not limited to, vertical or lateral deflections of suspension bridge towers due to temperature changes, or settling of cable anchor blocks over many months or years.

The NetForce system will be evaluated for its accuracy and applicability to monitoring various parts of major and unique TxDOT bridges. Mezure has advertised "sub-centimeter" level accuracy for the NetForce system. The system will be fully evaluated for its accuracy and the time required to achieve this accuracy.

To be fully applicable to TxDOT in the area of bridge monitoring, centimeter-level or better accuracy will be required. As testing results are presented, the applicability of the system will be discussed further.

2.4.1 NetForce System Operations

NetForce is a "plug and play" wireless system, where the system can be ready to take GPS data only moments after the equipment is delivered and power provided. Stand-alone weatherproof enclosures containing all hardware necessary for GPS measurements are delivered to the site and attached to the object that requires monitoring. Raw, unprocessed GPS data are received by the antenna, located within the fiberglass enclosure (which is relatively transparent to GPS signals), and logged by the receiver. An internal cellular modem encrypts the data, transforms them into packet form, and transmits them via a digital cellular signal. This service acts as a normal cellular telephone connection, except that the connection is always active, enhancing signal reliability.

After the cellular provider receives the data, as shown in Figure 2.1, they are then transmitted over a broadband Internet connection to Mezure's Network Operations Center (NOC), located in Bend, Oregon. Data are also sent to a series of remote mirror sites where copies of all data are stored. This allows the retrieval of past GPS data if there is a problem within the system.
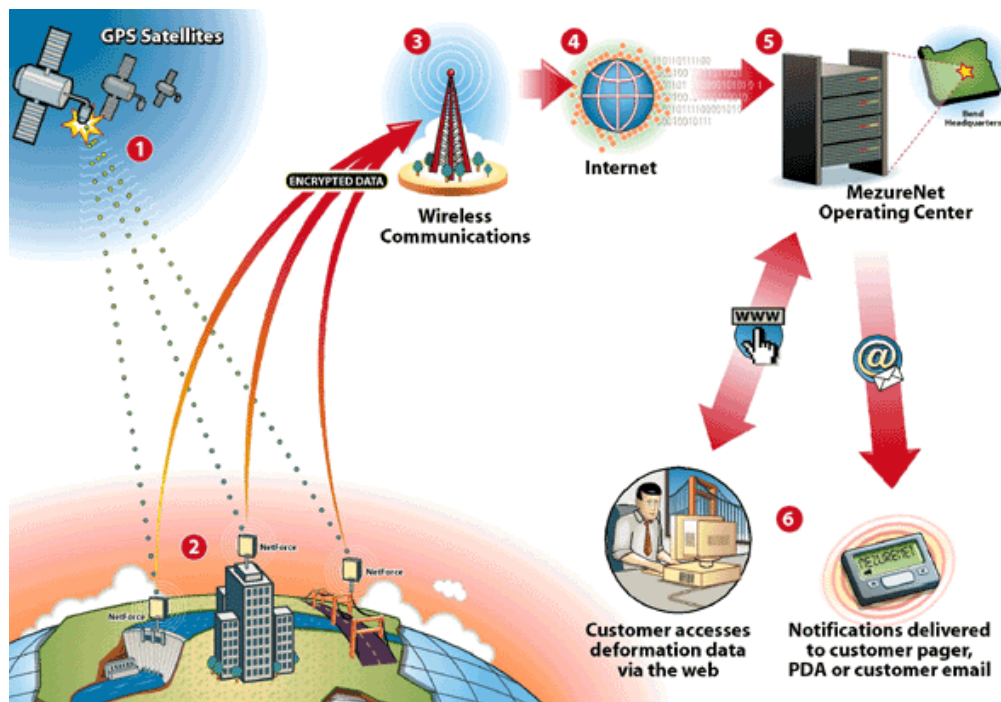
Figure 2.1: NetForce System Operations

Processing of the raw GPS data, called post-processing, is done by Mezure at the NOC. Unprocessed GPS data are stored in RINEX format (Receiver INdependent EXchange), which is widely accepted in the GPS field. RINEX data are processed using software by Novatel to obtain the actual coordinates of each GPS station in three dimensions. The horizontal coordinate values are given in degrees of Latitude and Longitude. The vertical coordinate is given in meters above mean sea level (MSL). A conversion formula was used to transform the horizontal coordinate values from units of degrees into units of meters. Once all three dimensions are referenced in units of meters, displacements can be computed by subtracting the coordinates of successive positions.

16

2.4.2   MezureNet Website

Users can access their GPS data at any time through a password-protected website called MezureNet. Each customer will have a custom website designed specifically for their set of NetForce stations. Customers can have a single or multiple passwords that allow them to view the current state of each GPS station through the Internet.

When a customer logs on to their MezureNet website, they are presented with an overview of the positions of each NetForce station. Each station is presented with a customer-specified name ("North Tower 1" or "West Abutment," for example). A photograph of each station can also be incorporated for easy station identification and user friendliness, as shown in Figure 2.2.

Figure 2.2: MezureNet Home Screen

Eight color-coded horizontal bar charts present the current state of certain parameters associated with each station, as seen in Figure 2.2. A consistent blue bar chart with a centered green square indicates that the value of that parameter is centered within its specified limits. If the green square moves off center, that parameter is approaching a limit value. When the entire bar chart is colored red, that parameter has exceeded its specified limits. An event that exceeds limits will trigger an alarm, which would in turn alert the user of a potential problem.

When navigating the website, the user can place the mouse pointer over each bar chart. This will display the last reported value of the associated parameter and the specified limit value. Each parameter's characteristics and definitions are given below:

- *Data Gap* – The amount of time, in seconds, since the station last reported GPS data to Mezure's NOC. The limit specified by Mezure is 300 s, but rarely does the actual value vary from 0 s. Units are very good at reporting data promptly and on time.

- *Horizontal Uncertainty* – The +/- margin of error, expressed in meters, of the horizontal position calculations with a confidence level of approximately 68% (1 standard deviation in two dimensions). The limit specified by Mezure is normally 0.1 meters. Observed values usually hover around 0.01-0.03 m.

- *Vertical Uncertainty* – The +/- margin of error, expressed in meters, of the vertical position calculations with a confidence level of approximately 68% (1 standard deviation in two dimensions). The limit specified by Mezure is normally 0.1 m. Observed values usually hover around 0.01-0.03 m.

- *Position Type* – This signifies the strength of the position solution obtained by the GPS software. As satellites move in and out of

range, or on-site conditions change, communications lock with each satellite may be compromised, causing a decrease in position type. Position Type ranges from zero (the best GPS solution) to 10 (the worst GPS solution). Limit values are normally set at 3.5, but rarely deviate from zero.

- *Down / Up* – Displacement along the vertical axis, in meters, from the control coordinate (a starting location for each GPS station that can be reset at any time). Limit values are user-set.

- *East / West* – Displacement along the east/west horizontal axis, in meters, from the control coordinate. Limit values are user-set.

- *North / South* – Displacement along the north/south horizontal axis, in meters, from the control coordinate. Limit values are user-set.

- *Horizontal Radial* – Straight-line displacement, in meters, from the control coordinate along the horizontal plane. This is derived using the Pythagorean theorem of right triangles and the values of East/West and North/South. Limit values are user-set.

The reference station will have its own information panel on the MezureNet website, similar to those for each rover station. However, only values for the Data Gap parameter will be displayed for the reference station. Since the reference station is stationary, displacement values are calculated relative to its position. Therefore, the reference station needs only to output its position reliably to maintain accuracy over the entire system. A stationary reference point makes differential GPS possible.

2.4.3   Graphical User Interface

MezureNet users can view plots of displacement versus time for each NetForce station. The "View Graphs" button on the information panel for each station will open a new Internet browser window. Three plots of displacement versus time are visible in this view port: latitude, longitude, and vertical. All three dimensions of displacements are plotted in meters.

Users may select to plot measured displacements over various amounts of time. These times include 1, 3, and 12 hr, 1, 3, 7, and 14 days, 1, 3, and 6 months, and 1, 2, 3, 4, 5, and 10 yr. By selecting the desired timeframe, each plot will be automatically rescaled using the most current positioning information.

One-hour plots allow the user to see individual 10-sec data points, along with the 5-min average points computed during that hour. These first averaging points begin show improved accuracy and clustering when plotting the displacement of a fixed position, as shown in Figure 2.3.
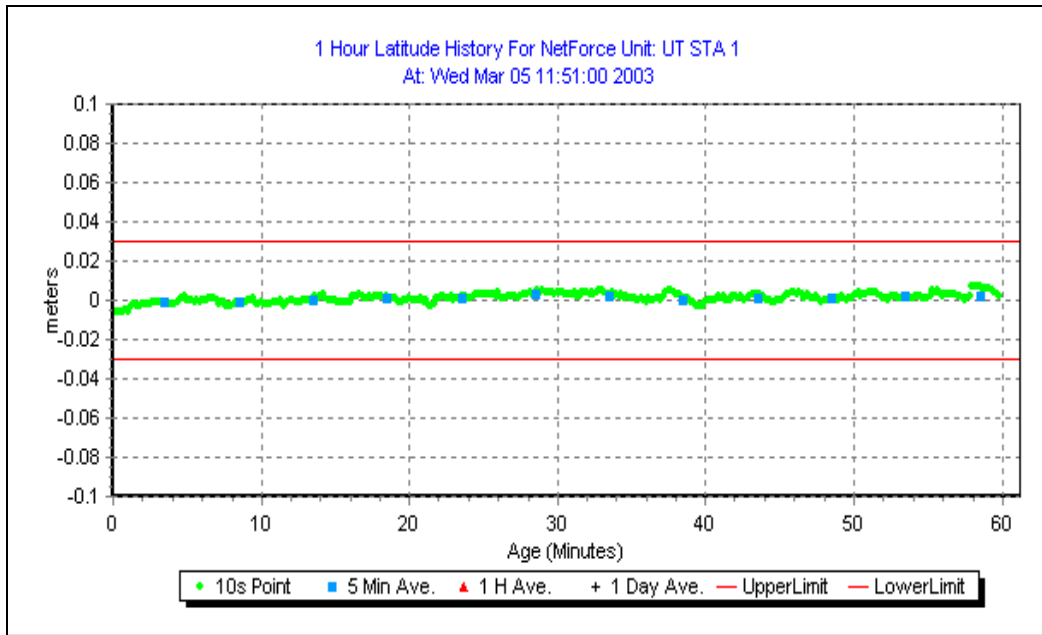
Figure 2.3: One-hour Latitude Displacement Plot

Three-hour plots show 10-sec data points, 5-min average points, and begin to show 1-hr average points. As the length of time plotted is increased, more frequent data points become obscured by the average points. When only averaged positions are plotted, a trend line of average displacement behavior is established. This trend line is a more accurate representation of the displacement behavior of that station over the long term (see Figure 2.4).
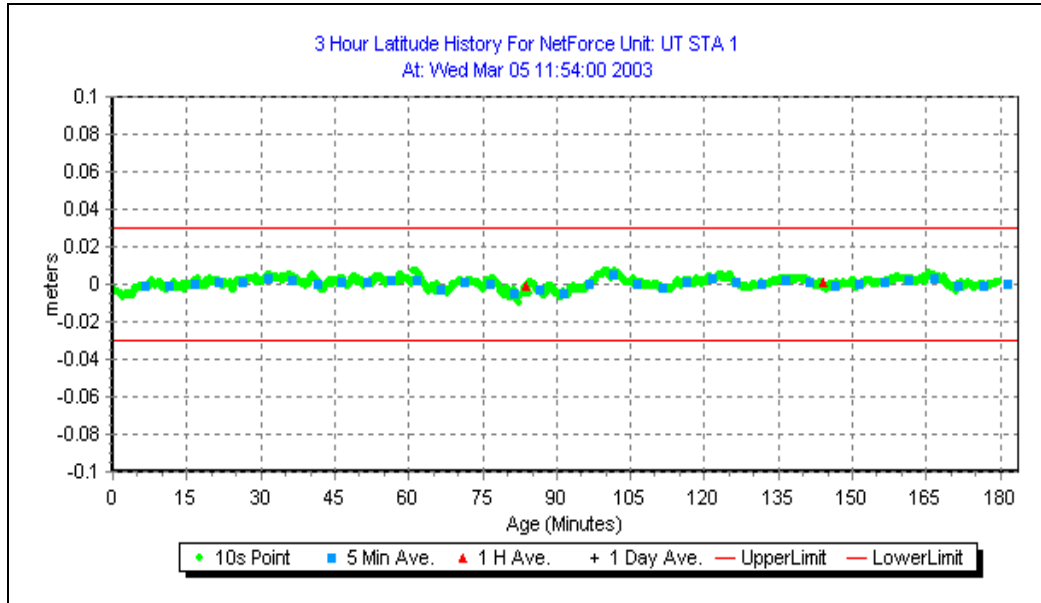
Figure 2.4: Three-hour Latitude Displacement Plot

Horizontal red lines represent user-specified limit values for displacements in each dimension. When measured data exceed these limits for a user-specified amount of time, an alarm can be triggered to alert the customer of the situation.

2.4.4 Data Download

Blocks of data acquired by the NetForce system are available to the user over the Internet. Unprocessed RINEX data can be downloaded in 24-hr segments through the Mezure website. The previous five days of raw data are stored for each NetForce station. RINEX data sets older than five days are available, as well, but only upon special request.

2.4.5 Displacement Limits and Alarms

The majority of NetForce users will elect not to perform their own post-processing of the raw GPS data. NetForce facilitates the outsourcing of data processing and interpretation duties, so that the end user can be free to perform other tasks. When the displacement of a monitored structural component exceeds rational limits, that is the time when the customer would like to be alerted. This directly defines what the Mezure system does best. Mezure's software and hardware monitors the stations without any personal attention, 24 hours a day. When displacements have exceeded customer-specified limits, the customer can be alerted to it in a variety of ways. These may include a personal telephone call or automated messages delivered via e-mail, pager, or personal data assistant.

2.4.6 Special Considerations

Units can be programmed to report a position as often as every 10 seconds, or as infrequently as the user wishes. However, as the reporting speed is increased, monitoring costs also increase.

On sites where cellular service is not yet available, a special cellular hub can be set up on-site for the exclusive use of the GPS modems. This hub will receive data from each NetForce station and transmit them via a dedicated Internet connection to Mezure's NOC. Once again, system costs will escalate with this requirement.

Alternating current (120 VAC) normally powers the NetForce units. Inside the weatherproof enclosure, a step-down transformer converts 120 VAC to 12 volts of direct current (VDC). The direct current supplies the power needs of both the GPS receiver and cellular modem, as well supplying the internal backup battery with current.

On sites where 120 VAC service is not accessible, each NetForce unit can be connected to a solar panel for remote powering. These panels power the hardware and recharge the internal backup battery during the exposure to sunlight. The backup battery powers the hardware during dark hours. Mezure has employed high-power cellular modems that draw very little current from the power supply. The GPS receiver itself also uses very little current, allowing reliable use of the solar panel. In the event of an external power loss, a fully charged backup battery will last approximately 30 hours during continuous operation.

Finally, when a project requires multiple GPS antennas to be in close proximity to each other, each GPS antenna can be mounted in any location with a clear view of the sky, while the GPS hardware package can be mounted away from this location. This will permit the cellular modems to transmit clearly without creating interference. Should GPS need to be employed in aesthetically sensitive areas, this technique can also be used to disguise the bulk of the GPS hardware by hiding it away from view. Accuracy of the data is not influenced by the distance between then antenna and the GPS hardware.

CHAPTER 3
Evaluation of Commercial GPS Data

This chapter discusses the collection and evaluation of data from the commercial global positioning system (GPS), NetForce, by Mezure, Inc. The conceptual design of the evaluation procedure and detailed design of the experiments used to evaluate the sensitivity of the results in the horizontal and vertical planes will be discussed. Important GPS data will also be presented.

3.1 CONCEPTUAL DESIGN OF EXPERIMENT

The focus of this experiment was to determine if the GPS data were sufficiently accurate to be used by the Texas Department of Transportation (TxDOT) for the long-term structural health monitoring of bridges. On TxDOT's "major and unique bridges," the Engineer or Inspector might wish to monitor the movement of components of the bridge at certain points over the long term. These may include the top of a support tower, mid-span of a bridge deck, suspension cable anchor blocks, or stay cable anchorage points. It would be important to monitor the location of each these points in three-dimensions with a certain degree of accuracy. This degree of accuracy must allow the user to measure movements that may signal the onset of a structural problem. On some structural components, a single centimeter (or less) of displacement could create a structural problem, while on other components, daily thermal fluctuations of a few centimeters may be common and overlooked. The user may wish to measure deflections relative to stable ground or relative to another point on the structure. To fulfill these requirements, a global positioning

system would therefore need to be versatile in its installation capabilities and highly accurate in its three-dimensional measurement capabilities.

3.1.1 Overview of Test

Mezure loaned three GPS stations to the project team for testing purposes. One station remained stationary at all times and served as the reference point for the remaining two stations. The remaining two stations, called 'rovers,' were placed away from the reference point. These stations moved to generate displacement data relative to the fixed reference station. Two rover stations were used to determine the repeatability of the experimental data. For the majority of bridge monitoring situations, the reference station would not be placed on the bridge. Relative displacements would therefore be measured from a known, fixed point.

To create the experiment, the rovers were displaced by known amounts to simulate the variety of scenarios that may be encountered on an actual bridge. Displacement data were then collected from these two stations, compared with the known displacements, and analyzed to determine the accuracy and sensitivity of the measurements. In each of the displacement sequences discussed in the following sections, nominally identical displacements histories were imposed on both rover stations.

Figure 3.1 shows the general layout of the testing site. The area pictured is the southwest corner of the J. J. Pickle Research Campus at the University of Texas at Austin. Both rover stations were placed near the center of a large field that would provide a clear view of the sky and the best possible GPS signals. It was desired to test the capabilities of the system for a long-span bridge installation, where a rover may be located relatively far from its

26

reference station. Accuracy of the GPS solution for a particular rover station will decrease as the distance between the rover and the assigned reference station increases. Therefore, the reference station was placed 560 ft from the rover stations.

Figure 3.1: Testing Site Layout

The rovers were placed as close to each other as possible to remove experimental differences caused by environmental variables such as atmospheric signal disturbances. Because of the high-power cellular signals being transmitted by each rover station, it was recommended by Mezure that the stations be separated by at least 100 ft. Therefore, the rovers were placed approximately 100 ft from each other, as shown in Figure 3.2.

Figure 3.2: Rover Station Layout

The reference station used in this experiment is shown in Figure 3.3. The hardware package for the reference station is exactly the same as for the rover stations, and will be described further in Section 3.1.2. To assure a fixed position, the NetForce hardware package was bolted to a 24" x 24" x 30" reinforced concrete block. Power was provided from a nearby building.

Figure 3.3: Reference Station Layout

The elevations of all three stations are approximately the same. The large buildings shown in Figure 3.1 to the north and west of the rover stations are not more than 40 ft in height. Short structure heights combined with distance from the structures help to reduce multipath effects to acceptable limits. Multipath effects, depicted in Figure 3.4, are caused by satellite signals being reflected off the ground, surrounding structures, or anything else that does not absorb radio waves. When the signal is reflected, it travels farther than a direct satellite signal. This extra distance requires additional travel time, giving the illusion that the satellite is farther away than it actually is. Normally, shielding on the underside of the GPS antenna absorbs some of the ground reflection. Unfortunately, it is not possible to shield against all reflective paths. These signals must be minimized to obtain the best GPS signals. For these reasons, all stations have a clear view of the majority of the sky at all times. This is the most important key to any successful GPS station installation.
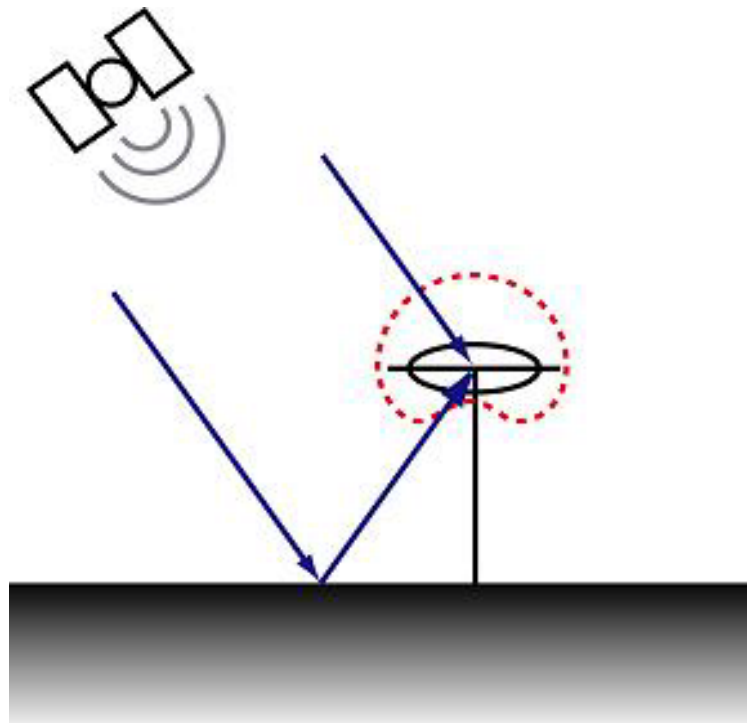
Figure 3.4: Ground Reflection Multipath Signal (Bilich, 2002)

The nature of the global positioning system dictates that the measured data in the vertical plane will be less accurate than the measured data in the horizontal plane, as mentioned in Chapter 3. On single-receiver systems, the decrease in vertical positioning accuracy ranges from 40% at a 95% confidence level to 67% at a 99.99% confidence level over the measured horizontal position accuracy. Therefore, if the horizontal component of the actual position were measured to be within 1.0 m of its true position with a 99.99% confidence level, the vertical component of the actual position could only be measured within 1.67 m of its true position at that confidence level (Hofmann-Wellenhof, et al., 1997).

Because of the difference in horizontal and vertical positioning accuracies, testing in the horizontal and vertical planes was divided into two separate phases. Testing of the GPS in the horizontal plane was conducted first, and will be discussed Sections 3.1.3, 3.2, and 3.3. The second phase involved vertical axis testing of the GPS, and will be discussed in Sections 3.4 and 3.5.

3.1.2 Hardware

The hardware package for each GPS station is enclosed within a 10" x 16" x 18" weatherproof fiberglass enclosure, shown in Figure 3.5. This enclosure and associated hardware weighs approximately 50 lb and was delivered fully assembled as shown in Figure 3.6. All necessary hardware for the operation of the each GPS station is located within this enclosure.

Hardware within each GPS station can be divided into five components: the GPS antenna (white disk located at the top of Figure 3.6), the GPS receiver (black box located immediately below the GPS antenna, situated horizontally), the cellular modem (black box located immediately below the GPS receiver, situated horizontally), the power supply (black box toward the lower-left corner of the enclosure), and the backup battery (black box toward the lower-right corner of the enclosure). The GPS antenna is responsible for receiving the radio signals transmitted from the orbiting satellites. The fiberglass enclosure does not interfere with communication between the satellites and the GPS antenna. After the antenna receives the satellite signals, the GPS receiver sends them via serial cable to the cellular modem. The modem then transmits the signals to Mezure's Network Operations Center (NOC) via cellular signal and the Internet.

Figure 3.5: GPS Hardware Package

Mezure has designed the complete hardware package to be mounted to the structural component(s) that will be monitored. When the structural component displaces, the hardware package will displace with that component. This will displace the antenna and the GPS data will be used to monitor the structural component.

Figure 3.6: GPS Hardware Package (cover removed)

Mounting the GPS unit is facilitated through the use of the supplied mounting bracket. This bracket is a galvanized steel cradle, shown around the base of the fiberglass enclosure in Figure 3.5, which can be bolted to any object using appropriate anchors. Once the bracket is mounted to the structure, the GPS enclosure is seated in the cradle and bolted from within using four ¼" galvanized bolts. When mounting is complete and 120 VAC power is supplied to the unit, the GPS hardware can be switched on and data collection can begin immediately.

3.1.3   GPS Analysis Methodology

The method used to evaluate all of the GPS positioning data is described in this chapter. Although GPS stations were fixed for some experiments and subjected to a variety of different displacement histories in other experiments, the same evaluation method was used in all cases. Note that the GPS data used in all analyses are raw GPS position data sent directly to the research team from Mezure. One position value is reported by the GPS stations every 10 sec. These are not the data that can be seen in the GPS position plots found on the MezureNet website.

A simple displacement history is shown in Figure 3.7. At time t_o, the GPS unit is moved from position x_A to x_B. The actual distance moved, $\Delta x = x_B - x_A$, is measured on the milling table by multiplying the number of crank revolutions by the travel per revolution listed in Table 3.1.
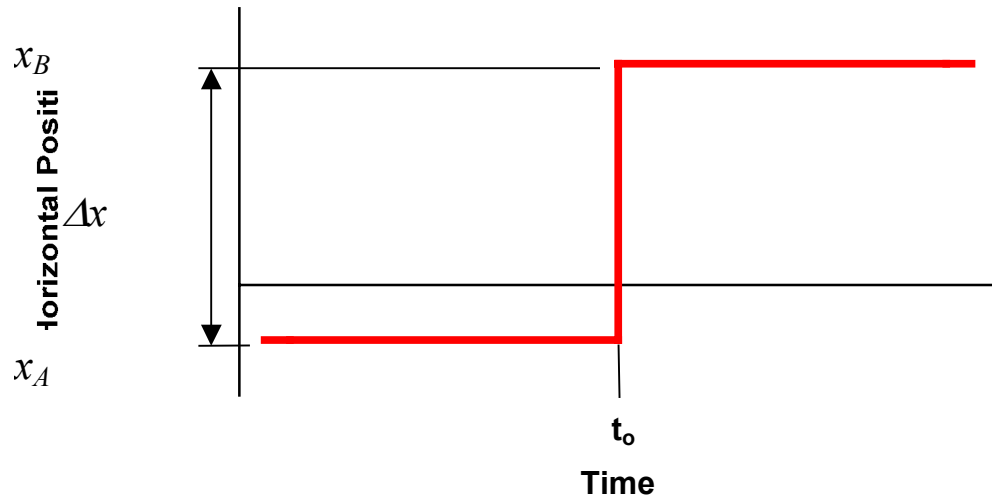
Figure 3.7: Simplified Displacement History

The GPS data recorded for the interval are plotted in Figure 3.8. Before t_o, the average value of the measured GPS data is $\overline{y_A}$ and after t_o, the average value of the measured GPS data is $\overline{y_B}$. Under ideal conditions, the difference between the two average positions, $\Delta GPS = \overline{y_B} - \overline{y_A}$, should equal the actual distance moved, Δx. However, the GPS data contain errors for the reasons described in Section 2.2. Therefore, ΔGPS will be compared with Δx to evaluate the accuracy and sensitivity of the GPS data.
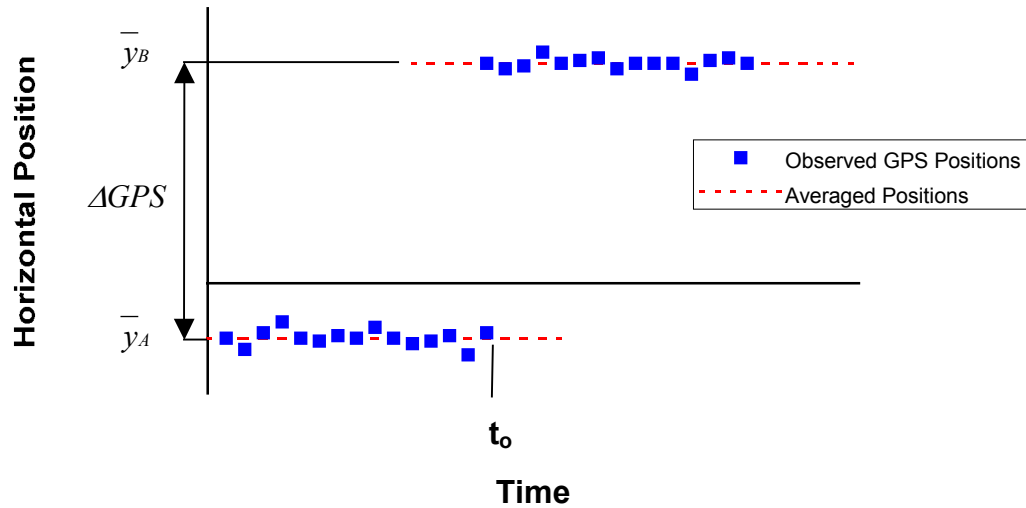
Figure 3.8: Sample Recorded Displacement History

One consequence of the setup used is that the rover GPS units were not repositioned instantly. Therefore, when comparing the GPS data with the actual displacement histories, it is important not to consider the period of time when rover GPS units are being moved. As shown in Figure 3.9, this period is called the block-out period, and is centered about time t_o. To be conservative, the entire block-out period was assumed to be 10 min, centered about t_o. Individual block-out times (t_b) were five minutes in duration.
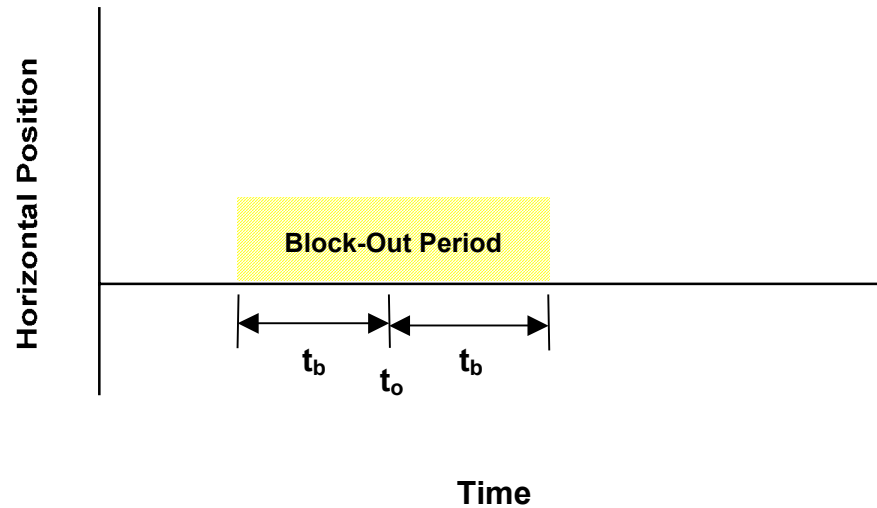
Figure 3.9: Data Block-out Period

In the analysis of the GPS data, the duration of the period used to determine the average values $\bar{y}_A$ and $\bar{y}_B$ was the primary parameter. This averaging period is shown as Δt in Figure 3.10. Values between 1 min and 24 hr were considered for Δt. The maximum value for Δt for each analysis of GPS displacement was dependent on the length of time between consecutive station displacements. During analysis of static tests, averaging durations were allowed to exceed the length of time between consecutive station displacements.
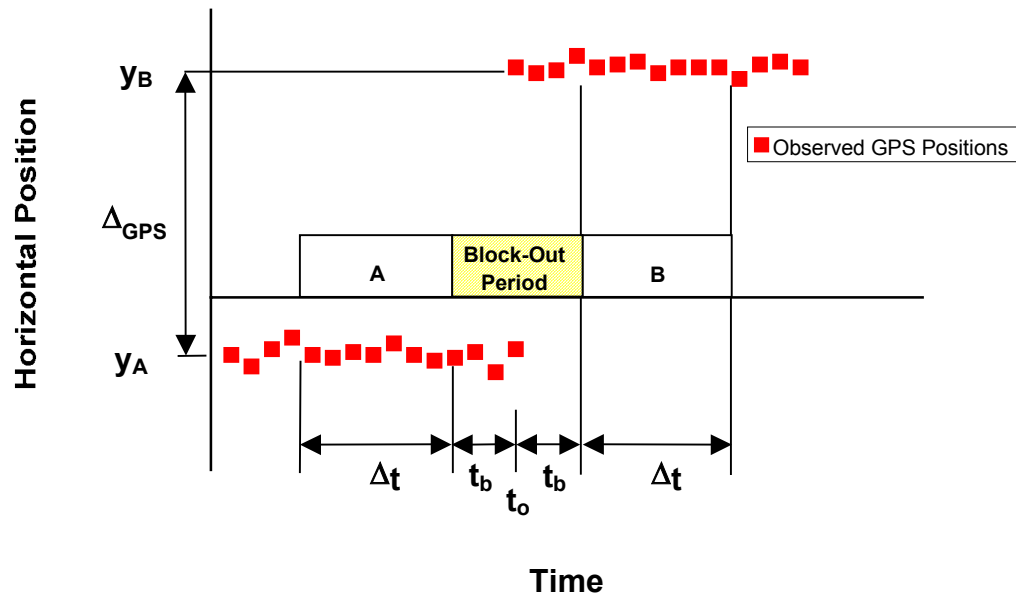
Figure 3.10: Data Averaging Periods

In the following discussion, *ΔGPS* values will be calculated for each GPS displacement using various values of *Δt*. These data will be used to determine the minimum durations over which the GPS data must be averaged to achieve a desired level of positioning accuracy.

3.2   HORIZONTAL TESTING SETUP

This section describes testing the NetForce GPS in the horizontal plane. It will discuss the goals of this phase of testing and profile the design and construction of the horizontal testing apparatus.

3.2.1   Goals

The goal of this phase of testing was to verify the horizontal positioning accuracy of the NetForce system in a variety of static and dynamic situations. This was achieved by precisely controlling the horizontal displacements of the rover stations.   Displacement data were collected from the rover stations, processed, and analyzed for accuracy when compared with the actual displacements.

3.2.2   Horizontal Movement Package

In order to evaluate the accuracy, sensitivity, and repeatability of the horizontal GPS data, a mechanism was developed to move the rover stations in a controlled manner. The entire station would have to be stable against wind and rain forces, and it must have the flexibility to allow horizontal movements in any direction.

To facilitate these requirements, 20" x 20" x 28" reinforced concrete blocks were selected as the foundations for each rover station.   Each block weighed approximately 1,000 lb. The blocks were moved on-site as shown in Figure 3.2 and leveled.

A Palmgren two-axis milling table was bolted to the top of each concrete block using lead anchors and ½" x 2" lag bolts.   A diagram of the milling table is shown in Figure 3.11. Milling table dimensions and directional precision data are presented in Table 3.1.

Table 3.1: Milling Table Specifications

Quantity		Dimension
Table Length	A	18-5/8" (473 mm)
Table Width	B	6" (152 mm)
Table Height	H	5-3/16" (132 mm)
Base Length	L	12" (305 mm)
Base Width	W	7-1/8" (181 mm)
East-West Travel		12" (305 mm)
North-South Travel		8" (203 mm)
Travel per revolution of adjustment screw		0.0787" (2.0 mm)
Reported precision of displacements		0.0008" (0.0203 mm)
Actual precision of displacements		0.009" (0.229 mm)
Weight		60 lbs.
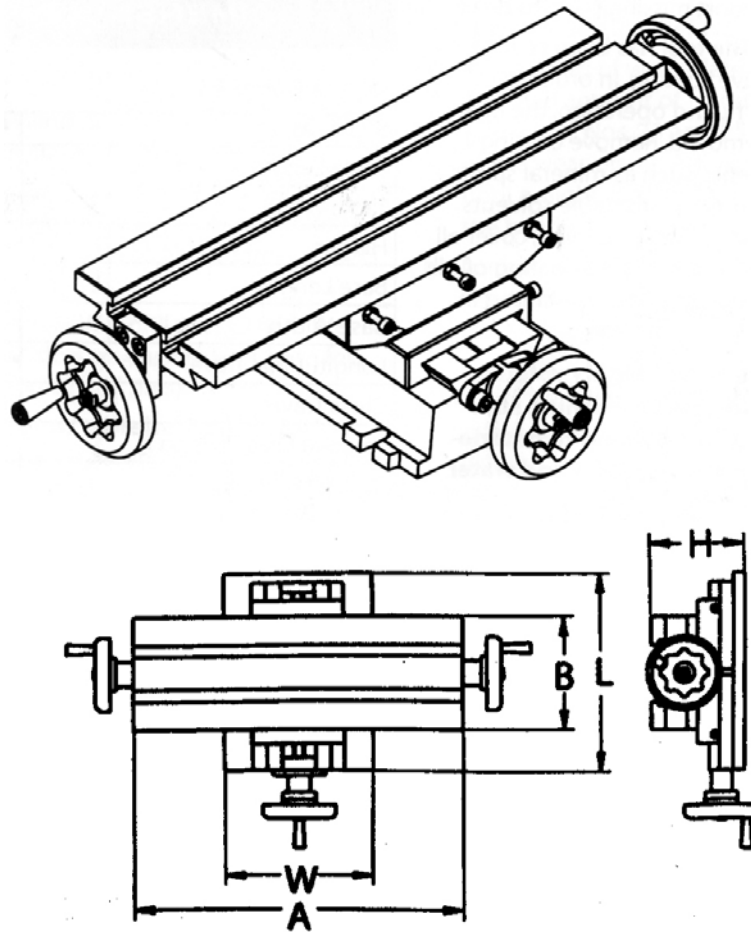
Figure 3.11: Palmgren Milling Table

The precision of each adjusting screw was specified by Palmgren to be 0.0008". However, because of backlash present in the adjusting screws, a reduced level of precision would be realized when changing direction. Assuming that a reversal of direction might occur during any test, both east/west and north/south precision were taken as the backlash present in the adjusting screws, 0.009". This

level of precision for horizontal movements was taken to be sufficient given the reported level of accuracy of the NetForce system.

Figure 3.12: Horizontal Testing Apparatus

To provide anchorage of the GPS hardware package, two 8"-long, 2" x 6" wood blocks were bolted to milling table using 5/16" diameter bolts. The GPS mounting cradle was anchored to the wood blocks using four 2½" coarse thread

wood screws. Finally, the GPS hardware enclosure was attached to the cradle using four ¼"-20 bolts and washers. The completed apparatus, shown in Figure 3.12, allows the precise movement of the GPS hardware enclosure in two directions along the horizontal plane.

3.3   RESULTS OF HORIZONTAL TESTING

Testing of the NetForce GPS in the horizontal plane was divided into three phases: long-term static testing, short-term static testing, and dynamic testing. The long-term static test involved leaving the GPS stations in one position for a single five-week period. Short-term static testing involved moving each GPS station three times over a period of approximately one month. Finally, the dynamic testing phase involved seven discreet displacement histories, each imposed over a relatively short period of time. Each sequence of movements was intended to test the horizontal positioning accuracy of the GPS while simulating an actual bridge installation condition.

3.3.1   Long-term Static Tests

Before imposing any displacement histories, both GPS stations were left in an arbitrary location for five weeks. Continuous data were evaluated over this five-week period. During evaluation of the data, averaging points (t_o) were set every three hours. Data were averaged about each t_o over eight different Δt durations: 5 min, 10 min, 20 min, 30 min, 1 hr, 2 hr, 12 hr, and 24 hr. Since no displacements were induced at any time, the measured displacements were considered to be background noise inherent in the system. This background noise is expected to correspond to the limit of horizontal accuracy of the NetForce system.

44

a) *Evaluation of Data*

To evaluate the performance during the long-term static tests, five weeks of data from both stations were divided into individual weeks. Each week contains 56 t_o averaging points, spaced at three-hour intervals. Because of this spacing, a single day would contain eight t_o points. The times of day corresponding to each t_o point would be the same each day of the five-week evaluation.

To investigate data trends relating to the time of day when the data were recorded, the seven *ΔGPS* values (one each day for seven days) computed at each time of day during a given week were averaged over that week. These t_o times of day are: 1 am, 4 am, 7 am, 10 am, 1 pm, 4 pm, 7 pm, and 10 pm (Central Standard Time). This evaluation technique will present specific times of day that may be problematic for GPS, and will examine these times over a five-week period.

Next, to investigate data trends relating to the duration of averaging (*Δt*) used to compute each *ΔGPS* point, the 56 *ΔGPS* values computed during a given week corresponding to a specific duration of averaging (*Δt*) were averaged over that week. This analysis shows how the system responds to different periods of averaging over an entire week, and examines those times over a five-week period.

Finally, to investigate how the system performs as a whole over a single day, the eight *ΔGPS* values computed during a single day corresponding to a specific duration of averaging (*Δt*) were averaged over that day. This was done once each day for a week. At the end of the week, this would show how the system performs on average for each day, and how the system responds to different durations of averaging (*Δt*) during each day.

b) *Variation with Time of Day*

Every geographic location on Earth will have times of day where satellite coverage is dense enough to provide good GPS solutions, but also times where satellite coverage is poor and good GPS solutions can not be achieved. Because satellite coverage repeats almost periodically every 24 hours + 4 minutes, time-of-day dependent behavior of the system is expected to be similar each subsequent day (Angus, 2002). However, when compared data sets are at least 15 days apart, the time offset is at least 1 hour and should be taken into account.

Figure 3.13 is a plot of accuracy versus time of day obtained from Station 2 during the first week of the long-term static evaluation (11/21/02-11/27/02). This illustrates the general system behavior when considering the time of day of data collection. Reported accuracy of 0 mm would be ideal, given that the GPS stations were not displaced at any time. Averages taken around most times of the day yield accuracy of 10 mm or less, regardless of the duration of averaging time (Δt) used, as shown in rescaled plot, Figure 3.14. This verifies Mezure's advertised "sub-centimeter" system accuracy.

However, when averages were taken around t_o = 13:00, accuracy was greatly affected. Averages taken at t_o = 10:00 and t_o = 16:00 are also affected, but to a much lesser degree. Short-duration averages at t_o = 13:00 yield errors of 350 mm. At least 12 hours of data averaging at t_o = 13:00 is necessary to obtain accuracy that can be obtained at other times of day.

Appendix A contains all 10 time of day accuracy plots generated from two stations observed for five weeks.
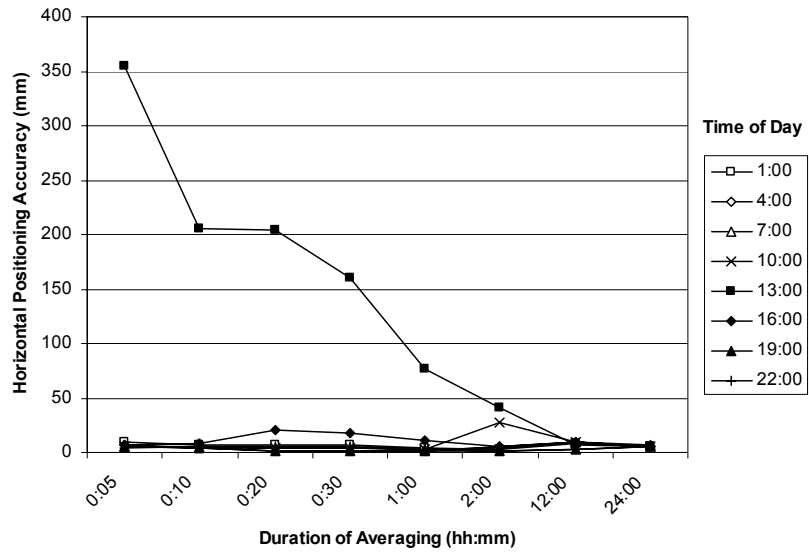
Figure 3.13: Horizontal Positioning Accuracy as a Function of Time of Day
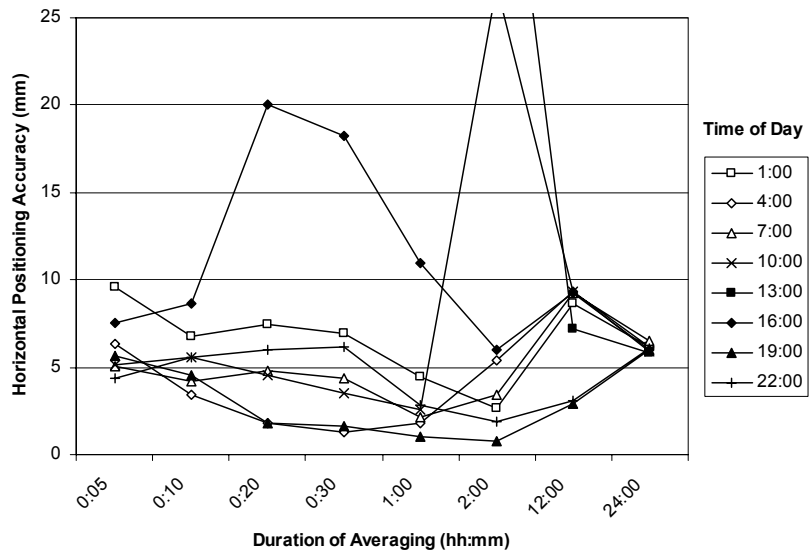
STA 2, Week 1

Figure 3.14: Horizontal Positioning Accuracy as a Function of Time of Day

STA 2, Week 1 - Expanded View

47
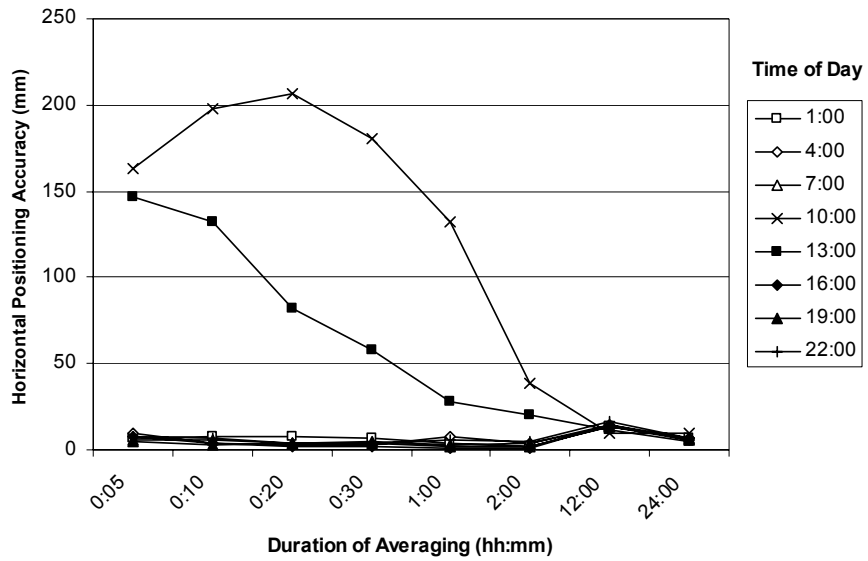
Figure 3.15: Horizontal Positioning Accuracy as a Function of Time of Day
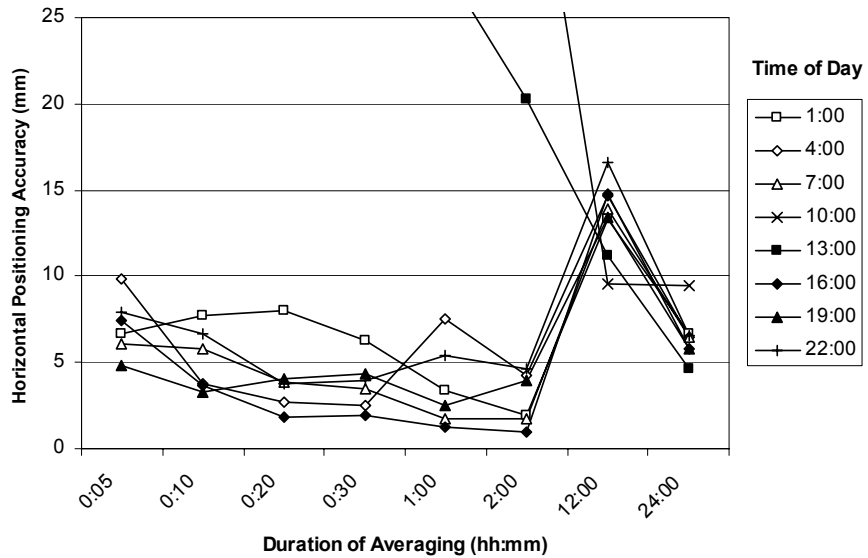
STA 1, Week 5

Figure 3.16: Horizontal Positioning Accuracy as a Function of Time of Day

STA 1, Week 5 – Expanded View

48

Figure 3.15 is a plot of accuracy versus time of day obtained from Station 1 during the fifth week of the long-term static evaluation (12/25/02-12/31/02). Figure 3.16 is the same plot rescaled to show details of 0 to 25 mm along the vertical axis. In these figures, changes in accuracy similar to those in Week 1 can be seen, but at different times of day. Accuracy around t_o = 13:00 showed improvements, while accuracy at t_o = 10:00 worsened. This effect can be explained by examining the pattern of periodic satellite coverage over the central Texas region. Figures 3.17 and 3.18 show the number of satellites in view as a function of the time of day. This information was calculated using the approximate latitude and longitude coordinates of the GPS stations, the date, and known satellite patterns to predict satellite availability patterns over a certain location on a certain date (Bilich, 2003).

To obtain the most basic GPS solution, four satellites must be in view of a particular GPS station. To obtain a more accurate GPS solution, more satellites are required. Given the constellation of 24 satellites distributed across the globe relatively equidistant from each other, a maximum of 12 satellites may be in view of a location at a given time.

Figure 3.17 shows that on November 21, 2002, satellite coverage was poor (5 satellites in view) for an extended period of time around 13:00, and for a very short time at 16:00. At other times, coverage was much better. As many as 11 satellites were in view at 06:00, but coverage remained high for the duration of the day. This supports the data shown in Figure 3.13 for the same date.

49
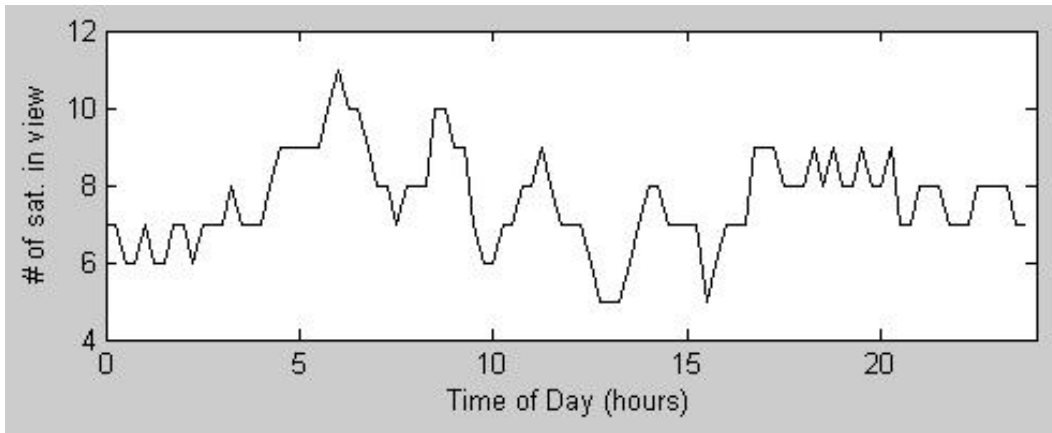
Figure 3.17: Number of Satellites Over Central Texas (11/21/02)

Figure 3.18 shows that on December 27, 2002, satellite coverage was poor around 10:00 and 13:00. At other times of day, satellite coverage was better, allowing for good GPS solutions. This supports the data shown in Figure 3.15 for the same date.
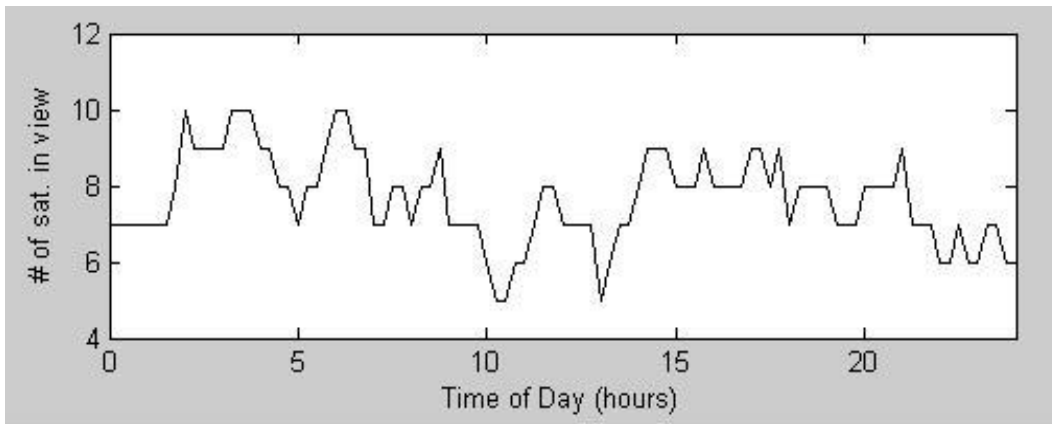
Figure 3.18: Number of Satellites Over Central Texas (12/27/02)

Each location on the globe will produce similar results, but at different times of day. GPS users should not be deterred by this behavior, as it is normal and cannot be avoided. Rather, all potential GPS installation sites should be fully investigated and thought given to the times of day when relevant GPS data are required and when they can be obtained at that site.

c) *Weekly Averages*

When every ΔGPS value corresponding to a given duration (Δt) is averaged over a complete week, daily and hourly anomalies are not as noticeable. Figure 3.19 shows five data series. Each series corresponds to a complete week of continuous averaged long-term static GPS data. Station 2 was chosen for Figure 3.19, as it best represented the overall behavior of the system.

Short-period averages ($\Delta t = 5$ min) were poor during a particular week (49 mm in Week 1), but became very good the following week (10 mm in Week 2). As Δt is increased, all weekly accuracies were within 15 mm when $\Delta t = 12$ hr and within 5 mm when $\Delta t = 24$ hr.
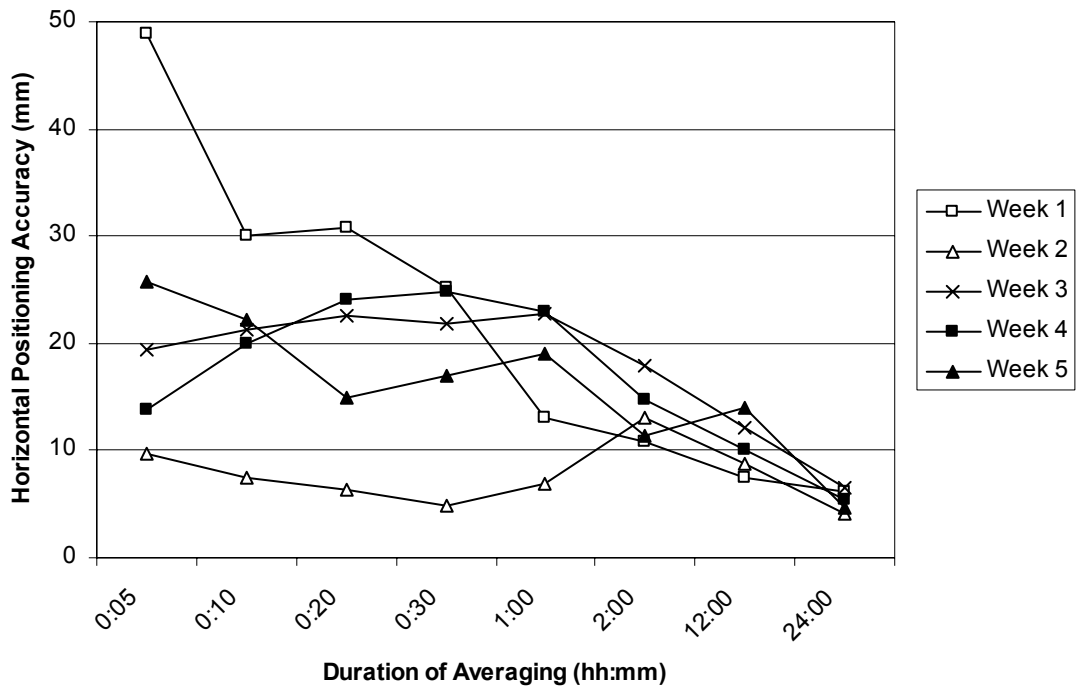
Figure 3.19: Weekly Averages of Horizontal Positioning Accuracy, STA 2

Figure 3.20 shows the same data retrieved from Station 2, but with the averages occurring when t_o = 13:00 removed from the analysis. Significantly greater accuracy is realized when averaging periods are relatively short (5 min < Δt < 2 hr). However, as averaging times approach Δt = 24 hr, accuracies are relatively unchanged between Figures 3.17 and 3.18. This observation shows again that specific times of day can adversely affect the accuracy of the GPS, but that averaging over time (in this case, averages over the period Δt > 12 hr) can remove these effects.

Appendix B presents the complete set of plots for Stations 1 and 2.
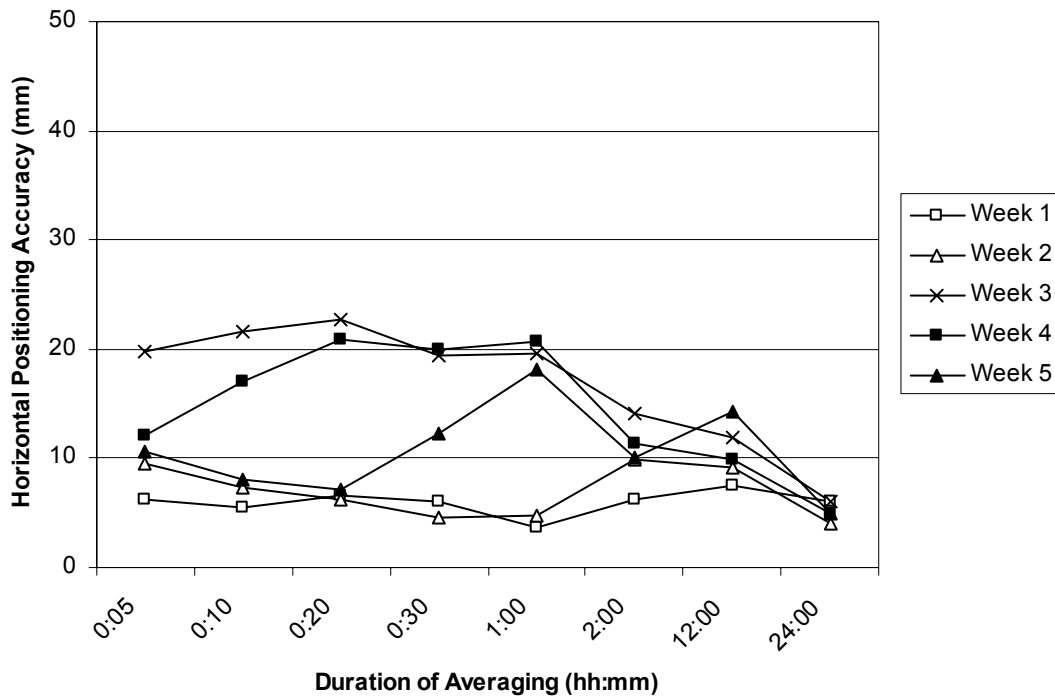
Figure 3.20: Weekly Averages of Horizontal Positioning Accuracy,
(13:00 averages removed), STA 2

d) Daily Averages

When data are averaged over a single day, rather than a full week, there is less chance of error in the GPS data on a given day. However, when errors are present in the GPS data, the effects can be greater because 24 hours of GPS data may not be enough to help average out the disturbance. This section considers the same data as in Section 3.3.1(c), but explores them in a different manner.

Figures 3.21 and 3.22 show the extremes over five weeks of continuous data when ΔGPS values are averaged daily. Figure 3.21 shows that good accuracy (less than 18 mm regardless of the duration of averaging, Δt) can be

obtained for an entire week. Most computed averages are within the sub-centimeter range, as specified by Mezure. However, Figure 3.22 shows an entire week where only 5 of 7 days achieved the desired accuracy while averaging the data over less than 24 hr.
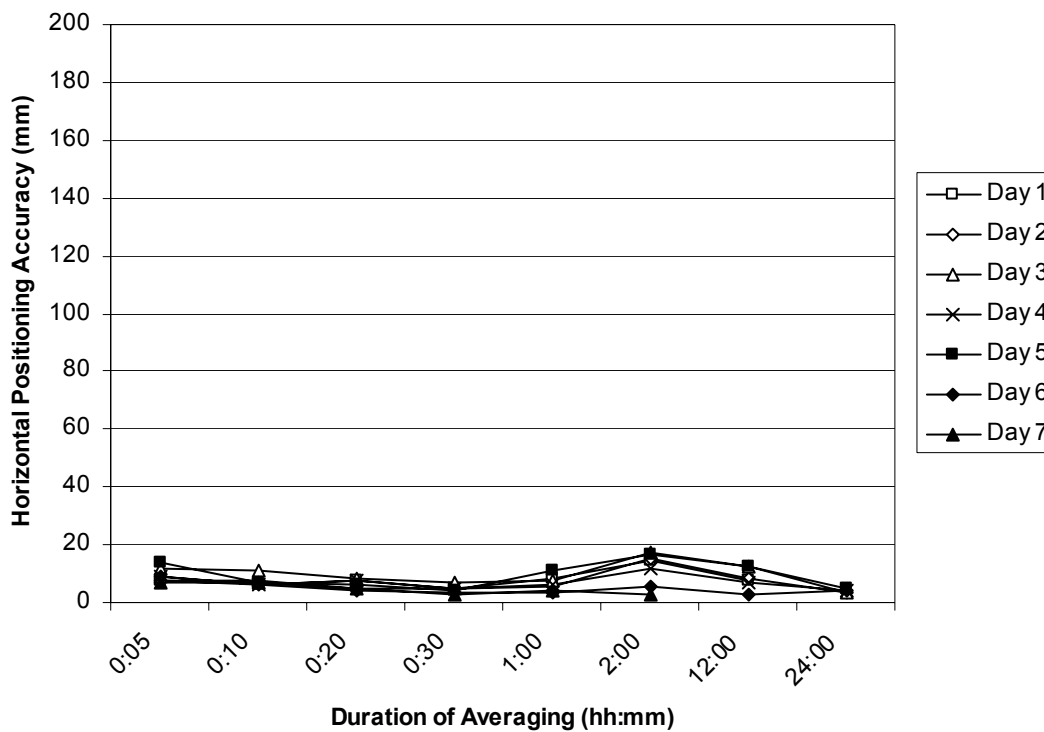
Figure 3.21: Daily Average of Horizontal Positioning Accuracy, STA 2, Week 2
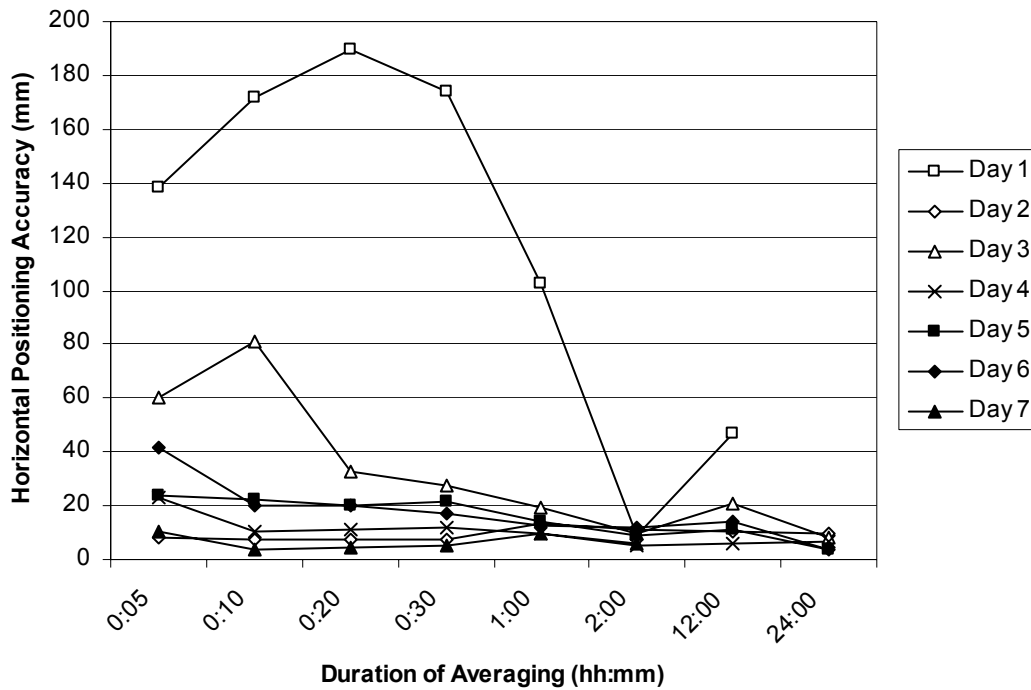
Figure 3.22: Daily Average of Horizontal Positioning Accuracy, STA 1, Week 5

Appendix C contains all 10 daily accuracy average plots generated from two stations observed for five weeks. On the whole, daily accuracies range from 10 to 25 mm depending on the duration of averaging, Δt. Only a few days in each week (zero days in some weeks) show disturbances in the GPS data that cause large errors in positioning. In all weeks, both stations generated accuracies of 10 mm or less when data were averaged over 24 hr.

3.3.2 Short-term Static Tests

Following long-term static testing, each GPS station was moved to a location and not moved from that position for a number of days. This was done three times in total. The magnitude and durations of the imposed displacements are listed in Table 3.2. These tests would simulate movements of the GPS stations on a bridge and allow time to observe the effects of averaging on data where actual displacements were induced.

Table 3.2: Short-term Static Testing Sequences

Movement Sequence	Horizontal Displacements		Duration of Test (days)	Date of Movement	Time of Movement (hh:mm)
	STA 1 (mm)	STA 2 (mm)			
1	120.0	100.0	7	10/01/02	16:00
2	123.7	104.4	2	10/08/02	15:50
3	28.3	28.3	26	10/10/02	20:30

a) Evaluation of Data

To evaluate the performance of the NetForce system in a short-term static environment, eight Δt values were used to compute ΔGPS values for each movement sequence. These eight Δt values were: 5 min, 10 min, 20 min, 30 min, 1 hr, 2 hr, 12 hr, and 24 hr. No averaging of DGPS values was performed in this analysis. Individual ΔGPS values are presented in Tables 3.3 and 3.4.

56

Appendix D contains a sample data set and computation sheet for the computing displacements during short-term static testing.

Table 3.3: Short-term Static Testing Averages – STA 1

Actual Displacement (mm)	Observed Displacements (mm)							
	5 min	10 min	20 min	30 min	1 hr	2 hr	12 hr	24 hr
120.0	105.4	102.4	84.9	76.2	95.0	92.6	113.4	111.8
123.7	131.7	120.4	155.5	158.0	140.4	117.1	119.6	120.5
28.3	25.7	25.7	26.9	27.2	27.4	26.9	31.8	24.9

Table 3.4: Short-term Static Testing Averages – STA 2

Actual Displacement (mm)	Observed Displacements (mm)							
	5 min	10 min	20 min	30 min	1 hr	2 hr	12 hr	24 hr
100.0	74.9	108.3	101.7	100.2	94.6	98.4	99.3	96.7
104.4	576.1	557.1	572.0	411.6	248.1	172.1	115.5	109.1
28.3	28.4	28.9	29.7	28.9	31.0	29.2	23.4	25.2

b) *Observations*

Of the six short-term static tests (three for each station), only one showed to have excessively poor accuracy. The second test of STA 2 reported positions that exceeded the displacement by a factor of 5.5 when $\Delta t = 5$ min. In this case,

the error exceeded 470 mm. However, measured displacements were within 11 mm when Δt = 12 hr and within 5 mm when Δt = 24 hr. In this case, an initially significant data disturbance was removed by averaging data over 12 to 24 hr.

Other tests generated accuracies of less than 10 mm when Δt = 10 min, and even greater accuracy when Δt = 12 to 24 hr. Test 3 of STA 2 displayed amazing performance, yielding accuracy of 0.1 mm when Δt = 5 min. This is not representative of the general system performance, but does show how potentially accurate GPS can be given the right atmospheric and site conditions, and a minimal amount of averaging time.

3.3.3   Dynamic Tests

a) Evaluation of Data

Table 3.5 summarizes seven series of dynamic tests imposed on both Stations 1 and 2. For dynamic testing, each GPS station was moved through the specified series of displacements at precise time intervals. Movement frequencies varied from one displacement each day to each 30 min. In some tests, the units were moved in the same direction and by the same amplitude each time. In other tests, the direction of the movements was varied, but the amplitude of the translation was constant. And in other tests, both the direction and amplitude were varied. This variety of testing situations was intended to replicate the variety of possible movements that a bridge structure may experience in a non-controlled environment due to daily fluctuations in temperature and due to structural degradation with time.

Table 3.5: Dynamic Testing Sequences

Movement Sequence	Horizontal Displacements		Movement Frequency (hours)
	N+/S- (mm)	W+/E- (mm)	
4	0	+20	24
	0	+10	
	0	+5	
	0	+4	
	0	+3	
	0	+2	
	0	+1	
5	0	+10	0.5
	0	+10	
	0	+10	
	0	+10	
	0	+10	
	0	+10	
	0	+10	
	0	+10	
6	0	+10	1
	+10	0	
	0	+10	
	+10	0	
7	0	-20	2
	0	-20	
	0	-20	
	0	-20	
8	+20	0	0.5
	0	-20	
	-20	0	
	0	+20	
9	+40	0	1
	0	-40	
	-40	0	
	0	+40	
10	-40	0	2
	0	-40	
	+40	0	
	0	+40	

To evaluate the performance of the NetForce system in a dynamic environment, multiple ΔGPS values were computed for each series of displacements. In tests where station movements occurred every 2 hr (Sequences 7 and 10), ΔGPS values were computed with Δt not exceeding 2 hr. All other sequences were approached in the same manner, where Δt would not exceed the smallest spacing between adjacent t_o values. Values of the averaging duration (Δt) for each displacement sequence are listed in Table 3.6.

Table 3.6: Dynamic Testing Averaging Durations

Movement Sequence	Averaging Duration (Δt)									
4	5 min	10 min	20 min	30 min	1 hr	2 hr	12 hr	24 hr		
5	1 min	2 min	3 min	4 min	5 min	10 min	20 min	30 min		
6	5 min	10 min	20 min	30 min	1 hr					
7	5 min	10 min	20 min	30 min	1 hr	2 hr				
8	5 min	10 min	20 min	30 min						
9	5 min	10 min	20 min	30 min	1 hr					
10	1 min	2 min	3 min	4 min	5 min	10 min	20 min	30 min	1 hr	2 hr

The shorter averaging periods ($\Delta t < 5$ min) found in Sequences 5 and 10 help relate accuracy to averaging duration as Δt approaches zero. The longer averaging durations ($\Delta t > 2$ hr) found in Sequences 4 and 10 help locate the limiting accuracy of the system.

When displacement increments within a particular sequence were of the same magnitude (as in Sequences 5 through 10), ΔGPS values corresponding to each Δt were averaged, as shown in Tables E2 – E7 and Tables E9 – E14. These

60

averaged *ΔGPS* values show how accurate the system is on the whole during a particular displacement sequence, rather than during a single displacement increment within the displacement sequence.

In the box-type displacement sequences (Sequences 6, 8, 9, and 10), closing values were computed for each *Δt* value. The closing value is the difference in the initial and final positions of the station. This value shows how accurate the system can be in a dynamic environment where displacement behavior repeats.

b) Cumulative Accuracy

This section examines dynamic movement Sequences 4 and 8. These sequences would help test the accuracy of the GPS hardware as smaller displacements accumulated. They would also help test the repeatability of experimental results from station to station. For this analysis, recorded GPS positions were plotted versus time, as shown in Figures 3.23 – 3.26. The induced station displacements, averaging durations, and averaged GPS displacements are given in Tables 3.7 – 3.10.

Figures 3.23 and 3.24 show the recorded GPS positions for Stations 1 and 2 during movement Sequence 4. Although the GPS data were recorded every 10 sec, every sixth point is plotted in these figures, yielding one data point each minute. A total of eight positions, each held for 24 hr, comprised the sequence. The data recorded during the first interval were averaged to obtain a baseline for the entire sequence. Recorded GPS positions were then plotted relative to this baseline.

Table 3.7: Averaged GPS Displacements, Dynamic Test 4, STA 1 (mm)

Actual Displacements (mm)		Averaging Durations							
N+/S-	W+/E-	5 min	10 min	20 min	30 min	1 hr	2 hr	12 hr	24 hr
0	+20	10.0	12.7	14.9	16.7	18.1	19.6	27.9	25.7
0	+10	1.9	8.4	9.0	9.5	9.5	10.1	14.4	16.4
0	+5	7.7	11.4	7.7	5.2	5.1	5.5	5.1	5.0
0	+4	8.4	6.4	5.7	5.3	5.6	5.7	5.9	2.7
0	+3	7.6	5.2	3.8	2.6	3.0	3.4	8.4	3.9
0	+2	4.9	8.8	5.8	1.7	1.2	3.2	5.1	9.3
0	+1	4.6	5.7	1.6	3.2	2.3	2.0	2.1	4.9

Table 3.8: Averaged GPS Displacements, Dynamic Test 4, STA 2 (mm)

Actual Displacements (mm)		Averaging Durations							
N+/S-	W+/E-	5 min	10 min	20 min	30 min	1 hr	2 hr	12 hr	24 hr
0	+20	7.7	19.0	17.0	18.0	18.6	19.5	21.4	23.2
0	+10	4.6	11.3	11.0	9.9	9.9	10.4	14.1	13.6
0	+5	7.9	12.9	9.1	7.3	5.0	5.5	13.6	6.1
0	+4	8.9	5.8	5.4	4.1	5.4	5.0	9.9	4.4
0	+3	11.6	4.8	4.6	3.6	2.2	3.0	11.6	6.8
0	+2	4.3	7.9	6.2	2.6	1.5	2.5	5.6	1.8
0	+1	6.1	5.4	2.5	1.2	2.7	1.2	4.1	6.9

Table 3.9: Averaged GPS Displacements, Dynamic Test 8, STA 1 (mm)

Actual Displacements (mm)		Averaging Durations			
N+/S-	W+/E-	5 min	10 min	20 min	30 min
+20	0	19.9	18.4	21.7	19.0
0	-20	19.2	17.5	17.9	19.5
-20	0	19.1	20.1	22.1	22.1
0	+20	20.2	21.6	21.0	20.3
Average		**19.6**	**19.4**	**20.7**	**20.2**
Closing Values		9.2	9.4	12.2	13.3

Table 3.10: Averaged GPS Displacements, Dynamic Test 8, STA 2 (mm)

Actual Displacements (mm)		Averaging Durations			
N+/S-	W+/E-	5 min	10 min	20 min	30 min
+20	0	20.1	21.6	20.9	21.9
0	-20	18.7	17.7	17.7	18.6
-20	0	19.1	18.8	18.7	18.7
0	+20	20.0	21.9	21.9	20.8
Average		**19.5**	**20.0**	**19.8**	**19.8**
Closing Values		2.7	3.8	5.6	9.2

As displacements were induced, data were clustered around the darker horizontal lines that represent the actual location of the GPS unit. Although variability is seen in the recorded positions, each group remained centered about its actual displacement. When the displacement increments fall below 3 to 4 mm, data begin to blend together horizontally, suggesting an accuracy plateau at this displacement level.

Times of particularly high error were noticed during each of the eight 24-hr periods. These periods are indicated in the figures by the large deviations from the expected values and occurred approximately 18 hr from the beginning of each 24-hr displacement increment. These times range from 10:00 – 11:00 am, corresponding to times when satellite coverage is lowest over the test site during the week of testing, 1/14/03 – 1/21/03. Although not shown on the plots, errors as large as 2,035 mm were observed during the sequence.

With 24-hour averaging durations, it is possible to reduce the effects of these data anomalies and resolve displacements as small as 3 or 4 mm. Unfortunately, because of these anomalies, even longer averaging durations will be required to resolve displacements smaller than 3 or 4 mm.

Figures 3.25 and 3.26 show the recorded GPS positions for Stations 1 and 2 during movement Sequence 8. In this sequence, four movements occurred at approximately 30-min intervals, moving each station in a 20-mm square. Thirty min of recorded GPS positions were averaged to obtain a baseline value for the displacement sequence. Each recorded GPS position was then plotted relative to this baseline.

Because of the nature of the GPS data provided to the research team by Mezure, it was not possible to resolve each movement into east/west and north/south components. The vector distance of the station from the starting point of the displacement sequence was the only available measurement (see Section

D.3 for further discussion on computational restrictions). The maximum vector displacement value during the 20-mm square displacement sequence occurred when the station was at the corner opposite the starting point. This maximum displacement value was 28.3 mm.

The recorded GPS positions in Sequence 8 exhibited reasonable clustering around the actual positions when the stations were displaced. Normal variability was observed in the individual GPS positions. Most data points were within 10 mm of the actual displacement at that time. No large-displacement variabilities were observed during this displacement sequence. This was likely aided by the time of day, 18:00 - 20:00, when satellite coverage over the test site was acceptable on 2/14/03.

After the sequence was completed and each station returned to the initial position, recorded GPS positions were 5 to 10 mm above the baseline zero. This depicts the random nature of unaveraged GPS positions taken over a brief period of time, such as the 30-min intervals in Sequence 8. Although 30 min of data were averaged to obtain a zero-displacement reference value, the GPS environment (satellite coverage, atmospheric conditions, etc.) had changed by the conclusion of the 90-min test. Rapid GPS movements can be sensed relatively quickly, but the true position cannot be calculated without sufficient averaging time.
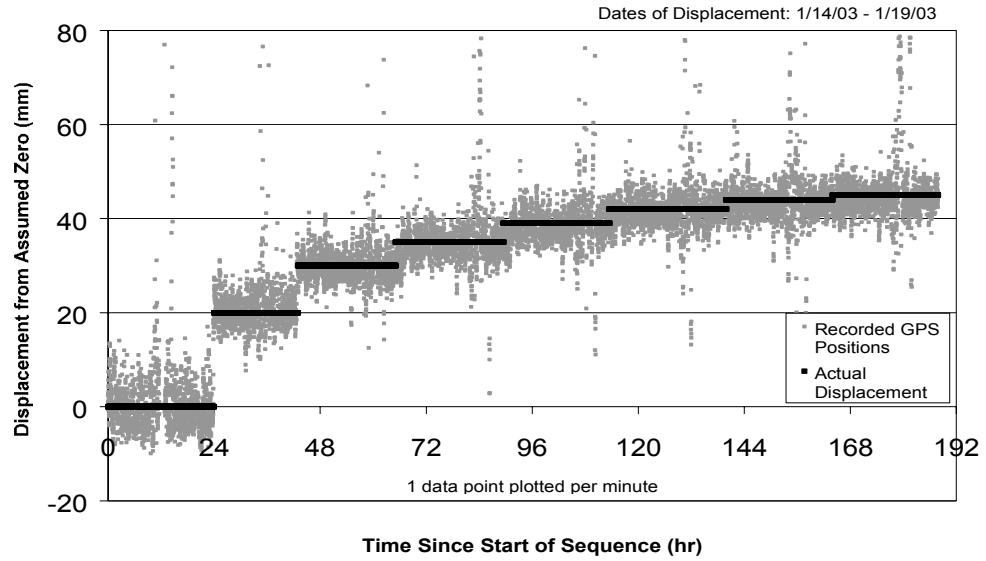
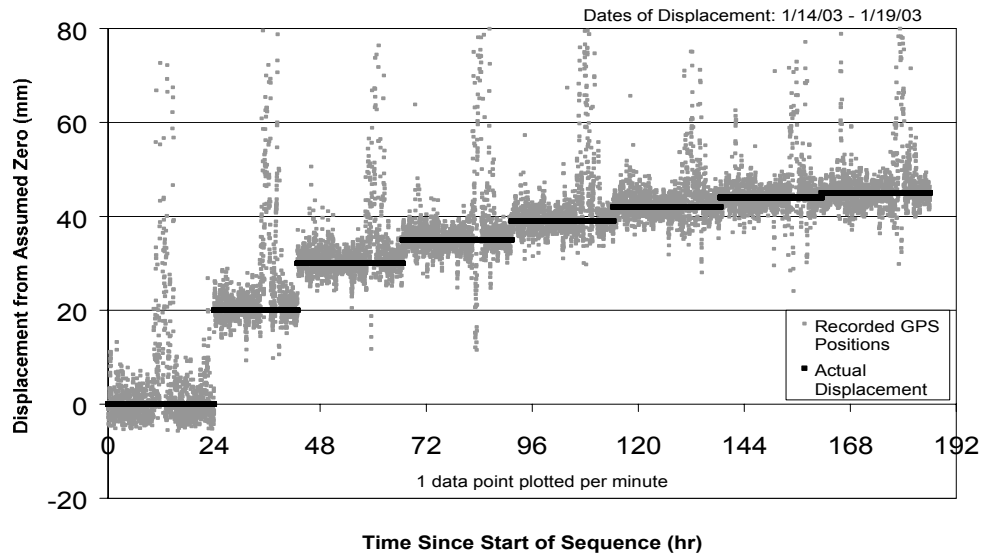*Figure 3.23: Displacement Sequence 4, STA 1*
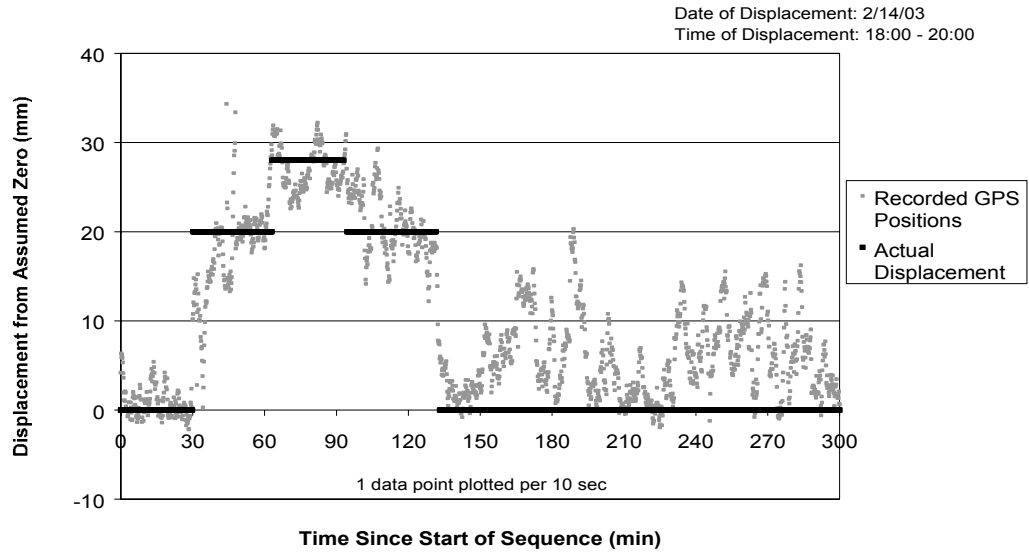

Figure 3.24: Displacement Sequence 4, STA 2

66

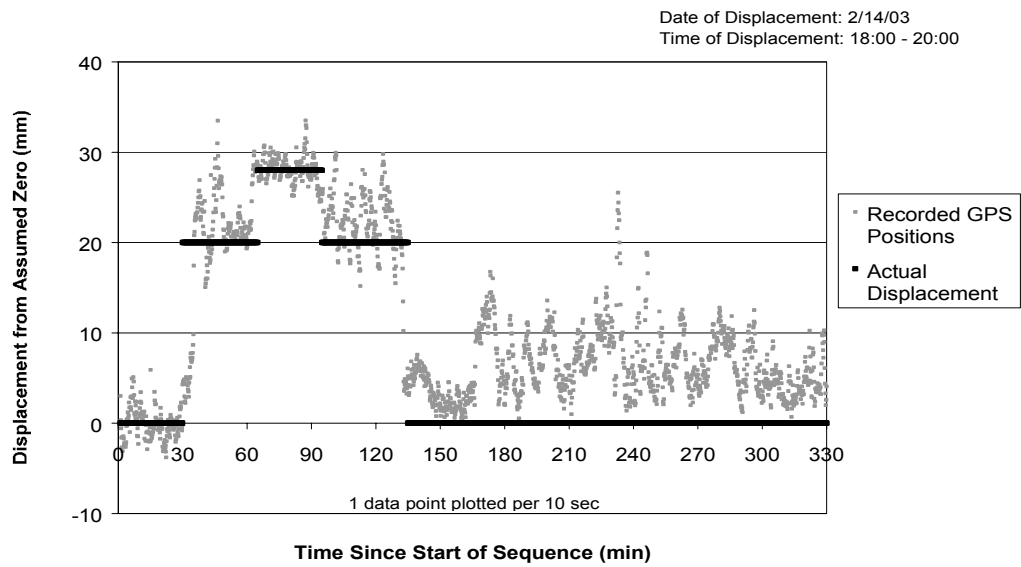*Figure 3.25: Displacement Sequence 8, STA 1*

Figure 3.26: Displacement Sequence 8, STA 2

67

c) Repeatability of Data

When comparing the data series for STA 1 and 2 for a single displacement sequence, repeatability of the experimental data can be assessed. Comparing Figures 3.23 and 3.24 for Sequence 4 and Figures 3.25 and 3.26 for Sequence 8, nearly identical data series are observed. Similar clustering of the data around each actual displacement is observed. During Sequence 4, nearly identical disturbances were observed simultaneously between stations. These results suggest exceptional repeatability of recorded GPS positions between stations.

d) General Observations

The averaged *ΔGPS* values in Appendix E show that all fourteen tests (seven sequences, two stations) produced accuracy at the sub-centimeter level. In most cases, accuracy was significantly better than the sub-centimeter level. Some disturbances were seen in the data, mostly due to loss of satellite coverage at specific times of day. When induced displacements were smaller than 3 to 4 mm, background noise inherent in the reported GPS positions (discussed in Section 3.3.1) caused a plateau in accuracy where it became difficult to measure displacements smaller than these values. This was taken to be the limiting accuracy of the system, regardless of the type or rate of dynamic displacements induced.

Increased averaging durations improved positioning accuracy, but only up to this accuracy plateau. This plateau was most likely due to predictable times of inadequate satellite coverage. In some tests, 24-hr averaging periods successfully resolved displacements less than 3 to 4 mm in magnitude. However, this behavior was not representative of the system behavior. It is possible that averaging durations greater than 24 hr could resolve displacements smaller than the plateau

value. This research, however, did not average values over durations greater than 24 hr.

Closing values for box displacement sequences were quite erratic in nature and lacked the accuracy present in other measurements. When the stations were returned to the initial position, displacement values ranged from 3 to 13 mm. Although some of the most accurate values were generated with 2 hr of averaging duration, others were generated with only 5 min of averaging duration. This unpredictable closing behavior was likely caused by changing GPS conditions and may have been aided by increased averaging durations.

e) *Alternative Evaluation of Data*

This section discusses an alternative method for analyzing the GPS data. Rather than comparing blocks of averaged data before and after each t_o time to obtain a relative displacement between the two blocks, data acquired immediately prior to each t_o time were averaged and compared with an assumed baseline value as shown in Figure 3.27. Additional averaging durations were used in this method, with values ranging from 10 min to 24 hr. The resulting plots yielded a smoother relationship between horizontal accuracy and duration of averaging than in the previous analysis.

The duration of averaging used to establish the baseline value for this analysis was 24 hr. Because all displacement data were compared with the same baseline value, the duration used to obtain the baseline value is relatively unimportant. The change in the relative displacements calculated for each averaging duration was the variable of interest.

The data acquired during Week 1 of the long-term static tests were analyzed using this alternative technique. Figures 3.28 and 3.29 examine the effect of the time of day on GPS accuracy by plotting horizontal accuracy versus

the duration of averaging. The data examined in these plots are those used to obtain Figures A1 and A6 (Week 1, STA 1 and 2).
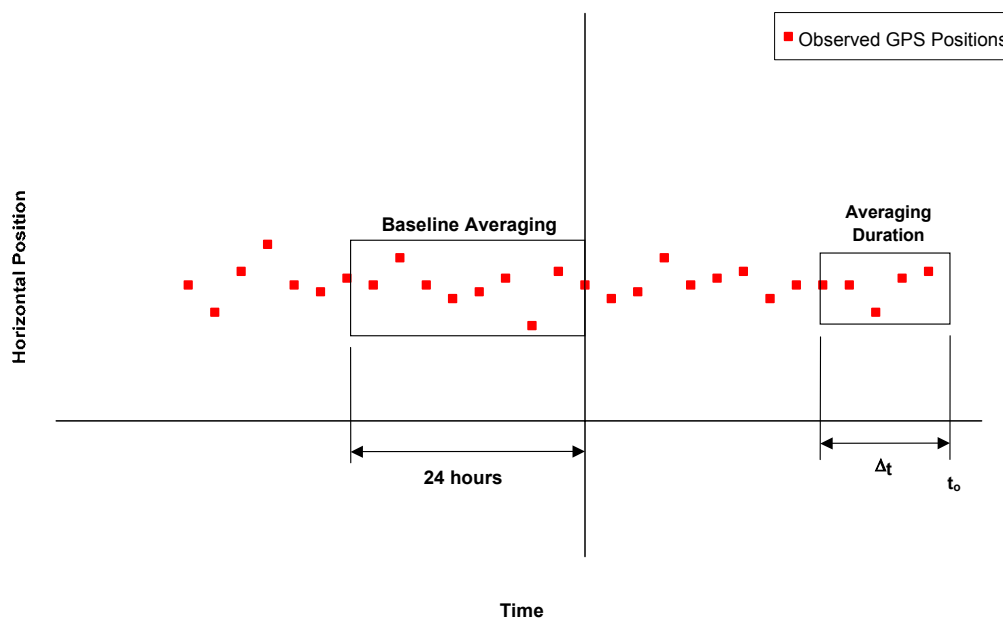
Figure 3.27: Alternative Analysis Method

Interesting trends not readily apparent in Figures A1 and A6 are shown in the plots below. As mentioned in Section 3.3.1(b), reduced satellite coverage occurred around 13:00 during Week 1 of the long-term static test. These figures support this observation. Data averaged immediately previous to $t_o = 13:00$ yield errors approaching 400 mm (not shown on these plots). As the averaging duration increases, limiting accuracy of the system is seen to be 4 mm for STA 1 and 6 mm for STA 2. These limiting values correspond to those resulting from the previous analysis technique.

As t_o moves farther away from 13:00, accuracy for the overall curve improves. However, when the duration of averaging is long enough to include data from 13:00, accuracy worsens dramatically. Once data from 13:00 has been included in the average, it becomes a challenge for the system to remove this error through averaging within a 24-hr period. Although short-term accuracy is very good at some times of day, the accuracy of the system on the whole is depicted by the behavior at the end of the curve, as averaging durations approach 24 hr. The accuracy plateau when averaging over 24 hr is found to be approximately 5 mm.
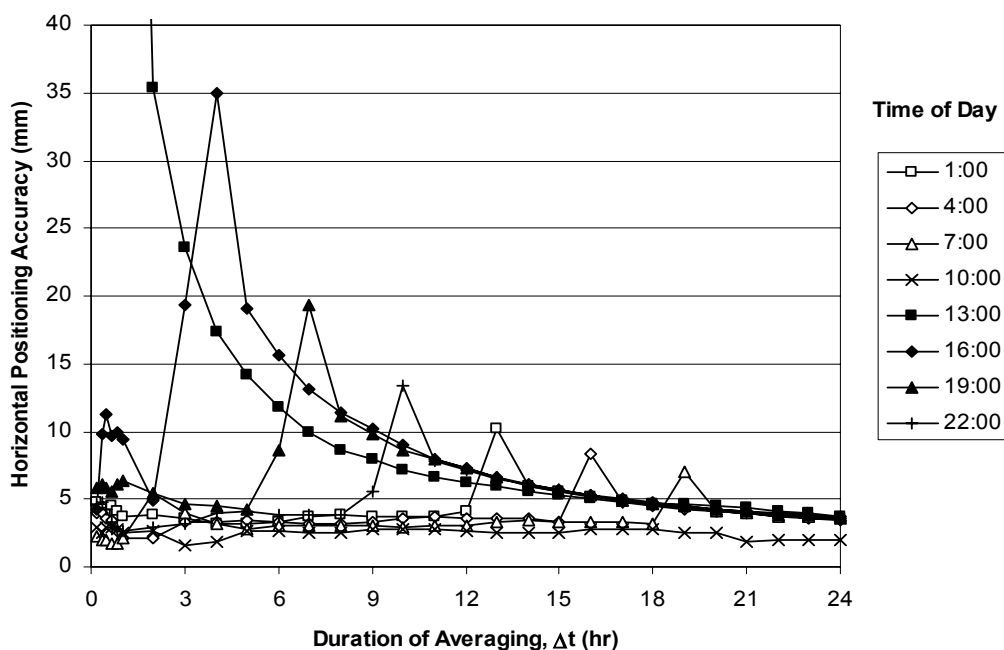
Figure 3.28: Horizontal Positioning Accuracy as a Function of Time of Day STA 1, Week 1
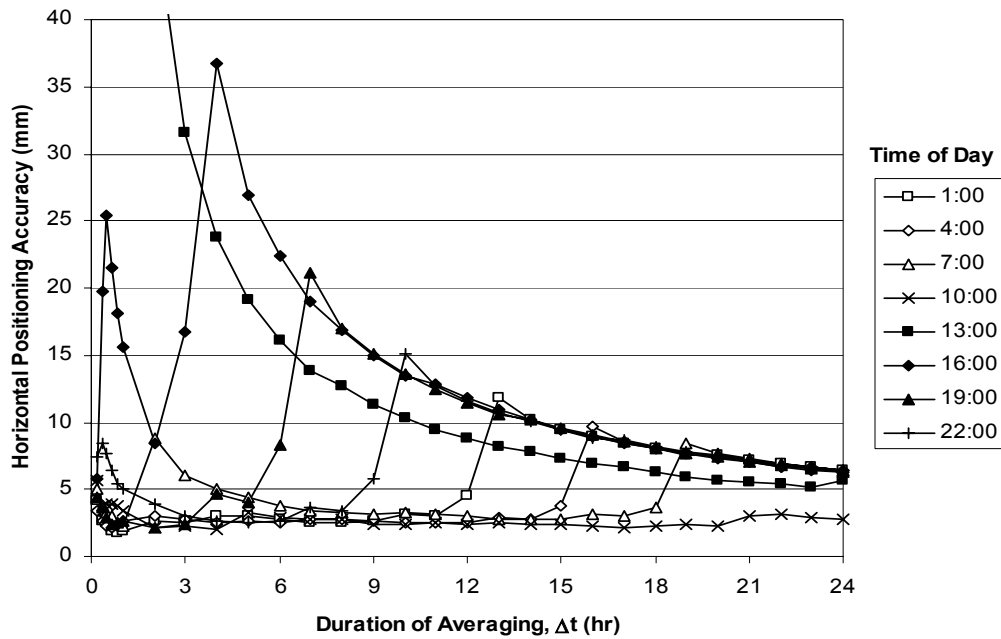
***Figure 3.29: Horizontal Positioning Accuracy as a Function of Time of Day
STA 2, Week 1***

f) Conclusion

The NetForce global positioning system generally performed at or better than the advertised sub-centimeter level of accuracy in a variety of dynamic testing environments. These tests showed that increased averaging durations did improve system accuracy up to a plateau. System accuracy may improve beyond this plateau with averaging durations greater than 24 hr.

3.4 VERTICAL TESTS

This section describes testing the NetForce GPS in the vertical plane. It will discuss the goals of this phase of testing and profile the design and construction of the vertical testing apparatus. Testing methodology will also be discussed.

3.4.1 Goals

The goal of this phase of testing was to verify the vertical positioning accuracy of the NetForce system in a variety of static and dynamic situations. This was achieved by precisely controlling the vertical displacements of the rover stations, while keeping them stationary in the horizontal plane. Displacement data were collected from the rover stations and processed. Section 3.5 will discuss the analysis of the vertical displacement data.

3.4.2 Vertical Movement Package

In order to evaluate the accuracy, sensitivity, and repeatability of the vertical GPS data, a mechanism was developed to move the rover stations in a controlled manner. As with the horizontal movement package, the entire station would have to be stable against wind and rain forces, and it must have the flexibility to allow vertical movements.

Upon completion of the horizontal testing phase, the existing horizontal testing apparatus (see Section 3.2.2) was altered to allow vertical movements. This was done by unbolting the GPS hardware enclosure from the milling table base, inserting rectangular steel shims of varying thickness, and affixing the enclosure to the milling table using four 6" C-clamps. The C-clamps allowed quick and easy insertion (or removal) of shims that would displace the station in the vertical plane by known amounts.

73

To induce a vertical displacement, shims were added or subtracted from beneath the GPS enclosure. After a vertical displacement was induced (positive or negative) and the station reaffixed to the milling table, the shim stack would be measured at all four corners. Measurement was performed using a dial caliper with an accuracy of 0.001". These four values were averaged and this number taken to be the mean height of the station above the milling table surface. The actual value of the induced vertical displacement was then calculated by subtracting the new station height from the previous station height.

3.5   RESULTS OF VERTICAL TESTING

The following section will discuss the sequences of induced vertical displacements. It will also discuss problems encountered with recovery of the vertical displacement data.

3.5.1   Vertical Displacement Sequences

Testing in the vertical plane was not divided into phases, as were the horizontal tests. Each station was displaced through seven discreet displacement sequences. Table 3.11 presents the vertical displacement sequences induced in this phase of testing.

Table 3.11: Vertical Testing Sequences

Movement Sequence	Vertical Displacements		Duration of Displacement
	STA 1 Up + / Down – (mm)	STA 2 Up + / Down – (mm)	
1	+19.1	+19.1	3 days
2	+18.9	+19.3	17 days
3	+6.6	+6.6	7 days
4	-6.5	-6.5	1 hour
	-6.4	-6.6	1 hour
	-6.4	-6.3	1 hour
	-6.3	-6.5	1 hour
	-6.4	-6.4	1 hour
5	-12.7	-12.8	13 days
6	+2.6	+2.6	4 days

Movement Sequence 4 was the only movement sequence that contained multiple, dynamic movements. This sequence was intended to replicate a structure experiencing rapid vertical movement. In this case, the structure would be sinking at a rate of approximately 6 mm per hour.

Other movement sequences were intended to test the maximum positioning accuracy of the system in the vertical plane, as well as the effects of different data averaging durations (t_o) on system accuracy.

3.5.2 Data Recovery Issues

Immediately following the final movement sequence on April 14, 2003, attempts were made to contact Mezure, Inc., requesting transfer of the final GPS data set. This is the data set that contains the vertical displacement data for all seven displacement sequences. Over the next month, Mezure did not answer repeated telephone calls or return repeated e-mail messages. As of May 1, 2003,

the MezureNet website as well as the company homepage were no long accessible. Still no contact had been made with Mezure.

As of the end of July, Mezure has yet to respond. The whereabouts of Mezure and its personnel are unknown, but a possible explanation is that Mezure is experiencing financial difficulties and can no longer offer services to the public.

This being said, a recommendation must be made to evaluate the financial stability of any company fully before entering a long-term contract of service with that company. A thorough evaluation of the company done previous to the start of GPS testing may have uncovered such instabilities within Mezure. With that knowledge, another firm offering GPS hardware and monitoring services would have been contacted to provide research support. This in turn may have allowed the completion of this portion of the research.

CHAPTER 4

Autonomous Data Acquisition System for Strain

Over the past twenty years, a large number of researchers have measured the response of bridges in the field and then analyzed the data to evaluate the condition of the bridge. While this method of operation has proven to be effective in the research environment, the data acquisition systems and data reduction algorithms are not well suited to the needs of a Department of Transportation which must inspect all bridges on a bi-annual basis. The data acquisition system described in this chapter was designed specifically for these frequent inspections.

Each data acquisition unit is battery powered, small enough to sit on the bottom flange of a steel girder, and records data from a single, 120-K strain gage. Perhaps most importantly, the unit has been designed to generate rainflow counts directly, so that the inspection team can evaluate the stress ranges experienced at a given location on the bridge rather than analyzing thousands of points of strain data. The research team believes that there are many applications for this type of autonomous data acquisition system.

This Chapter is divided into three sections. The ASTM E 1049-85 rainflow counting algorithm is briefly described in Section 4.1. An overview of the features of the data acquisition system is given in Section 4.2, and the system is evaluated critically in Section 4.3.

4.1   RAINFLOW COUNTING

Rainflow counting is a method of simplifying a complex strain history into a histogram of cycle amplitudes. By counting the number of times that a structure experiences cycles of a given level of strain, the likelihood of fatigue damage and the remaining fatigue life can be predicted (Downing and Socie, 1982).

The rainflow counting algorithm is described using the sample loading history shown in Figure 4.1, which was taken from ASTM E 1049-85 specification for rainflow counting. The loading units in this sample history can be assumed to be directly proportional to both stress and strain in the specimen.
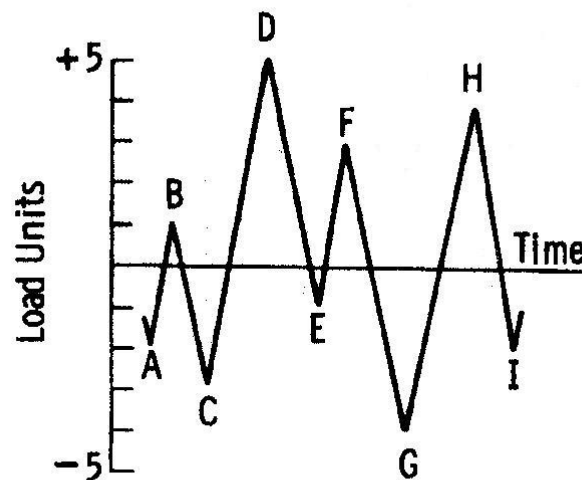

Figure 4.1: Example Loading History (ASTM E 1049-85)

The ASTM algorithm for rainflow counting me be used to evaluate previously recorded data, as well as strain histories that are measured, counted, and discarded in real time. The strain history is examined point-by-point,

beginning with the first observed data point, A.   A simple series of Boolean checks are performed to compare the current strain with the adjacent maximum and minimum strains in the history. In this manner, the number of cycles within predetermined ranges of strain are calculated.

The strain history shown in Figure 4.1 can be used to demonstrate the algorithm. The following notation is used in this discussion: X denotes the strain range under consideration; Y denotes the strain range before X; and S denotes the starting point in the strain history.

As shown in Figure 4.2, the rainflow counting algorithm begins by setting the starting point, S, at the first point in the history, A. Range A-B in labeled as Y and range B-C is labeled as X. The absolute values of ranges Y and X are three and four, respectively. Because X > Y and range Y contains the starting point S, the range A-B is counted as a half-cycle with an amplitude of three, as shown in Table 4.1. Point A is then discarded, and the starting point S is moved to Point B.

Range B-C is now labeled as Y and range C-D is labeled as X. Because X > Y and range Y contains S, the previous actions are repeated: Range B-C is counted as a half-cycle with an amplitude of four, Point B is discarded, and the starting point is moved to Point C.

Range C-D is now labeled as Y and range D-E is labeled as X. Because X < Y, range C-D is bypassed, but not discarded, without modifying the cycle counts. Range D-E is now labeled as Y and range E-F is labeled as X. Because X < Y, actions are repeated: range D-E is bypassed and the cycle counts remain unchanged.

Range E-F is now labeled as Y and range F-G is labeled as X. Because X > Y and the starting point S is outside range Y, range E-F is counted as a full cycle with an amplitude of four and both points E and F are discarded. This leaves the range D-G in place of the points D-E-F-G. The starting point S is still

79

at point C.   Therefore, range C-D becomes Y and range D-G becomes X. Because X > Y and S is within range Y, range C-D is counted as a half-cycle with an amplitude of eight, point C is discarded, and the starting point S is moved to Point D. Range D-G becomes X and the range G-H becomes Y. Because X < Y, range D-G is bypassed and the remaining ranges are relabeled.   Range G-H becomes Y and range H-I becomes X.

Because point I is the last data point in the series, all remaining ranges (D-G, G-H, and H-I) are counted as half-cycles and logged as shown in Table 4.1.
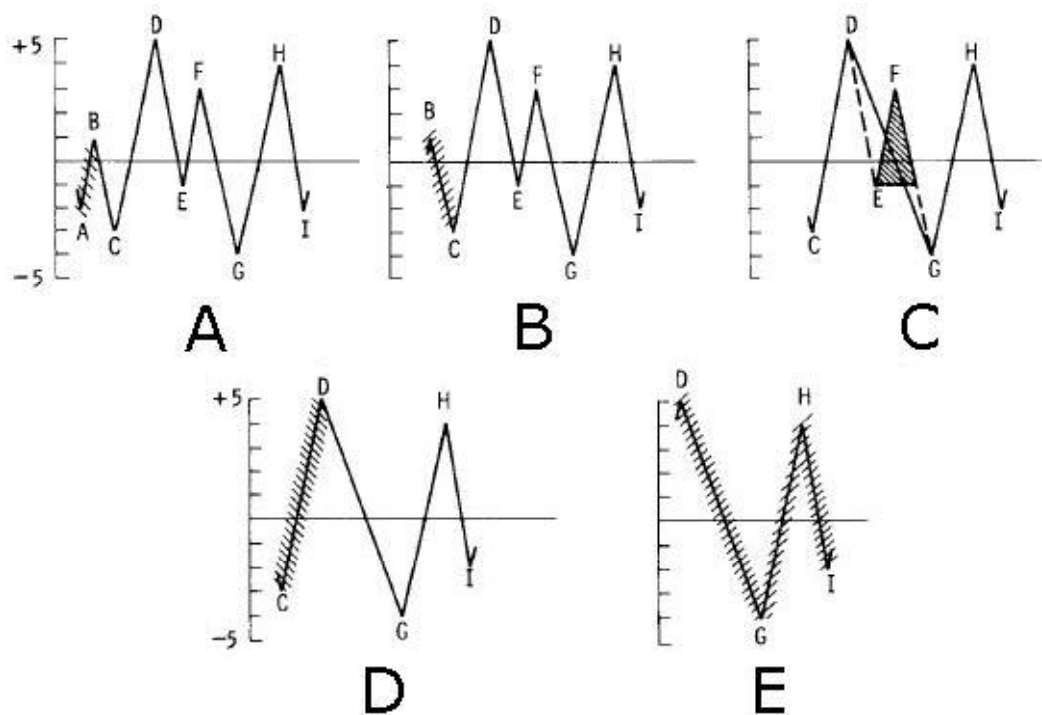

Figure 4.2: Rainflow Counting Methodology (ASTM E 1049-85)

When actual data are acquired in a realistic environment, many cycle counts are recorded in a given strain history and recorded values of strain are not

80

integers. If this rainflow counting algorithm were used with actual data, an extensive table of stress ranges, each likely to have only a single or half-cycle, would be generated. These data would be voluminous and difficult to interpret.

Range bins allow individual cycle counts to be combined into more meaningful groups. An example of binned data is shown in Table 4.2. The size of each range bin is 3 units. Cycles from 0 to 3 units are counted in the first bin, cycles from 3 to 6 units are counted in the second bin, and cycles from 6 to 9 units are counted in the third bin. Cycles falling on the edge of a bin (range = 3, for example) can be counted in either bin at the discretion of the rainflow algorithm programmer. The resulting table (Table 4.2) is a more condensed version of Table 4.1, where data are easier to interpret and more meaningful in fatigue life analysis.

Table 4.1: Rainflow Cycle Counts for ASTM Example

Stress Range (units)	Cycle Counts	Events
1	0	
2	0	
3	0.5	A-B
4	1.5	B-C, E-F
5	0	
6	0.5	H-I
7	0	
8	1.0	C-D, G-H
9	0.5	D-G
10	0	

Table 4.2: Binned Cycle Counts for ASTM Example

Range Bin (units)	Cycle Counts	Events
0-3	0.5	A-B
3-6	2.0	B-C, E-F, H-I
6-9	1.5	C-D, G-H, D-G

4.2   THE MICROSAFE SYSTEM

This section describes the features of a commercially available, autonomous strain recording device called MicroSAFE. MicroSAFE stands for "Micro-miniature Stress Analysis and Forecasted Endurance," and was developed by Invocon, Inc., located in Conroe, Texas.

4.2.1   Background

MicroSAFE is a single-channel data acquisition system intended to aid in fatigue life estimation of structural elements. Invocon began development of this technology for the National Aeronautics and Space Administration (NASA) in the late 1990's. Early versions recorded raw strain data on the space shuttle for analysis upon mission completion. These devices would monitor and record strains within the structural components of the space shuttle during launches and landings. Upon mission completion, the devices would be removed, and the data would be downloaded and analyzed. These data were used to determine the amount of fatigue damage done on each mission and predict the remaining amount of service life for each shuttle.

4.2.2   First Generation

In 2000, researchers at the University of Texas at Austin contacted Invocon to build a series of similar devices that could be used to monitor bridges. Only one unit from this first generation was ever constructed. This device is shown in Figure 4.3 and measured 30 mm x 30 mm x 15 mm. The system could record data at 7.1 Hz and compute rainflow counts as data were acquired. An internal battery with an expected life of 36 hours provided power. Once programmed for acquisition, the system was 100% autonomous.

Figure 4.3: First Generation MicroSAFE Device

Limited testing was done using this device, all previous to the start of this research. Available battery power was deemed to be the limiting factor in repeated data acquisition. Also, this unit was not enclosed in a weatherproof container.

4.2.3 Second Generation

This research was begun using the second generation of the MicroSAFE devices. Invocon delivered 11 second-generation units to the University in late 2001, along with an updated software package that facilitated the programming of this generation of devices. Over the next 2 years, Invocon worked closely with the University research team to test, evaluate, and update the devices.

This generation of devices was designed to be weatherproof. Each device was potted using epoxy material and used weatherproof rubber connectors. Power was provided by an external, non-rechargeable battery pack, which also utilized epoxy potting material and weatherproof connectors. This battery pack was designed to power a single MicroSAFE unit for three months of continuous data acquisition, removing battery life as the limiting factor for monitoring applications. Figure 4.4 shows the battery pack (larger device on left) connected to the MicroSAFE hardware (smaller device on right).
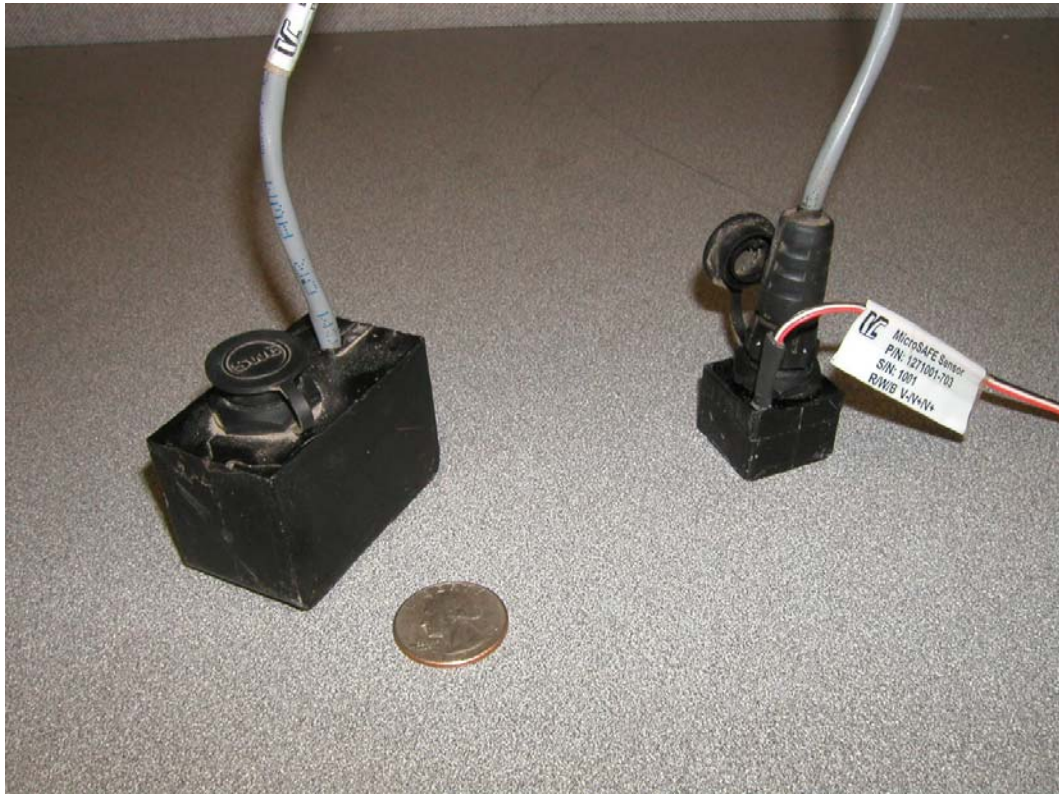
Figure 4.4: MicroSAFE Battery Pack and Hardware

An updated graphical user interface (GUI) was provided with this generation of MicroSAFE devices. The GUI is a computer program that is used to communicate with the MicroSAFE devices, program them for data acquisition, download data sets when the unit has completed data acquisition, and view downloaded data sets graphically in a variety of ways.

During the programming of the unit for data acquisition, various options are available. These options include the type of data acquisition, data acquisition mode, gage factor, data sampling rate, and bin size for rainflow analysis. The user can select the start and stop times for data acquisition, the number of consecutive data acquisition cycles, and the time between cycles.

Data acquisition can be started by setting a specific time or by an event-detection mode. In the event-detection mode, the unit would power off and "sleep" for a user-determined amount of time. It would then power on, "wake up," and monitor the strain gage for an event where strains were larger than a user-set threshold value. If the strain event contained strains over the threshold value, the unit would acquire the desired amount of data (number of cycles, length of data acquisition, etc.) before powering off and starting the process over. If the strain event did not cross the threshold value, the unit would power off and wait for the next time when it would power on and monitor the gage again. This function was intended to allow very long periods of observation where insignificant strain events (those below the threshold value) would not be recorded, preserving both battery life and available memory.

Because of the speed of traffic on in-service bridges, a single strain gage would most likely only experience an extreme strain event (a large truck passing overhead) for a few seconds. The odds of this event being observed within the brief event-detection window are small. If the event did happen to be captured in the event-detection window, the duration of the event would not be long enough to be captured once the unit has powered on and started to record data. For these reasons, the event-detection mode did not seem practical for monitoring strain events on a bridge and will be removed in future versions of the GUI.

A variety of data could be captured with this generation of devices. These included raw strain data capture only, raw data capture and immediate, onboard rainflow counting of this data, and rainflow counting only. During the "rainflow counting only" acquisition mode, no raw data would be saved in memory. The option for raw data capture would allow the user to perform a variety of analyses following data capture, while the rainflow option would allow the user to see how the structural element was performing immediately after data capture. The "raw

86

and rainflow" option allowed the user to have both a rainflow count for the recorded strain history and the raw strain data from which the rainflow count was obtained. Any time raw data are captured, available memory on the MicroSAFE device becomes the limiting factor in data acquisition time.

The data rate could be specified to be 8, 16, or 32 Hz. At the maximum data acquisition rate, available memory would be fully utilized after only 34 min of continuous data acquisition. This was viewed as a limitation to the MicroSAFE devices and may be addressed in the next generations.

Data acquisition time is also limited to 34 min per cycle while taking rainflow data only. Though the available memory will be only 1.2% full with a single 34-min rainflow-only cycle, the maximum rainflow acquisition time per cycle was still limited by the GUI. If more than one sampling cycle was requested, the MicroSAFE unit would have to sleep for 8 sec to log the rainflow counts to a data file before beginning the next cycle. After downloading the completed rainflow data, each cycle would be represented in a separate data file.

If the user wished to observe the behavior of a structural component over a 24-hr period, 48 30-min cycles would have to be programmed. Following download, all 48 sets of rainflow cycle counts would need to be combined to get a clear picture of how the structural component behaved for that 24-hr period. In February 2003, Invocon released a Rainflow Combining Utility that allowed the graphical viewing of multiple rainflow files at one time, and the combination of the values found in each bin of these files. Although the addition of this program allowed the creation of 24 hr of continuous sampling, these extra steps proved to be confusing and difficult. These concerns will be addressed in the next version of the GUI and will be described in depth in the following section.

The majority of tests discussed in the following sections of this chapter were performed using MicroSAFE devices from the second generation. As

testing progressed, communication between the research team and Invocon produced five new versions of the GUI (versions v2.0 through v2.4), each more refined than the previous version. MicroSAFE hardware remained the same throughout these tests.

4.2.4   Third Generation

In early 2003, the Invocon discovered a problem with the manner in which individual rainflow counts were assigned to bins during data acquisition. This scheme was hard-coded within the MicroSAFE devices and could not be reprogrammed. All 11 devices were returned to Invocon in March 2003, for repair. Invocon replaced the non-programmable internal hardware with programmable chips and returned the units. Functionality of the units remained the same between generations, but the identified errors were corrected. This marked the beginning of the third and final hardware generation. Limited testing was done using this generation, and will be discussed later in this chapter.

Following the return of the third generation of devices, the research team discovered a slight but significant error in the rainflow counting algorithm. This error had been present in all previous generations of the MicroSAFE product. In May 2003, Invocon rewrote the rainflow counting algorithm to perform the correct rainflow counts. The units were returned to Invocon in July 2003 for reprogramming.

4.3   Micro**SAFE E**valuation

To evaluate the MicroSAFE system and determine if TxDOT could use the units effectively, the research team tested the units in a variety of environments. First, the accuracy of recorded strains was verified in a laboratory environment. Next, raw data and rainflow recording abilities were tested in a field environment. The durability of the hardware was tested in a corrosive, outdoor environment. Finally, rainflow recording abilities were further tested in a laboratory environment.

4.3.1   Verification of Data Acquisition

The first step in evaluating the MicroSAFE system was to verify the accuracy of the raw strain data recorded by the units. As stated previously, MicroSAFE can record raw strain data and perform onboard rainflow counting as data are taken. It can be assumed that accurate rainflow counts cannot be obtained without accurate strain data. Therefore, it was necessary to verify the accuracy of the recorded strains before proceeding with further testing.

A Measurements Group 1550A Strain Indicator Calibrator was used to produce simulated strains that could be recorded by the MicroSAFE device. Before using the 1550A as a strain benchmark, it was checked for output accuracy using a Measurements Groups P-350A Strain Indicator. Strains of various magnitudes were simulated using the 1550A calibrator. These strains ranged from 100 $\mu\varepsilon$ to 4,000 $\mu\varepsilon$. The results are summarized in Table 4.3.

Percent error of the 1550A calibrator increased as simulated strain increased. The maximum error level was 0.23% at 4,000 $\mu\varepsilon$. This level of strain corresponds to approximately 138 ksi of stress in structural steel (assuming the

steel does not yield). This value exceeds the maximum tensile stress that would be resisted by any structural steel shape (AISC 1998).

Table 4.3: Strain Indicator Calibrator Verification

Strain Calibrator (aY)	Strain Indicator (aY)	Percent Error
100	100	0%
200	200	0%
300	300	0%
400	400	0%
1000	999	0.10%
2000	2001	0.05%
3000	3003	0.10%
4000	4009	0.23%

Four of the 11 MicroSAFE units were selected at random for strain verification using the 1550A calibrator. Units were tested one at a time, recording strain data for 30 sec as the calibrator was cycled through each of the eight strain levels listed in Table 4.3. Each strain was held for approximately 3 sec. The recorded strain values were then compared with the input strain values. Results of the four tests are summarized in Table 4.4.

Table 4.4: MicroSAFE Strain Verification

Recorded Strain (aɣ) for Each Unit

Strain Indicator (aɣ)	#1000	#1001	#1003	#1005	Average Percent Error
100	101	100	100	100	0.3%
200	199	201	200	198	-0.3%
300	299	302	300	299	0.0%
400	394	402	400	399	-0.3%
999	998	1004	1000	997	0.1%
2001	1998	2005	2000	1998	0.0%
3003	2998	3006	3000	2996	-0.1%
4009	3998	4008	3999	3993	-0.2%
				Average	**-0.1%**

Individual recorded strains were within 1.0% of the corresponding input strain. When errors corresponding to a single strain value were averaged for all four units, maximum error was reduced to 0.3%. From this examination, it can be concluded that the MicroSAFE devices would record sufficiently accurate strain data for strains up to 4,000 aɣ.

During the recording of a static strain, a certain level of background noise is recorded by each MicroSAFE device. This level varies from unit to unit, peaking at 10 aɣ and averaging 3 - 4 aɣ. A 3-sec history as a constant input strain is shown in Figure 4.5. This strain history would produce rainflow cycle counts with magnitudes ranging from 0 - 8 aɣ due to background noise, which would

saturate the smallest bin(s) in the rainflow histogram. Bins of larger magnitude than the observed background noise would continue to contain reliable counts.

This background noise cannot be removed. For this reason, the new GUI will include a function that will ignore cycles with magnitudes lower than a threshold value specified by the user. These cycle counts will be removed from the rainflow histogram so that it will more accurately represent the number of cycle counts at lower strain ranges. The discarded cycle counts will be logged in the full data file for retrieval upon demand.

Background noise is present at all times during strain measurement. The magnitude of the background noise is random, but remains small in comparison to the magnitudes of strain cycles that will affect the fatigue life of a steel structure. Therefore, the level of background noise present in the MicroSAFE strain measurement will not adversely affect fatigue life predictions using this system.
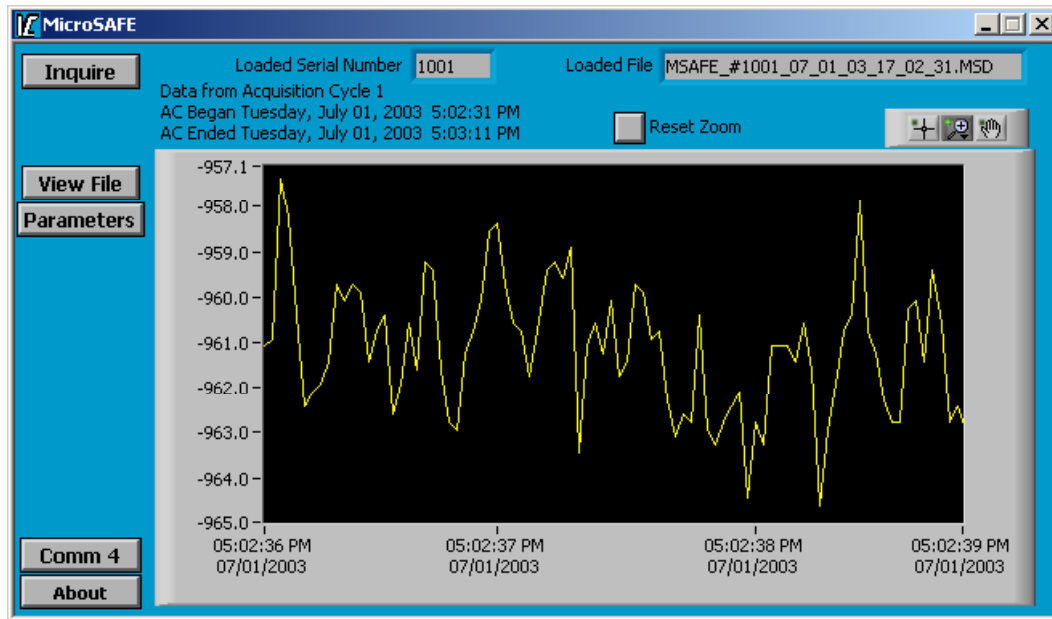
Figure 4.5: MicroSAFE Background Noise Sample

4.3.2 Field Testing on U.S. 183 / 71 Bridge

Field-testing of the MicroSAFE units was performed on a bridge located in Austin, Texas. This bridge carries westbound Texas State Highway 71 over U.S. Highway 183 (Figure 4.6). This structure was selected because the layout permitted access to the girders at midspan without obstructing traffic.

The TX 71 / U.S. 183 overpass is a 6-girder steel bridge with a concrete deck. Steel girders are continuous over pinned supports at the concrete bent caps. The concrete deck acts compositely with the steel girders over five spans. All testing was performed at midspan of the center span.

Figure 4.6: U.S. 183 / Texas 71 Overpass

Ten MicroSAFE units were tested in this field study. Units were mounted on the top face of the bottom flange of the interior girders. Placement on the lower flanges of interior girders at midspan ensured the highest possible tensile strain signals during traffic loadings. The units were arranged in five pairs. Strain gages in each pair were arranged in a nose-to-nose fashion, as shown in Figure 4.7.

Figure 4.8 shows a pair of MicroSAFE units installed on the bridge. All gage pairs were installed with identical configurations. Because both gages in a given pair were positioned in almost identical locations on the structure, this configuration allowed a pair of MicroSAFE units to record identical strain data

simultaneously in the field. Figures 4.9 through 4.12 contain plots of the measured data. These figures show nearly identical strain histories when corrected for minor initial strain and time differences between MicroSAFE units. These corrections are discussed later in this section.

Figure 4.7: Paired Strain Gage Placement

Figure 4.8: MicroSAFE Units Paired on Bridge

Testing on the TX 71 / U.S. 183 overpass lasted approximately one year. Over this period, the units were acquiring data approximately 10-20% of the time. Performance and durability of the units were very good. More than 200 acquisition sequences were programmed during field testing. The units acquired the appropriate data in approximately 97% of the sequences. In one case, there were no data present on the MicroSAFE device following acquisition. In two cases (on two different MicroSAFE units), data were present on the unit but download was not possible. Following reprogramming, each unit performed normally for the duration of its service. In another case, one unit would acquire strain data, but returned zero cycle counts when programmed to take rainflow data. This was later traced to an internal programming error in the auto-zero function within that particular MicroSAFE device. The unit was reprogrammed by Invocon and has been functioning normally since.

The units were programmed to acquire both raw strain data and rainflow data an acquisition rate of 32 Hz for most of these tests. A few tests were performed using acquisition rates of 8 or 16 Hz. As expected, the peaks and valleys were less pronounced in the strain histories when the data were captured at the slower data acquisition rates. As a result, acquisition rates for all subsequent tests were set at 32 Hz.

Each round of tests was conducted by programming all 10 units to perform the same type of data acquisition using the same bin size. Bin sizes were varied between tests, starting at 10 aɣ and increasing by 10 aɣ for each successive round of testing. When bin size reached 50 aɣ, all observed stress ranges were being logged in the first half of the bins. The maximum bin resolution was no longer being used. Bins were therefore limited to 50 aɣ.

Acquisition periods for these tests were set at the maximum of 34 min. As stated previously, 34 min of continuous raw strain and rainflow data recorded at

32 Hz filled the available memory completely. The maximum acquisition time was employed to acquire the maximum number of strain cycles during an acquisition, helping to test the rainflow counting algorithm. However, even when using the maximum acquisition time of 34 min, most of the bins in the rainflow histogram contained zero cycles. There were not enough high strain cycles occurring within the 34-min acquisition window to populate all bins. Longer rainflow acquisition times would likely capture a few cycles of higher strain, however it was not possible to record raw strain data during the longer acquisition windows.

In an attempt to collect data over a longer duration, the same series of tests were performed again (using maximum acquisition time and varying bin sizes for each round of tests), but the start times for the five gage pairs were staggered so that acquisitions could be performed sequentially. Approximately 2.5 hr of continuous raw strain and rainflow data could now be acquired on the structure. Although each gage pair was not positioned at exactly the same location on the structure, the technique was successful in creating a combined, continuous raw strain history and a corresponding set of rainflow counts.

An interesting observation was made during field-testing on the TX 71 / U.S. 183 overpass. When two MicroSAFE units were programmed to begin identical acquisitions at the same time, small timing discrepancies between the two units were observed. This discrepancy results from the manner in which time is kept on each MicroSAFE unit.

When a unit is programmed for acquisition, the internal clock on the MicroSAFE device is synchronized to the computer clock. The clock speeds of the microprocessors within each MicroSAFE unit are used to count time once an acquisition has been programmed. Due to variability in the manufacturing of the microprocessors, the clock speed of each microprocessor is slightly different.

Therefore, there will be a minor time mismatch between all MicroSAFE units that cannot be removed. This mismatch will not vary more than a few seconds during a given acquisition (Haigood, 2002).

These effects can best be seen in Figures 4.9 through 4.12. MicroSAFE units #1001 and #1004 were programmed to take both raw strain data and rainflow data beginning at the same time. Raw strain data versus the time since the start of data acquisition (according to each unit) are plotted in these figures. Near the start of the acquisition period (approximately 108 sec into the 2000-sec acquisition period) the data series recorded by unit #1004 had to be shifted left by 0.27 sec to overlap the data series recorded by unit #1001, as shown in Figure 4.9. This value was called a *time offset*, because it represents the time shift between two units due to different clock speeds.
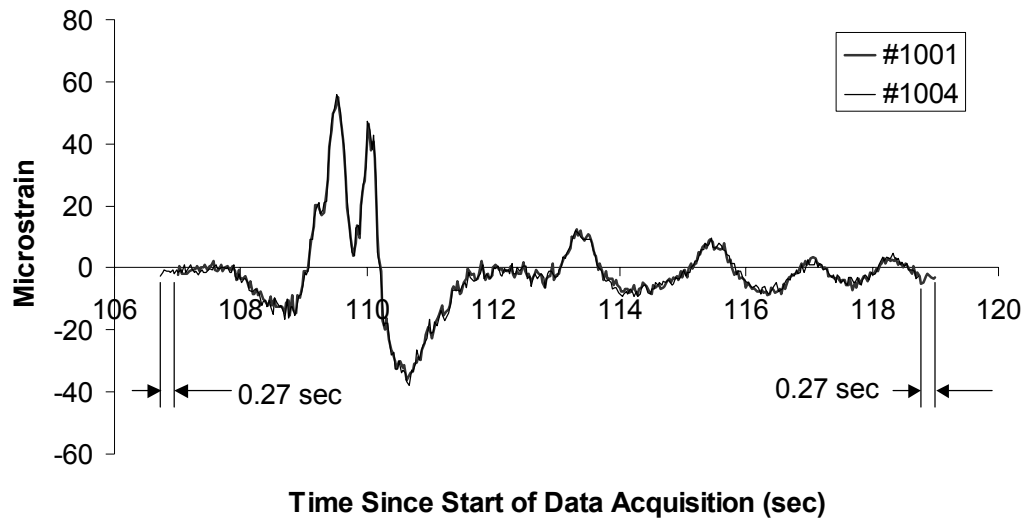
Figure 4.9: Corrected Strain vs. Time Approximately Two Minutes into Acquisition Period
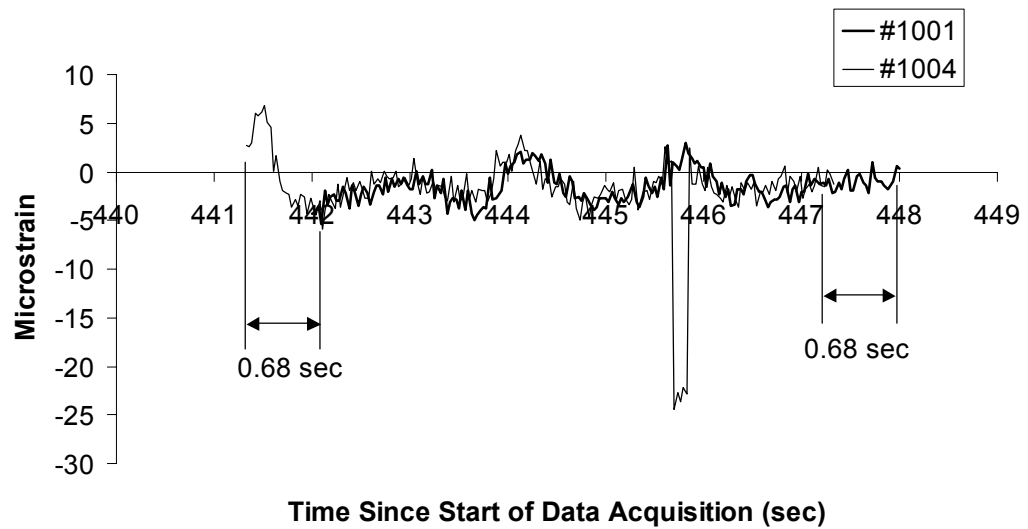
Figure 4.10: Corrected Strain vs. Time Approximately 7.5 Minutes into Acquisition Period

99
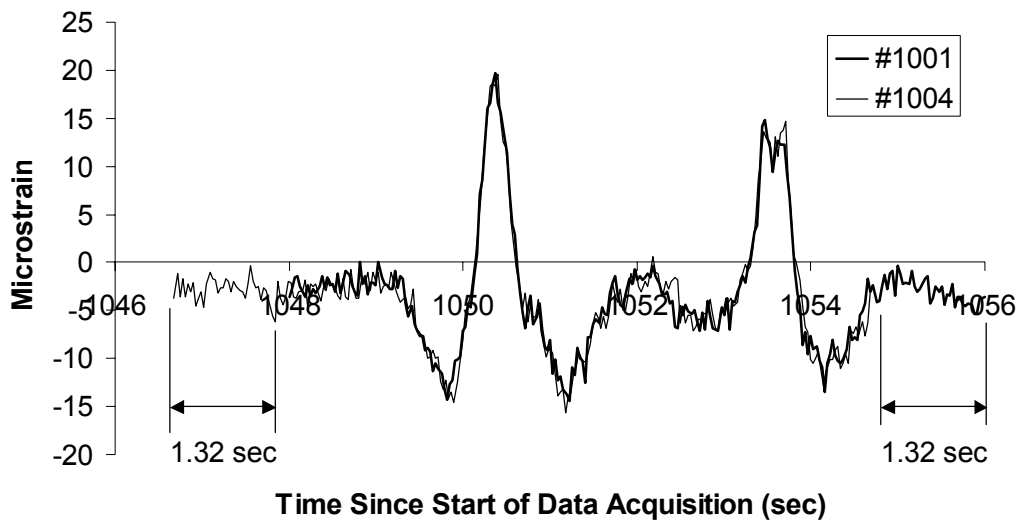
Figure 4.11: Corrected Strain vs. Time Approximately 17.5 Minutes into Acquisition Period
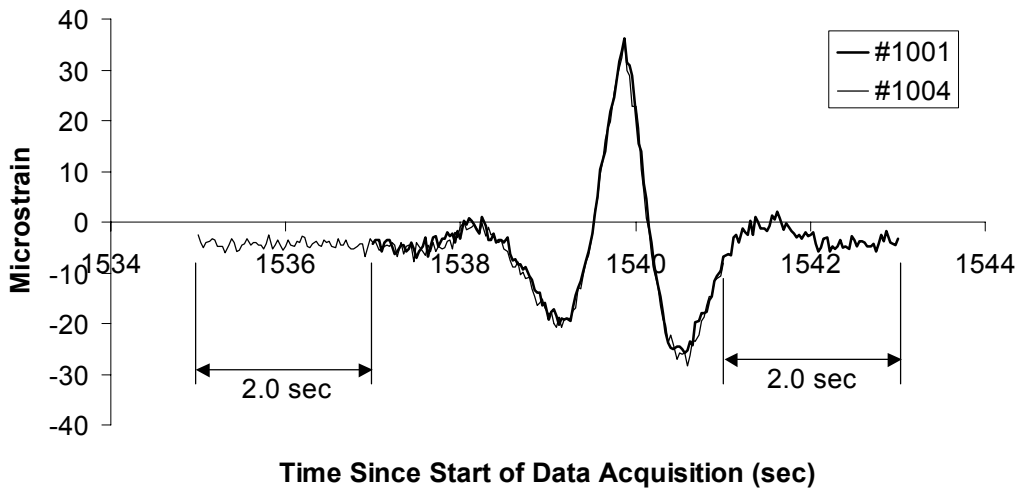
Figure 4.12: Corrected Strain vs. Time Approximately 25.5 Minutes into Acquisition Period

100

Near the end of the acquisition period (Figure 4.12, at approximately 1536 sec into the 2000-sec acquisition), 2.0 sec of adjustment was required to produce overlap in the data series. By computing time offsets at other points between 0 and 2000 sec, shown in Figures 4.10 and 4.11, the offset was found to vary linearly with time. These results, shown in Table 4.5, were expected because the time offset is due to differences in the clock speed between microprocessors.

Strain offsets were also observed at various times between 0 and 2000 sec. These values were used to correct the strain values and produce agreement in the data series. They are listed in Table 4.5, as well. Strain offsets were found to be generally increasing with time, but they did not increase linearly. It is most likely that these variations in strain between data sets are caused by background noise.

When both strain and time offsets are considered, Figures 4.9 through 4.12 show that data agreement between the two MicroSAFE devices is very good. Small variations (2 – 3 a∀) between the two devices are visible at times due to background noise. However, overall, the strain histories are so similar that it is difficult to distinguish one from another.

Figure 4.10 shows a brief but significant disturbance in the strain history for unit #1004. The cause of this disturbance is unknown. However, this was the only signal disturbance recorded during field testing that was not attributed to background noise.

Table 4.5: Strain and Time Offset Values

Time (sec)	Time Offset (sec)	Strain Offset ($a\Upsilon$)
108	-0.27	-1.5
442	-0.68	-1.0
1048	-1.32	-3.0
1536	-2.0	-5.0

Regardless of the cause of the time and strain offsets, they should not adversely affect acquisition of raw strain data or the corresponding rainflow data.

4.3.3 Durability Testing on Fred Hartman Bridge

To test the durability of the MicroSAFE system in a corrosive environment, a single MicroSAFE unit was installed at the center of the main span of the Fred Hartman Bridge. This bridge (Figure 4.13) spans the Houston Ship Channel between Baytown and LaPorte, Texas. The environment in this area is known for being highly corrosive and was therefore selected for this durability study.

Figure 4.13: Fred Hartman Bridge (TexasFreeway.com, 2003)

The duration of the study was one month. The MicroSAFE unit tested in this study was provided and managed by Invocon for the duration of the study. This unit, provided by Invocon, was the only second-generation unit not currently being used for testing by the University.

Various acquisitions were programmed during this month. According to Invocon, the unit performed flawlessly during all acquisitions. The physical condition of the unit following the study was also very good.

Figure 4.14 shows the unit installed on the Fred Hartman Bridge. The battery shown in this figure is a prototype of the new battery pack, where individual cells can be replaced without replacing the entire battery pack structure. According to Invocon, this battery pack performed as expected during the month of acquisitions. No special attention was required during acquisition.

Upon removal and inspection, there was no evidence of corrosion within the battery pack.

Figure 4.14: MicroSAFE Unit on Fred Hartman Bridge

4.3.4 Milling Machine Tests

It was also desired to verify the accuracy of the rainflow counting algorithm from unit to unit. An apparatus was devised that would reproduce a given strain history an arbitrary number of times. This could allow identical strain signals to be sent to any number of MicroSAFE devices. The return of identical rainflow counts between units would then verify that all MicroSAFE devices were retrieving the same data and performing identical operations on it.

A 1" x 12" x 1/8" aluminum bar was chosen as the test specimen for these tests. The bar was attached to the surface of a computer numeric controlled (CNC) milling machine. Figure 4.15 shows the test bar and the CNC milling machine. 1" of the bar (the right end of the bar in Figure 4.15) was clamped to the milling surface (clamp not shown in figure). 1" of the bar at the left end was pressed between a double-roller support, used to eliminate localized moments at the free end of the beam. The double-roller was then fixed in the stationary head of the milling machine. As the milling surface was displaced by computer control, relative displacements between the ends of the bar were induced. This arrangement created a cantilevered beam with a clear span of 10".

The CNC milling machine could be programmed to displace the milling surface with respect to the fixed head at up to 45 in./min. At this speed, actual displacements of the milling surface would be within 0.001" of the programmed displacement. The displacement scheme generated strains in the cantilevered bar, which were recorded by the MicroSAFE units.

Figure 4.15: Test Beam on CNC Milling Machine

Two strain gages were mounted on the bar, one on each side. Both gages were located 1" from the fixed end, where high strains were expected. Terminal blocks were attached to each strain gage to facilitate easy attachment of the MicroSAFE lead wires.

During a given test, one side of the beam is in compression while the other is in tension. Because the cross section of the beam is symmetric, and both gages were placed at the same distance from the fixed end, the absolute values of the strain magnitudes experienced by each gage would be identical. The signs of the strains would, however, be reversed. Although mirror-image strain histories would be observed when both gages are acquiring data simultaneously, rainflow counts for these histories would be identical. This hypothesis was verified during testing. MicroSAFE units recording data simultaneously produced identical rainflow counts.

106

Six MicroSAFE units were chosen at random for this test. The first three tests were performed with units #1006 and #1007, adjusting bin sizes between each test until proper bin sizes were selected. Following this, four additional MicroSAFE units were selected and tested. All six units sampled the strain history shown in Figure 4.16. From this strain history, each unit produced an identical rainflow count. A representative rainflow count is shown in Figure 4.17. These tests proved that the rainflow counting algorithms on each MicroSAFE unit worked identically.

Because of the background noise effects discussed in Section 4.3.1, the first bin in the rainflow cycle count table becomes saturated relative to the number of counts in the remaining bins. Though the MicroSAFE GUI enabled the user to change the values on both the X- and Y-axis, effectively scaling the plot into any desired window, not all data analysis will be done using the GUI. Therefore, when plotting the rainflow data as they are stored, the saturated bin will affect the visibility of counts in the other bins, as shown in Figure 4.17

Figure 4.18 shows the same rainflow cycle counts, but with the background noise removed from the first bin. All cycles less than 8 a_Y in magnitude were removed from the first bin, using a simulation of the new GUI that will be released in August 2003 and discussed in Appendix F. As a result, the plot is rescaled and the data in the larger bins become easier to interpret and more meaningful.
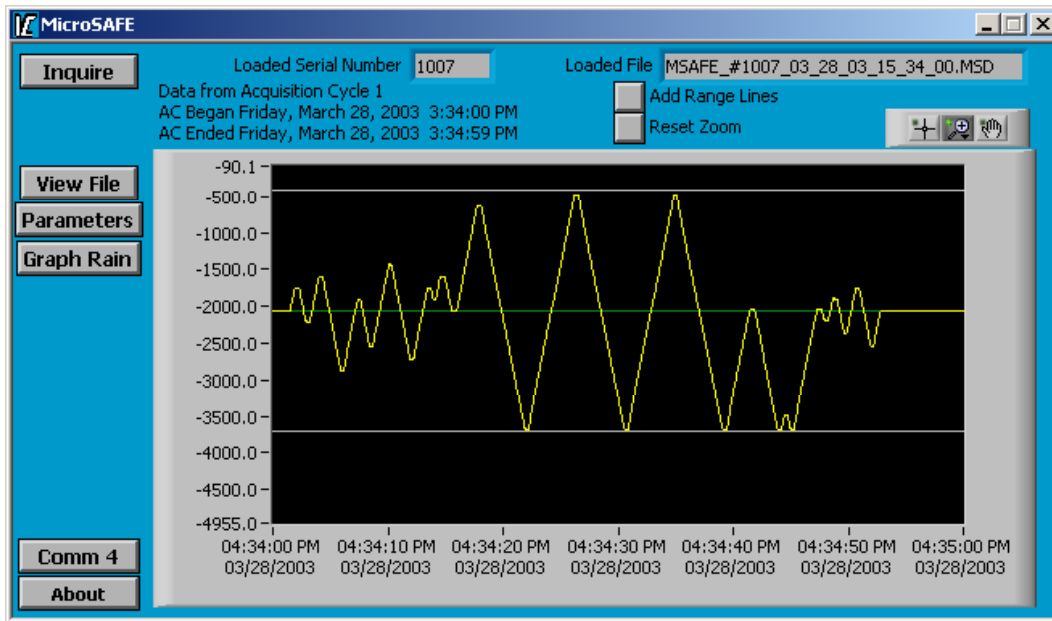
Figure 4.16: Strain History Induced During Milling Machine Tests
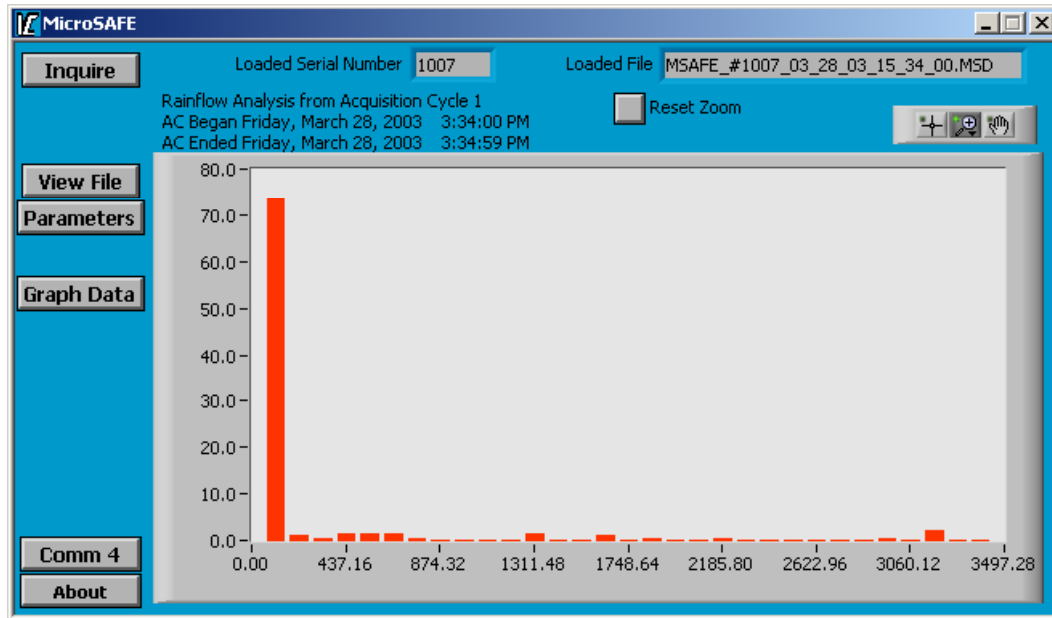
Figure 4.17: Rainflow Count from Milling Machine Tests
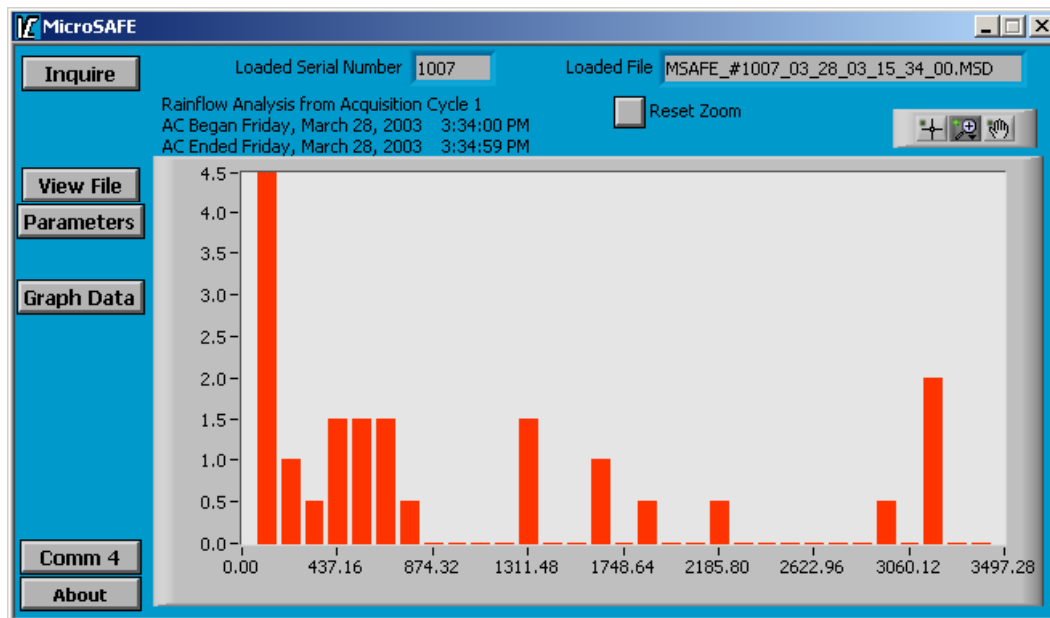
Figure 4.18: Rainflow Count from Milling Machine Tests with Background Noise Removed

4.3.5   Rainflow Verification

Following field-testing on the TX 71 / U.S. 183 overpass and testing on the CNC milling machine, many sets of raw strain data and corresponding rainflow data were available for analysis and confirmation. Two commercially available computer programs were used to verify the accuracy of the rainflow counting algorithm. The first of these programs, called "Crunch," is widely accepted in the structural analysis community (Buhl, 2003).   The second program used for verification was a Matlab script available for download from MathWorks, Inc. This script allows the Matlab software package to compute rainflow counts for any strain history, and is also widely accepted in the structural analysis field (Neislony, 2003).

Initially, ten 34-min strain histories were input into each program to verify that identical rainflow counts would be generated. Two of the examined strain histories are shown in Figures 4.19 and 4.20. Tables 4.6 and 4.7 show the resulting rainflow counts for these two strain histories. Both programs produced an identical rainflow count for each examined strain history.

Each program was also run using values taken from the example loading history depicted in Figure 4.1, discussed at the beginning of this chapter. This history was selected as a test history because the correct rainflow counts are know, given in the ASTM specification, and repeated again in Table 4.1. Both Crunch and Matlab produced the correct rainflow counts for this history. These results verified the accuracy of both programs, allowing either to be used as a benchmark for verifying the accuracy of the MicroSAFE algorithm.
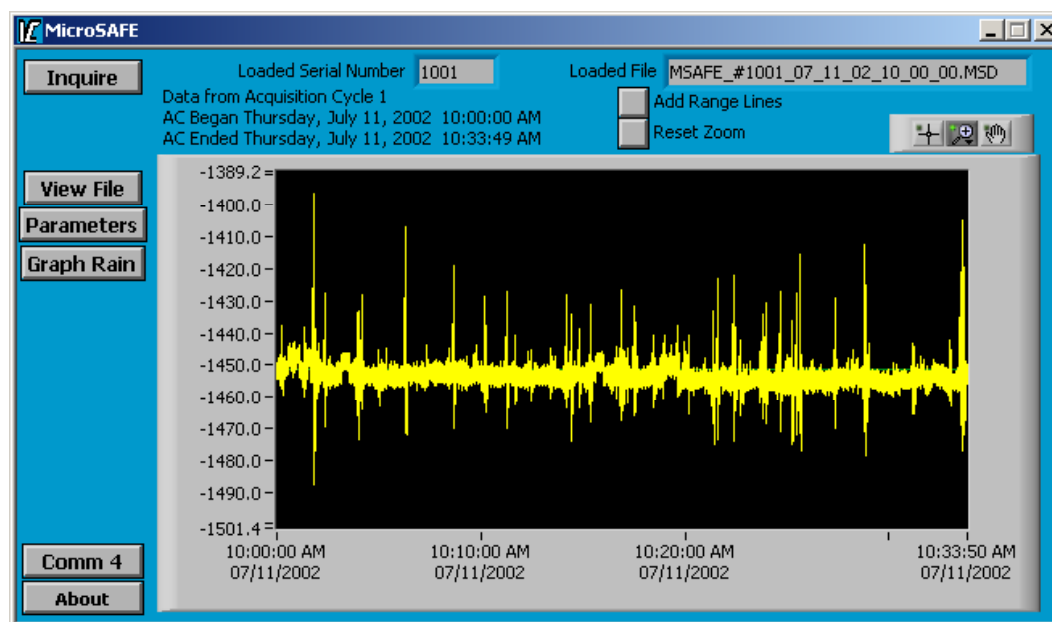
Figure 4.19: MicroSAFE #1001 Strain History

110
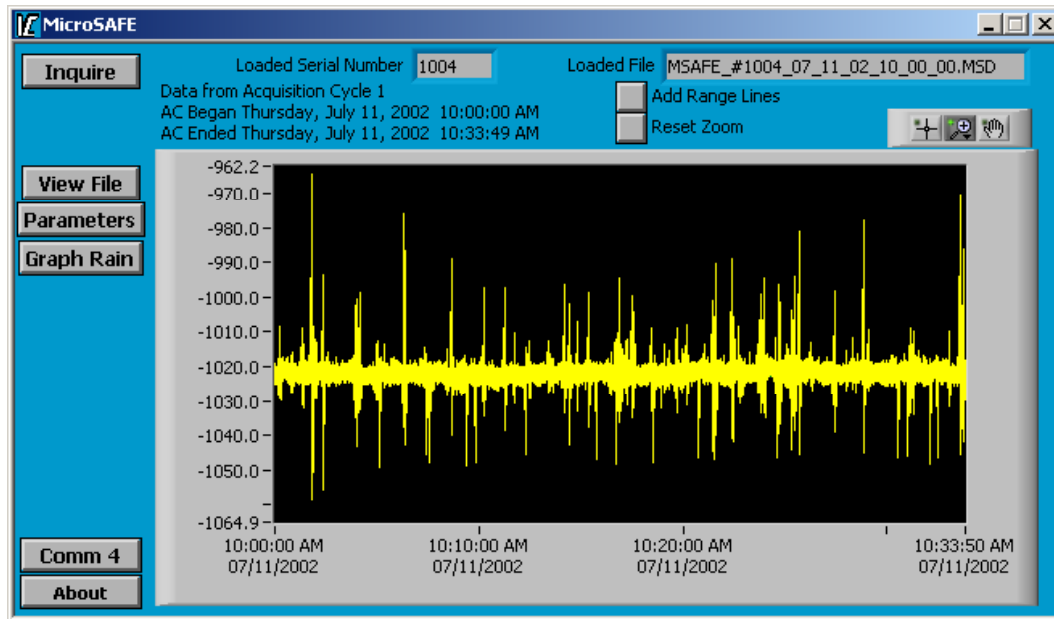
Figure 4.20: MicroSAFE #1004 Strain History

When comparing MicroSAFE-generated rainflow counts to those generated by either Crunch or Matlab, results were not identical. Conversations with Invocon uncovered an error in the manner in which rainflow cycle counts were assigned to the bins. Upon correction of this error, MicroSAFE rainflow counts performed on the previously examined strain histories changed slightly. In some cases, fewer counts were observed in the first and/or second bins. In other cases, there were no differences in cycle counts when using the revised binning scheme. In all cases, cycle counts in the remaining bins still did not match the rainflow counts of the benchmark programs. These bins contained the counts for the higher strain ranges, those that would be most important to fatigue life prediction.

Table 4.6: Rainflow Program Verification – Unit #1001 Strain History

Bin (microstrain)	Counts Crunch	Matlab
0-6	19707	19707
6-12	301	301
12-18	39	39
18-24	23	23
24-30	6	6
30-36	5	5
36-42	7	7
42-48	6	6
48-54	5	5
54-60	1	1
60-66	1	1
66-72	1	1
72-78	1	1
78-84	0	0
84-90	0	0
90-96	1	1
All other bins	0	0

Table 4.7: Rainflow Program Verification – Unit #1004 Strain History

	Counts	
Bin (microstrain)	**Crunch**	**Matlab**
0-6	19856	19856
6-12	307	307
12-18	35	35
18-24	24	24
24-30	12	12
30-36	5	5
36-42	6	6
42-48	7	7
48-54	6	6
54-60	3	3
60-66	2	2
66-72	1	1
72-78	2	2
78-84	0	0
84-90	0	0
90-96	1	1
All other bins	0	0

Table 4.8: MicroSAFE Rainflow Verification – Unit #1001 Strain History

Bin (microstrain)	Counts		
	Original MicroSAFE	Corrected MicroSAFE	Crunch
0-6	2709	2709	19707
6-12	15.5	143.5	301
12-18	22	22	39
18-24	18	18	23
24-30	6.5	6.5	6
30-36	7	7	5
36-42	7	7	7
42-48	4	4	6
48-54	3.5	3.5	5
54-60	0.5	0.5	1
60-66	1	1	1
66-72	2	2	1
72-78	0	0	1
78-84	0.5	0.5	0
84-90	0	0	0
90-96	0.5	0.5	1
All other bins	0	0	0

Table 4.9: MicroSAFE Rainflow Verification – Unit #1004 Strain History

Bin (microstrain)	Counts		
	Original MicroSAFE	Corrected MicroSAFE	Crunch
0-6	8445	8445	19856
6-12	61	61	307
12-18	25.5	25.5	35
18-24	20.5	20.5	24
24-30	8	8	12
30-36	6	6	5
36-42	6	6	6
42-48	7	7	7
48-54	3	3	6
54-60	4	4	3
60-66	0	0	2
66-72	3	3	1
72-78	0	0	2
78-84	0.5	0.5	0
84-90	0.5	0.5	0
90-96	0	0	1
All other bins	0	0	0

Tables 4.8 and 4.9 show examples of the differences between the original MicroSAFE rainflow counts, the corrected MicroSAFE rainflow counts, and Crunch-generated rainflow counts.

Following further discussion with Invocon regarding these differences, an issue was uncovered pertaining to the manner in which the rainflow counts were performed by MicroSAFE. To improve computational accuracy, Invocon attempted to simplify the rainflow counting method described by ASTM E 1049-85. Instead of comparing the actual values of measured strains using Boolean operators as described in Section 4.1, Invocon chose to count the number of times that a particular strain range crossed a predetermined set of range lines. The range lines, as set by Invocon, were the same size as the user-specified bins. Figure 4.21 shows range lines added to the milling machine strain history, previously shown in Figure 4.16.
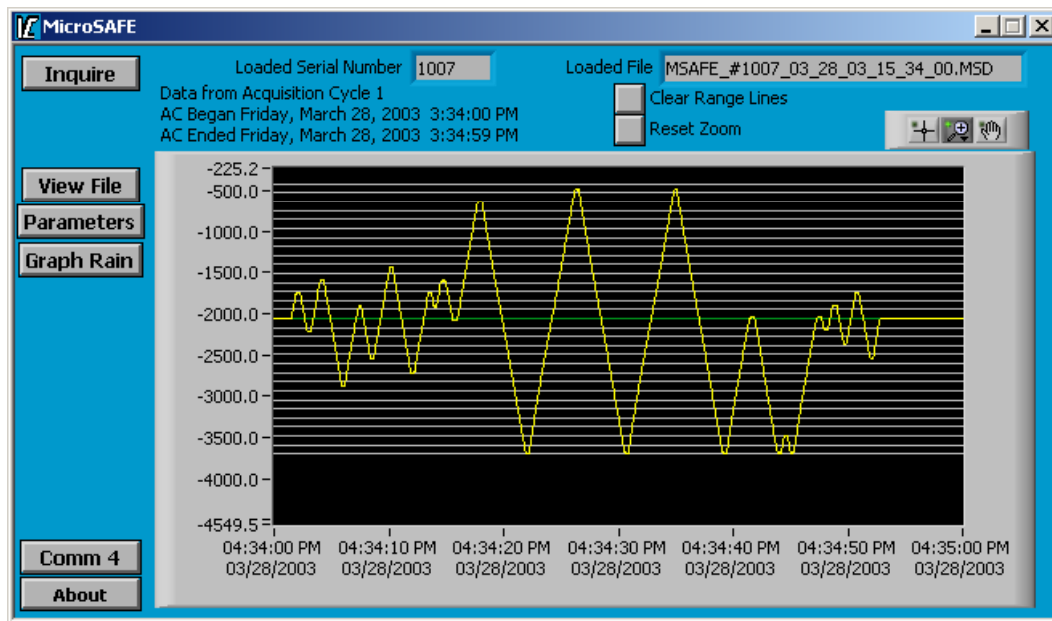
Figure 4.21: MicroSAFE Milling Machine Strain History (range lines added)

When using this simplified method to perform a rainflow count, cycles that exist in the strain history but do not cross any range lines will be not be counted as cycles. The background noise sample shown previously in Figure 4.5 is a prime example of this phenomenon. Bin sizes were set at 20 aY for this acquisition. Strain ranges in the noise sample never exceeded 8 aY. If this entire strain history falls between two range lines, spaced 20 aY apart, no cycles will be counted for this strain history. This will produce significantly lower counts in the first bin(s), as shown in Tables 4.8 and 4.9.

Consider also the sample strain history in Figure 4.22. Here, the first data point in the strain range (point A) lies between two range lines, and the next data point in the sequence (point B) lies immediately below the next higher range line. The line representing this strain range crosses only one range line, placing a half-

cycle count in the first bin (0 – 5 aɤ) according to the simplified rainflow counting algorithm.

If the magnitude of this strain range is examined, it is clear that this half-cycle will not be placed in the first bin. Its range is greater in magnitude than 5 aɤ, but lesser in magnitude than 10 aɤ. Therefore, the half-cycle count should be placed in the second bin, 5 – 10 aɤ.
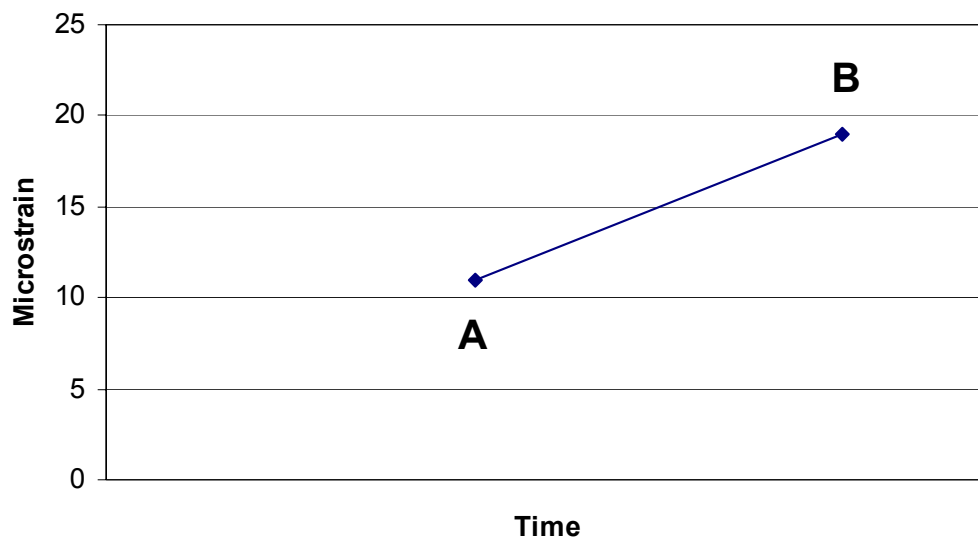
Figure 4.22: Sample Strain History

Though this scheme was computationally more efficient than that specified by ASTM E 1049-85, it did not produce the correct rainflow counts. Following a meeting with Invocon in May 2003, it was decided to revise the rainflow counting scheme to that described in the ASTM specification and reprogram the MicroSAFE devices.

118

As of July 2003, Invocon had corrected the rainflow counting algorithm and had run many successful computer simulations. All 11 MicroSAFE units were sent to Invocon on July 16, 2003 to have the new rainflow algorithms downloaded and add an algorithm for data correction due to temperature fluctuations during long-term rainflow acquisitions. The upgraded units are expected to be returned by August 1, 2003.

Final verification of the recoded MicroSAFE devices will commence following the return of the devices. No further problems are expected with this system.

Although over 200 data acquisition sequences were performed in the field and in the lab, only a fraction (less than 10%) were actually used in the analyses discussed in this chapter. As mentioned previously, many acquisition sequences conducted in the field were repeated almost identically. Programming variables, most notably the bin size, were changed between acquisition sequences to refine the output of the system.

CHAPTER 5

Conclusions and Recommendations

The goal of this research was to provide options for use by TxDOT to monitor the structural health of unique bridges. Two proprietary data acquisition systems were selected for testing and evaluation in satisfying these goals. The first system discussed was a global positioning system called *NetForce*. The second system discussed was an autonomous data acquisition system for strain called *MicroSAFE*.

5.1 CONCLUSIONS

Both technologies discussed in this thesis are viable for use by TxDOT. Each system is user-friendly, providing immediate return of meaningful engineering data with minimal effort on the part of TxDOT.

The MicroSAFE system can record raw strain data and compute rainflow counts for use in fatigue analysis of structural components. The system is compact, inexpensive, simple to use, and immediately generates meaningful engineering data that are easy to interpret. As areas of interest are identified during routine inspections, a single TxDOT inspector can install the system and program it to acquire rainflow data in a matter of minutes. When data acquisition is complete, rainflow data acquired over consecutive 24-hr periods show how the structural component is performing under service loads and the likelihood of fatigue damage can be immediately assessed. As a result, important questions regarding the condition of the structure can be answered in a very short period of time, and with a minimum of effort on the part of the engineer or inspector.

120

The NetForce system measures structural displacements over the long-term more accurately than the advertised sub-centimeter level. Once the system hardware is purchased from Mezure, it will be installed, monitored, and maintained by Mezure personnel. Both current and previous displacement data will be available at any time via a secure website. Large amplitude displacements will trigger preset alarms and alert TxDOT personnel.

5.2 CAVEATS

Based on the tests described in this thesis, the research team cautions that short-term GPS data may be unreliable due to daily fluctuations in the satellite coverage. Only displacement values averaged over time will generate stable and reliable information using a GPS-based system. As a result, data should be averaged for 24 or more hours before making any conclusions. This may limit the possible applications of the GPS-based system.

Also, when selecting a system that will be maintained and monitored by an outside firm for a long duration, the purchaser of the system must evaluate the financial stability of that firm before entering a long-term contract for services. The research team had been unable to contact Mezure for the last three months.

The use of preprogrammed data acquisition systems is appealing because the data are expressed in terms that can be included directly in engineering calculations. However, detailed evaluation of the algorithms is essential before adopting the systems.

5.3 FUTURE WORK

The monitoring technologies described in this thesis appear to meet the objectives established for structural health monitoring. Field testing will be implemented in the next stage of this project.

APPENDIX A

Variations of GPS Data with Time of Day

These plots pertain to the discussion found in Section 3.3.1(b). Figures A1 – A10 contain plots of GPS system accuracy versus the duration of averaging (Δt) used to compute the average values. Each plot represents a given week of observation (Week 1 through Week 5) for a given GPS Station (STA 1 or STA 2). Within each plot, eight data series are presented. Each data series corresponds to a different time of day (t_o) at which each set of average values was computed.
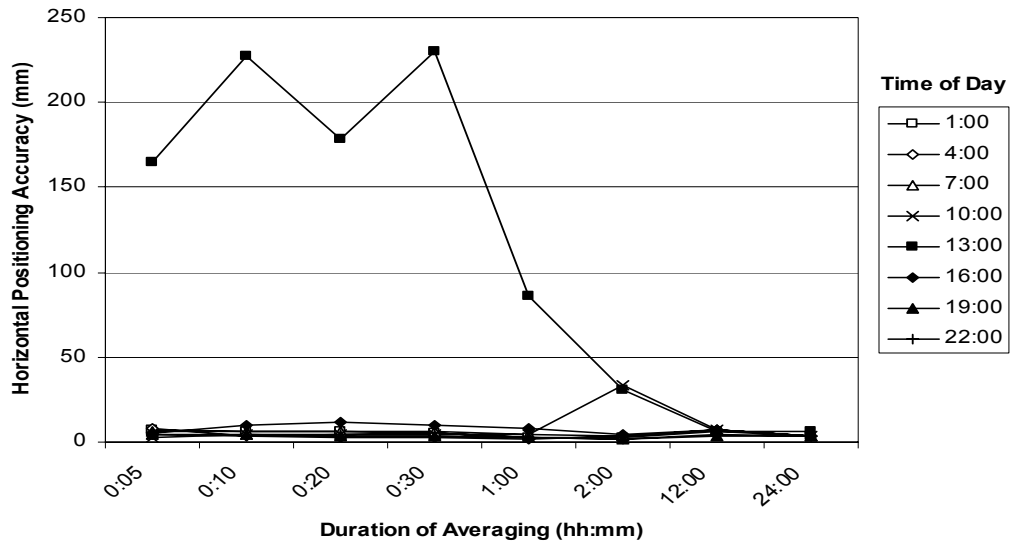
*Figure A1: Horizontal Positioning Accuracy as a Function of Time of Day,
STA 1, Week 1*
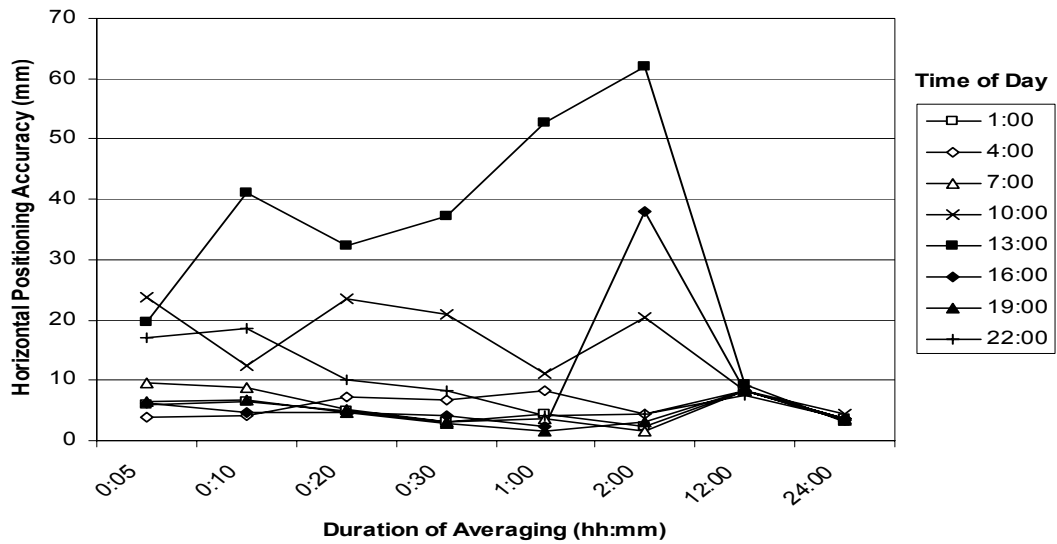
*Figure A2: Horizontal Positioning Accuracy as a Function of Time of Day,
STA 1, Week 2*

123
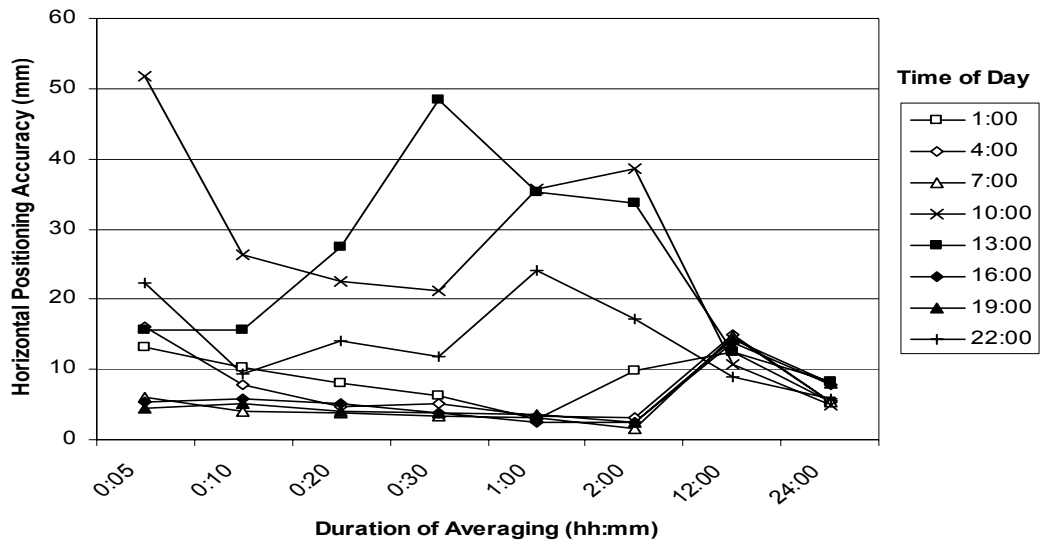
Figure A3: Horizontal Positioning Accuracy as a Function of Time of Day,

STA 1, Week 3
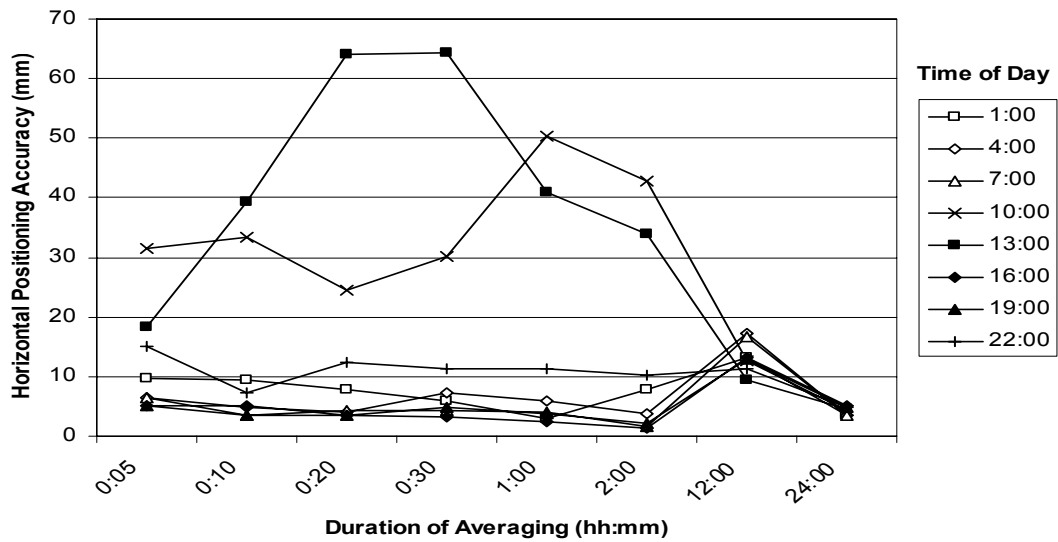
Figure A4: Horizontal Positioning Accuracy as a Function of Time of Day,

STA 1, Week 4

124
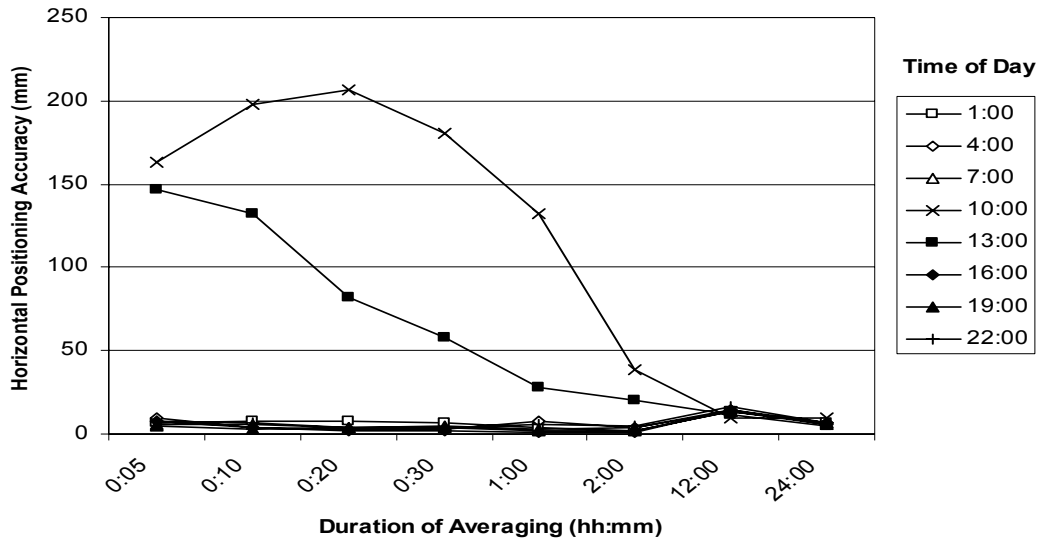
Figure A5: Horizontal Positioning Accuracy as a Function of Time of Day,

STA 1, Week 5
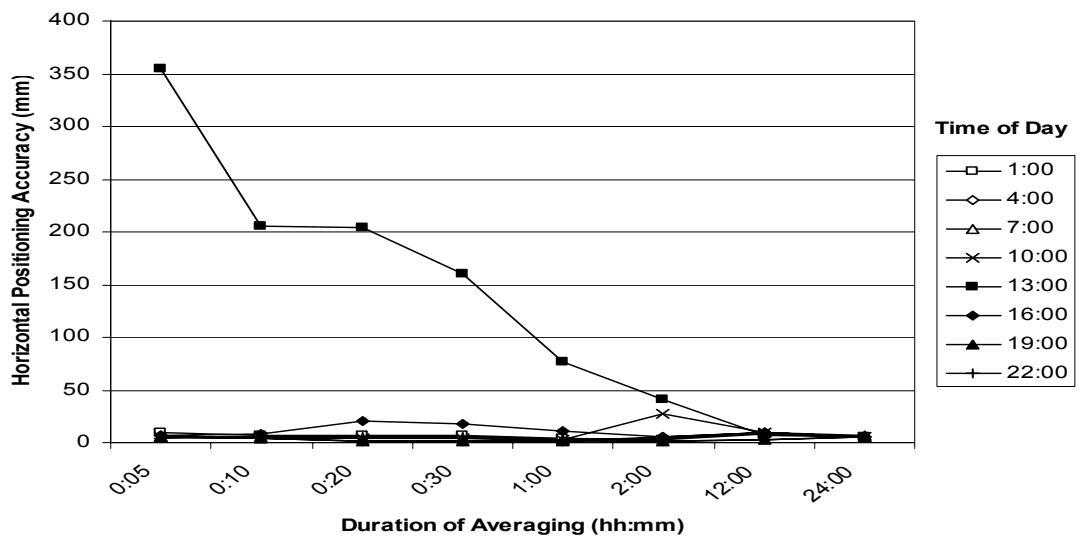
Figure A6: Horizontal Positioning Accuracy as a Function of Time of Day,

STA 2, Week 1

125
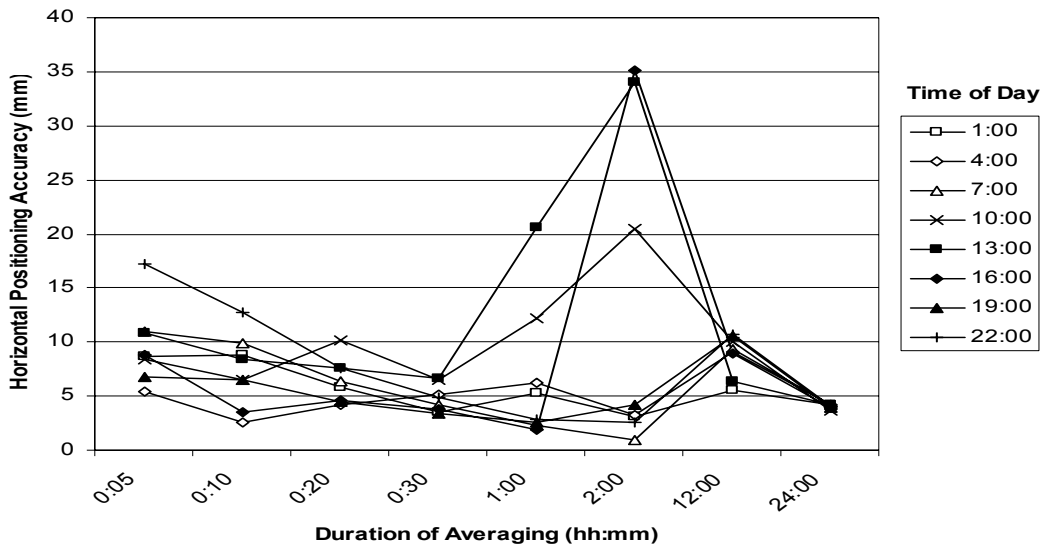
Figure A7: Horizontal Positioning Accuracy as a Function of Time of Day,

STA 2, Week 2
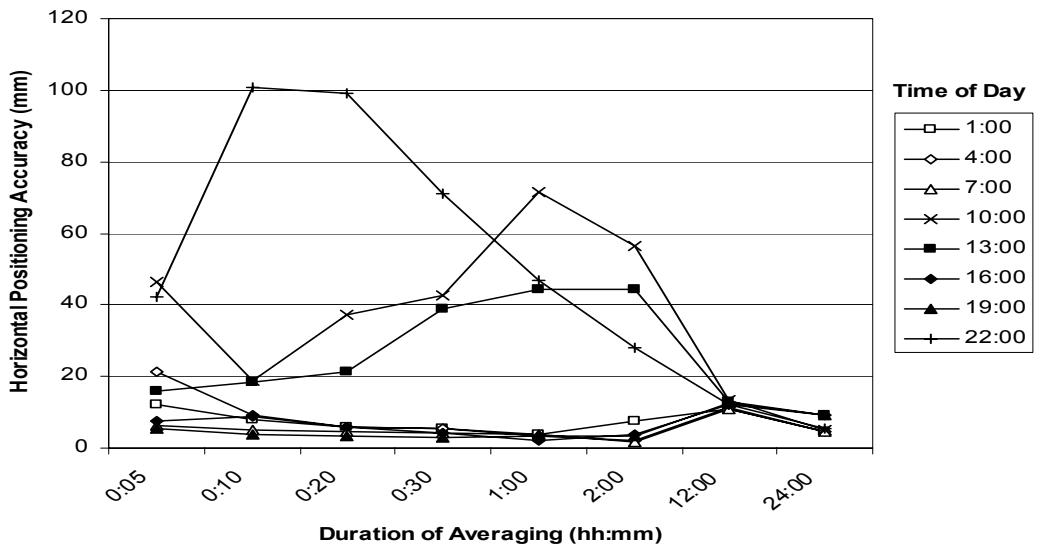
Figure A8: Horizontal Positioning Accuracy as a Function of Time of Day,

STA 2, Week 3
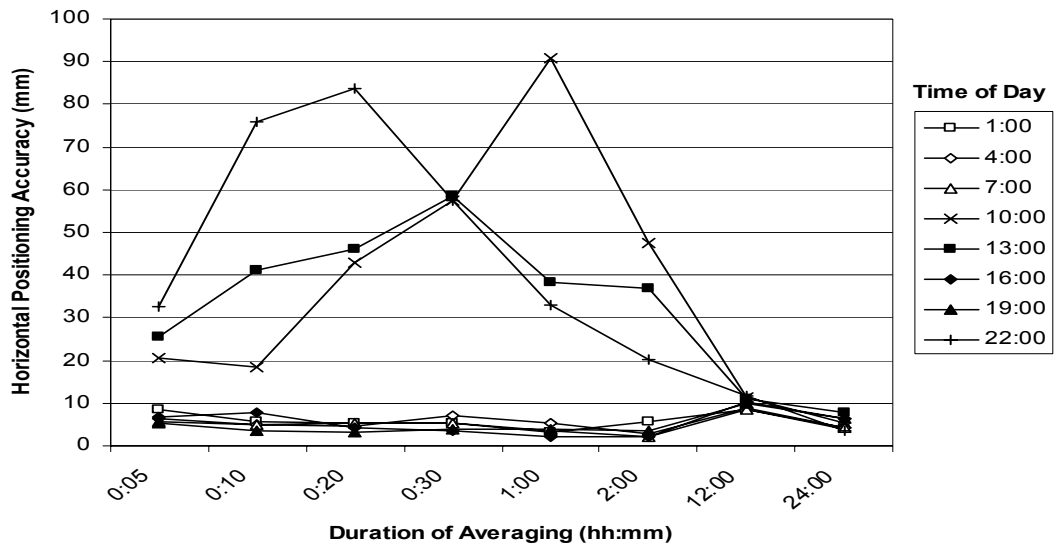
Figure A9: Horizontal Positioning Accuracy as a Function of Time of Day,

STA 2, Week 4
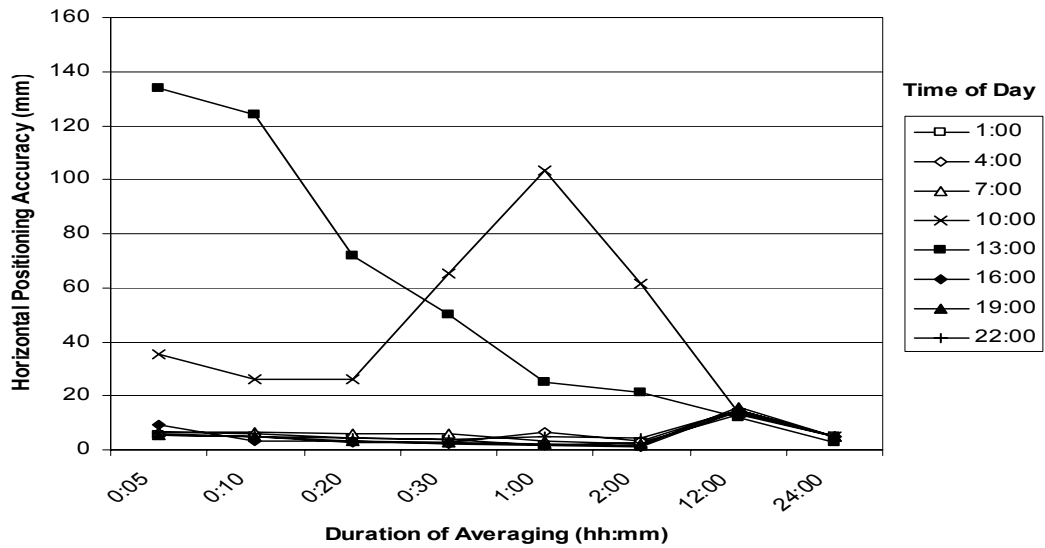
Figure A10: Horizontal Positioning Accuracy as a Function of Time of Day,

STA 2, Week 5

127

APPENDIX B

Weekly Averages of GPS Data

These plots pertain to the discussion found in Section 3.3.2(c). Figures B1 – B4 contain plots of GPS system accuracy versus the duration of averaging used to compute the average values. Each plot shows five sets of weekly averages for a given GPS Station (STA 1 or STA 2). Figures B1 and B2 show the recorded data sets, while Figures B3 and B4 show the same data sets, but with the averages taken about t_o = 13:00 (1 pm each day) removed from the analysis.
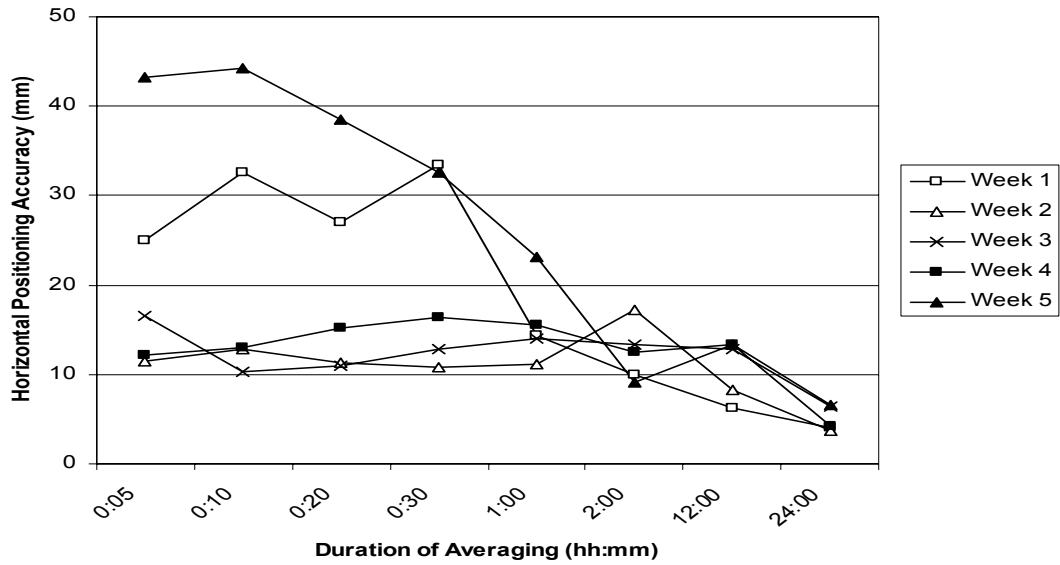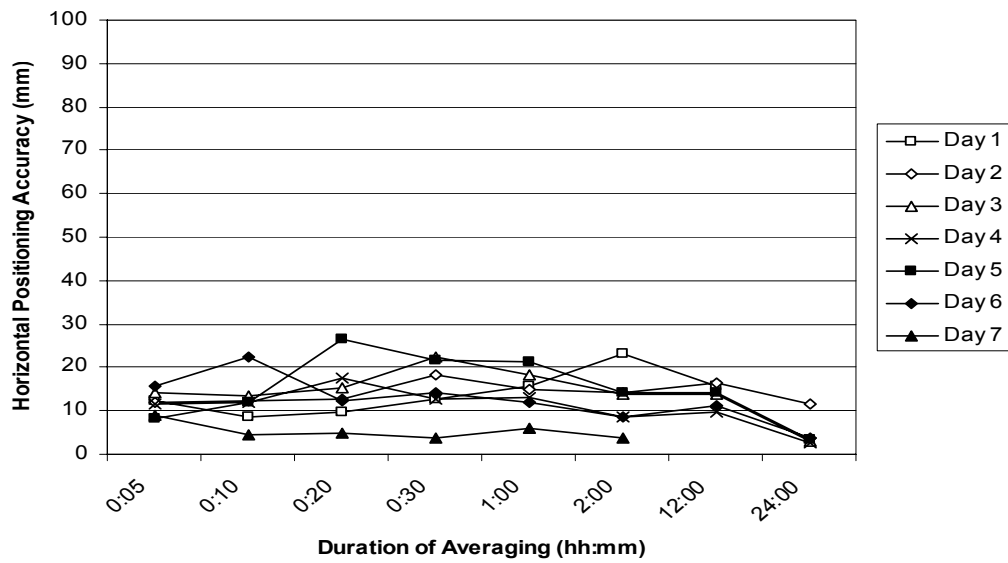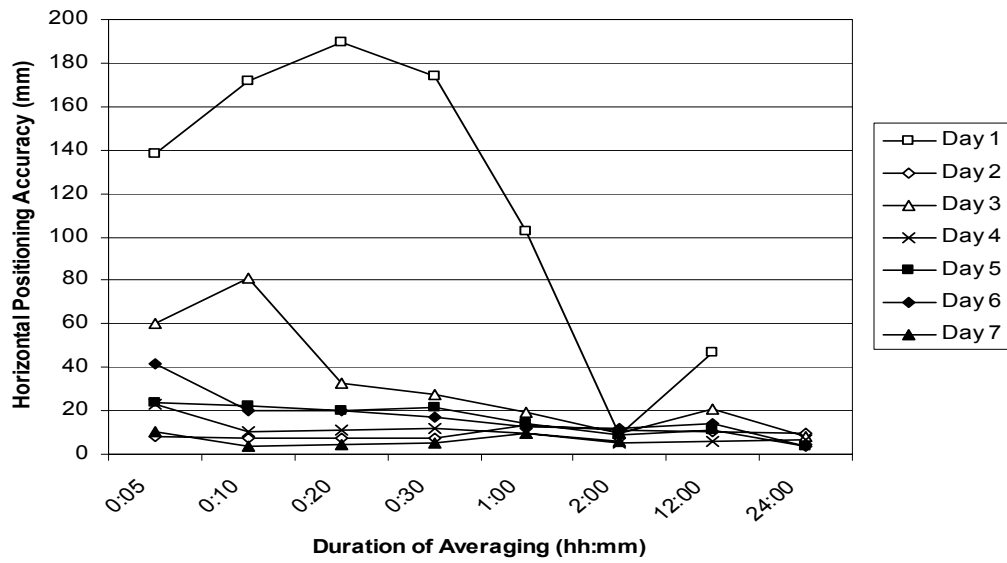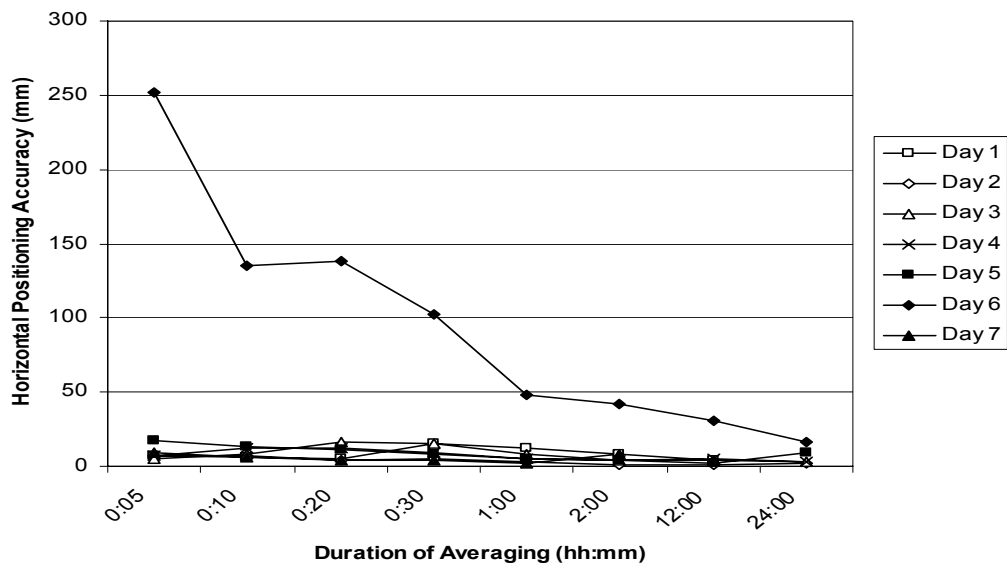
Figure B1: Weekly Averages of Horizontal Positioning Accuracy, STA 1
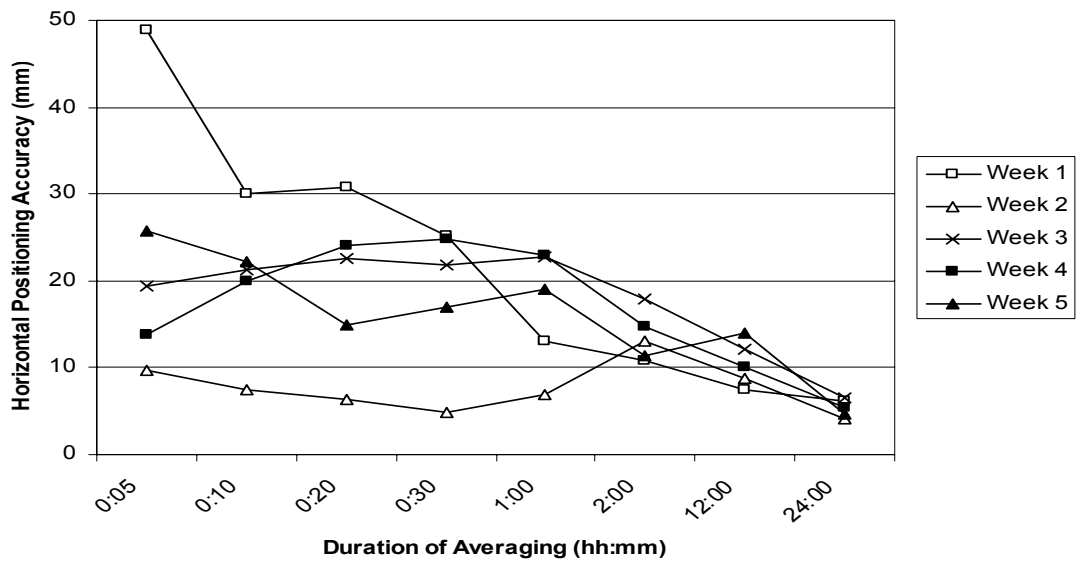
Figure B2: Weekly Averages of Horizontal Positioning Accuracy, STA 2

129
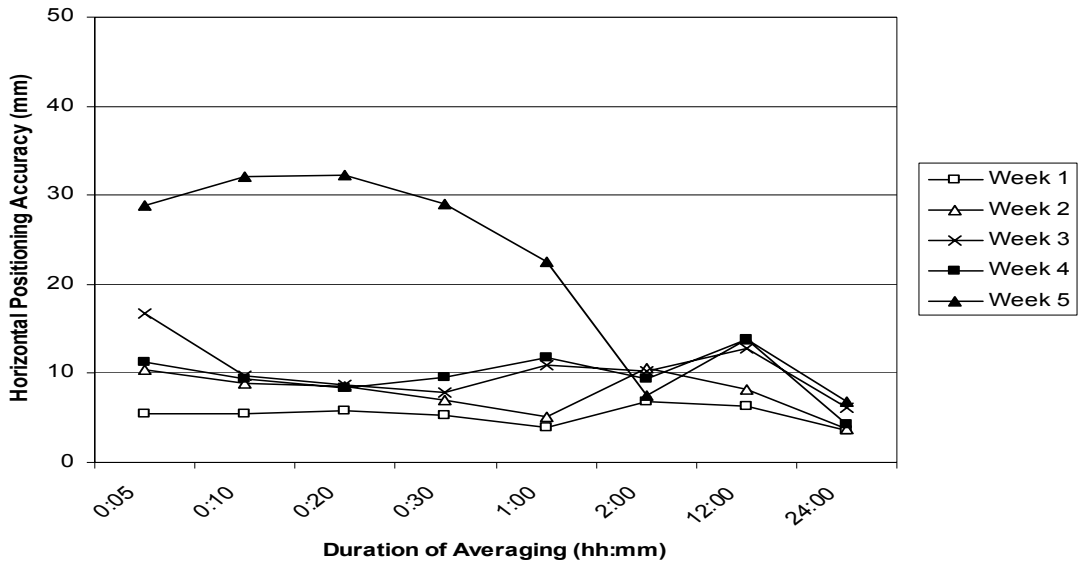
*Figure B3: Weekly Averages of Horizontal Positioning Accuracy
(13:00 averages removed), STA 1*
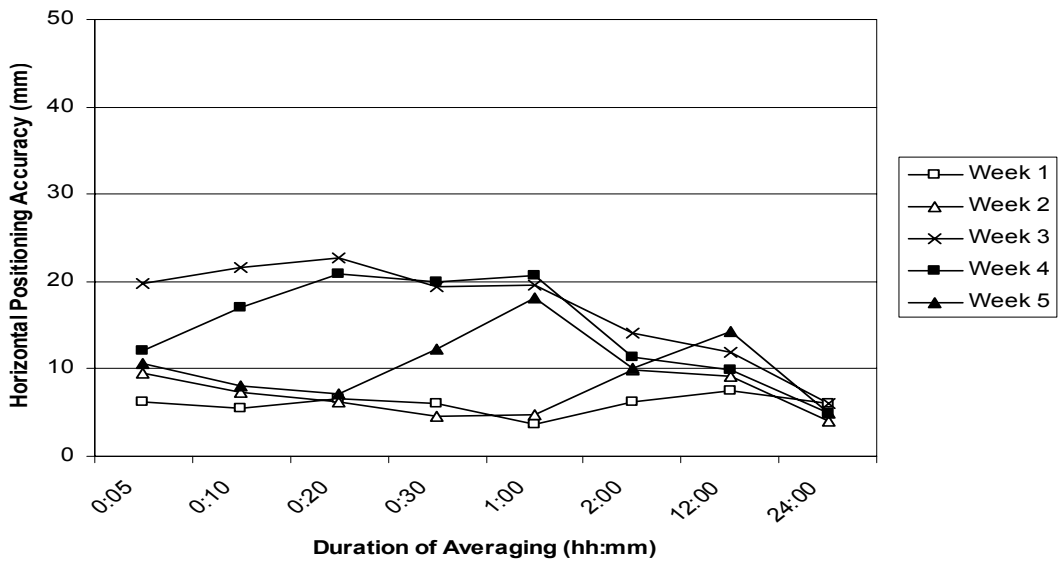
*Figure B4: Weekly Averages of Horizontal Positioning Accuracy
(13:00 averages removed), STA 2*

APPENDIX C

Daily Averages of GPS Data

These plots pertain to the discussion found in Section 3.3.1(d). Figures C1 – C10 contain plots of GPS system accuracy versus the duration of averaging used to compute the average values. Each plot represents a given week of observation (Week 1 through Week 5) for a given GPS Station (STA 1 or STA 2). Within each plot, seven data series are presented. Each data series corresponds to a day of the week for which each set of average values was computed.
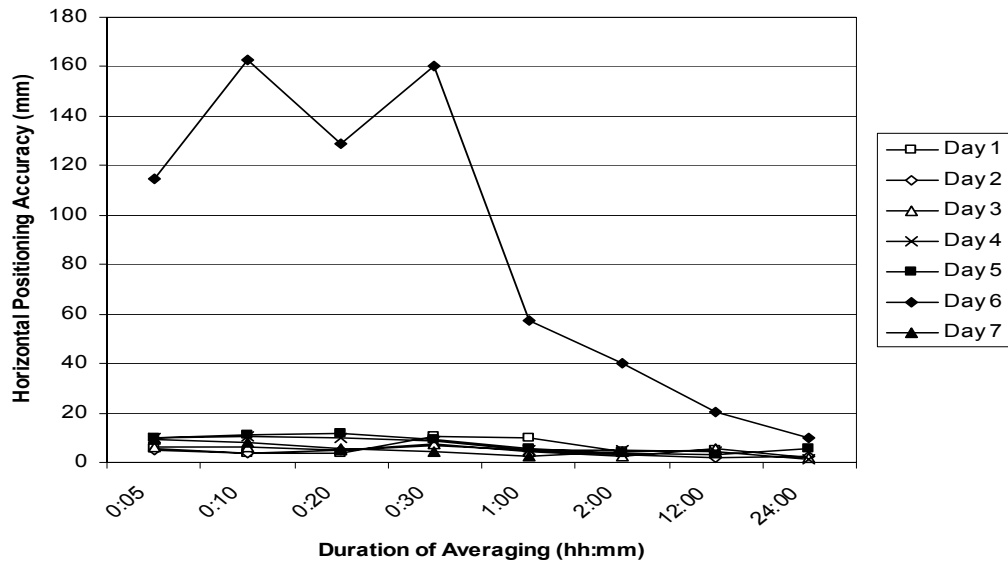
Figure C1: Daily Averages of Horizontal Positioning Accuracy, STA 1, Week 1
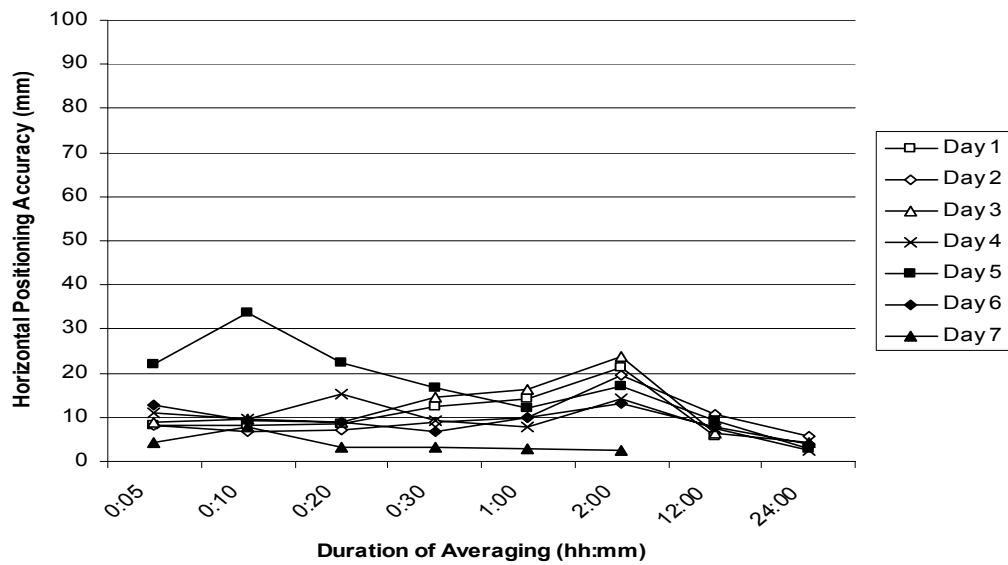
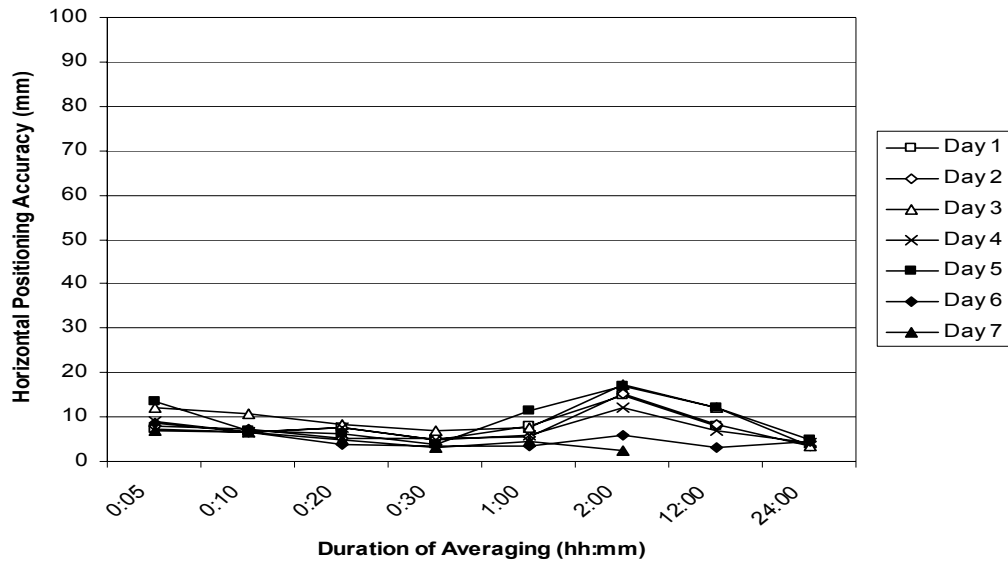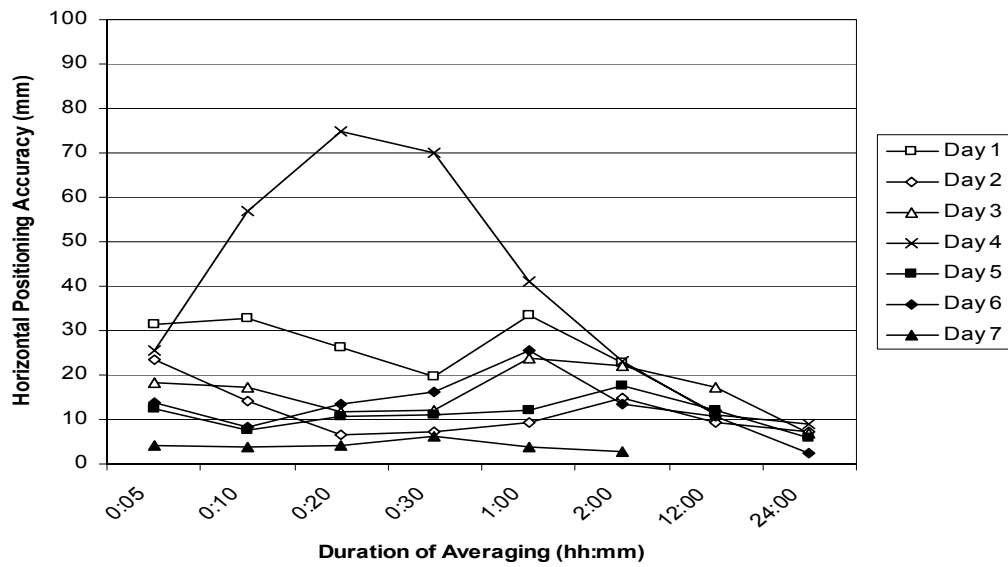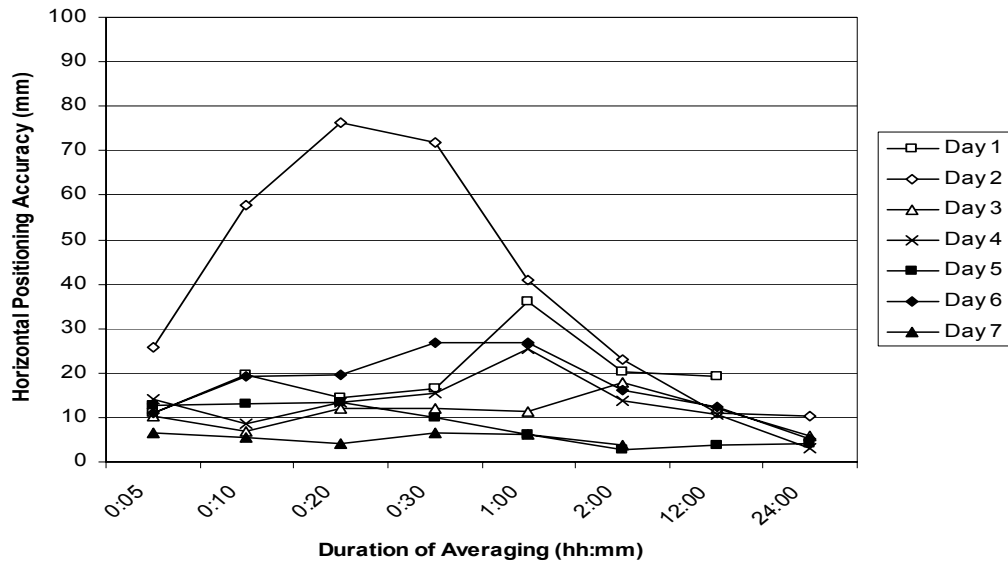*Figure C2: Daily Averages of Horizontal Positioning Accuracy, STA 1, Week 2*

132
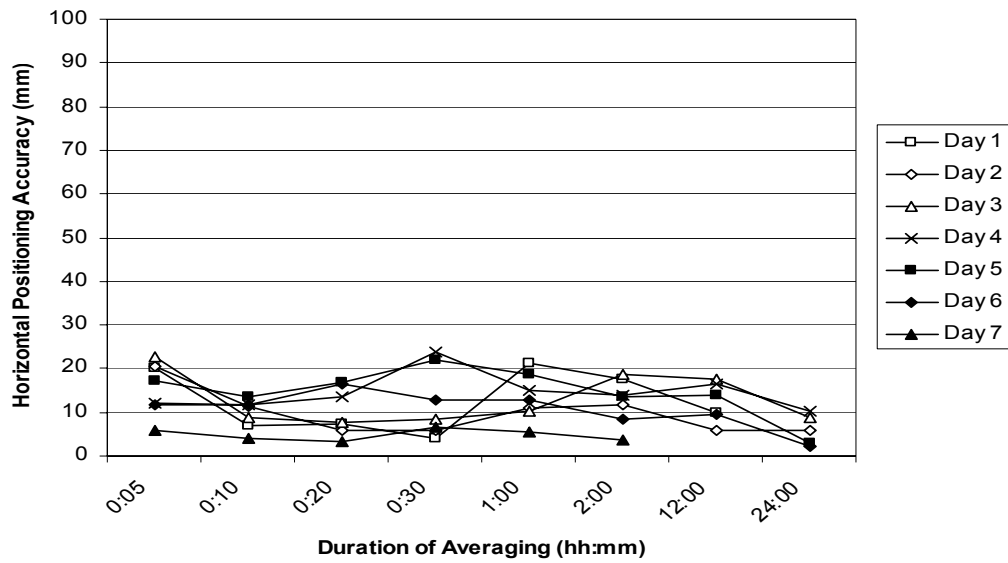
Figure C3: Daily Averages of Horizontal Positioning Accuracy, STA 1, Week 3

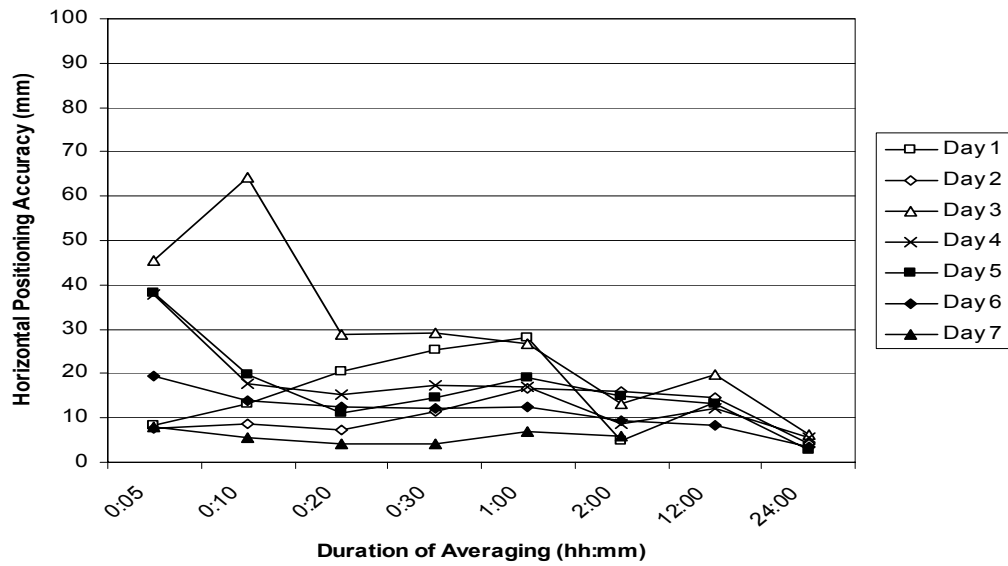*Figure C4: Daily Averages of Horizontal Positioning Accuracy, STA 1, Week 4*

Figure C5: Daily Averages of Horizontal Positioning Accuracy, STA 1, Week 5

Figure C6: Daily Averages of Horizontal Positioning Accuracy, STA 2, Week 1

Figure C7: Daily Averages of Horizontal Positioning Accuracy, STA 2, Week 2

Figure C8 Daily Averages of Horizontal Positioning Accuracy, STA 2, Week 3

135

Figure C9: Daily Averages of Horizontal Positioning Accuracy, STA 2, Week 4

Figure C10: Daily Averages of Horizontal Positioning Accuracy,
STA 2, Week 5

136

APPENDIX D
GPS Position Calculation

D.1   SAMPLE DATA SET

     Figure D1 contains a sample data set taken with Station 1 at its initial position.   Column A identifies the station ("41" = STA 1, "42" = STA 2). Column B identifies the current GPS week. This is the number of weeks elapsed since the declared beginning of GPS time on January 6, 1980. Column C is the number of seconds elapsed since the beginning of the given GPS week. Values in this column increment every 10 sec. This indicates that data are reported back from the GPS stations at a rate of one point for every 10 sec. This is the fastest rate at which NetForce can report data. Columns D and E are the reported latitude and longitude, respectively, of the GPS station. Units are in degrees. Column F is the reported height of the GPS station about mean sea level (MSL), given in meters. More significant figures are given in the actual data files than are shown here.

Figure D1: Sample Data File

D.2 DATA CONVERSION SPREADSHEET

Figure D2 contains a sample data conversion spreadsheet taken with Station 1 at its initial position. This spreadsheet format was used to convert the GPS positioning data from units of degrees of latitude and longitude into units of meters. Consistent units were required for three dimensions to calculate usable displacements of a GPS station.

The first column in Figure D2 lists total time in seconds from the beginning of the GPS week. This value is copied directly from the data files given by Mezure. Column B is the date of the recorded GPS position, calculated from the total time value (Column A). Column C is the time of day of the

138

recorded GPS position (hr:min:sec), calculated by Excel using the total time value (column A). Columns B and C allow easy reference of the date and time of each recorded GPS position.

Figure D2: Sample Calculation Spreadsheet

The data returned by Mezure (in Figure D1) are in the Latitude, Longitude, and Height (LLH) coordinate system. For this analysis, these values must be transformed into a reference frame with consistent units. The most common reference frame is the Earth Centered Earth Fixed (ECEF) coordinate system, employed by GPS users since 1987. This system takes the center of the Earth and places it at the origin of a set of three-dimensional axes. The shape of

139

the Earth is defined by the WGS-84 (World Geodetic System 1984) ellipsoid, a geocentric system defined by the coordinates of over 1,500 terrestrial sites (Hofmann-Wellenhoff et. al., 1997). In the ECEF coordinate system, each recorded GPS position is transformed into three distances, one along each principal axis. These distance values locate each GPS position on the Earth's surface relative to the center of the WGS-84 ellipsoid.

To begin the coordinate transform, n is calculated for each GPS position using Equation D.1. n is a constant that is dependent on the longitude value for each recorded position and is the primary value used to transform LLH coordinates to ECEF coordinates. RE is the equatorial radius of the Earth (semi-major axis) according to the WGS-84 ellipsoid. $RE = 6,378,137$ m. b is the length of the semi-minor axis of the WGS-84 ellipsoid. $b = 6,356,752.314$ m. Y_{LLH} is the longitude value of each recorded GPS position, given in the Mezure data files, converted to units of radians.

$$n = \frac{RE^2}{\sqrt{RE^2 \cos Y_{LLH} + b^2 \sin Y_{LLH}}} \tag{D.1}$$

Equations D.2 – D.4 are used in conjunction with Equation D.1 to calculate the absolute X, Y, and Z values in the ECEF coordinate system. X_{LLH}, Y_{LLH}, and Z_{LLH} are the longitude, latitude, and height (above MSL) values given in the Mezure data files (Angus 2002).

$$X_{ECEF} = (n + Z_{LLH}) \cos Y_{LLH} \cos X_{LLH} \tag{D.2}$$

$$Y_{ECEF} = (n + Z_{LLH}) \cos Y_{LLH} \sin X_{LLH} \tag{D.3}$$

$$Z_{ECEF} = \left[\frac{b^2}{RE^2} n + Z_{LLH} \right] \sin Y_{LLH} \tag{D.4}$$

D.3 POSITION AVERAGE CALCULATION SPREADSHEET

Figure D3 contains a sample spreadsheet used for calculating the position average values discussed in Chapter 3. As noted in Section 3.1.3, five minutes of data both before and after (t_b = 5 min) the recorded time of displacement (t_o) were blocked out of the analysis. Three columns of data (X_{ECEF}, Y_{ECEF}, and Z_{ECEF}) were averaged over the appropriate durations both before and after the block out times. These averaged values were then subtracted from each other to obtain the displacement of the station in three principal directions. Finally, the three-dimensional distance formula ($X_{ECEF}^2 + Y_{ECEF}^2 + Z_{ECEF}^2 = \Delta GPS^2$) was employed to obtain the displacement of the GPS station (ΔGPS), given in bold numbers in the last column (in units of millimeters).

In this analysis, operating within the ECEF coordinate system and using the three-dimensional distance formula, ΔGPS values are used to find the straight-line displacement between two points. Because each transformed GPS position is located relative to the fixed center of the Earth, it is possible to resolve straight-line displacements into East/West and North/South components. Although the MezureNet website contained plots of East/West and North/South displacements versus time, Mezure was unable to produce the formulas that were used to obtain these values. Because the exact component displacement values could not be reproduced, displacement sequences were structured such that individual displacements within each sequence would contain only one direction of movement at a time. Each displacement would therefore be easily calculated as a

straight-line displacement. Figure D3 shows eight such calculations as discussed above, one calculation for each averaging duration. Calculated straight-line displacements are given in bold on the right of the calculation sheet, while averaging durations are given in bold type on the left.

Figure D3: Sample Average Calculation Spreadsheet

APPENDIX E

GPS Data from Dynamic Tests

E.1 DYNAMIC TEST RESULTS – STATION 1

Tables E1 – E7 contain the results of the seven dynamic tests performed on Station 1. These figures pertain to the discussion found in Section 3.3.3.

Table E1: Averaged GPS Displacements, Dynamic Test 4, STA 1 (mm)

Actual Displacements (mm)		Averaging Durations							
N+/S-	W+/E-	5 min	10 min	20 min	30 min	1 hr	2 hr	12 hr	24 hr
0	+20	10.0	12.7	14.9	16.7	18.1	19.6	27.9	25.7
0	+10	1.9	8.4	9.0	9.5	9.5	10.1	14.4	16.4
0	+5	7.7	11.4	7.7	5.2	5.1	5.5	5.1	5.0
0	+4	8.4	6.4	5.7	5.3	5.6	5.7	5.9	2.7
0	+3	7.6	5.2	3.8	2.6	3.0	3.4	8.4	3.9
0	+2	4.9	8.8	5.8	1.7	1.2	3.2	5.1	9.3
0	+1	4.6	5.7	1.6	3.2	2.3	2.0	2.1	4.9

Table E2: Averaged GPS Displacements, Dynamic Test 5, STA 1 (mm)

Actual Displacements (mm)		Averaging Durations							
N+/S-	W+/E-	1 min	2 min	3 min	4 min	5 min	10 min	20 min	30 min
0	+10	9.5	12.6	10.7	10.1	10.7	9.5	9.8	9.6
0	+10	8.0	5.8	9.2	11.6	14.4	13.7	10.1	11.3
0	+10	10.8	10.4	8.6	8.2	7.7	8.6	7.8	10.3
0	+10	13.1	12.9	12.6	12.8	12.8	11.8	11.6	12.1
0	+10	9.0	9.1	8.6	8.3	8.3	9.4	10.1	10.3
0	+10	9.2	11.6	12.7	13.3	13.5	14.8	17.2	15.2
0	+10	9.0	10.9	11.9	13.1	13.4	14.6	14.8	13.0
0	+10	7.4	9.6	9.1	9.6	9.6	10.2	10.4	10.4
	Average	**9.5**	**10.4**	**10.4**	**10.9**	**11.3**	**11.6**	**11.5**	**11.5**

Table E3: Averaged GPS Displacements, Dynamic Test 6, STA 1 (mm)

Actual Displacements (mm)		Averaging Durations				
N+/S-	W+/E-	5 min	10 min	20 min	30 min	1 hr
0	+10	10.7	13.5	10.7	11.5	11.9
+10	0	9.0	9.8	9.5	9.3	7.2
0	+10	8.5	8.5	12.6	13.3	14.4
+10	0	9.9	9.0	12.6	17.1	13.5
	Average	**9.5**	**10.2**	**11.4**	**12.8**	**11.8**

Table E4: Averaged GPS Displacements, Dynamic Test 7, STA 1 (mm)

Actual Displacements (mm)		Averaging Durations					
N+/S-	W+/E-	5 min	10 min	20 min	30 min	1 hr	2 hr
0	-20	17.8	17.6	16.6	17.6	19.2	21.3
0	-20	15.0	18.1	18.7	20.1	18.9	21.7
0	-20	22.7	22.5	22.8	20.1	19.7	20.0
0	-20	17.4	18.4	21.0	19.6	20.6	21.2
	Average	**18.2**	**19.2**	**19.8**	**19.4**	**19.6**	**21.0**

Table E5: Averaged GPS Displacements, Dynamic Test 8, STA 1 (mm)

Actual Displacements (mm)		Averaging Durations			
N+/S-	W+/E-	5 min	10 min	20 min	30 min
+20	0	19.9	18.4	21.7	19.0
0	-20	19.2	17.5	17.9	19.5
-20	0	19.1	20.1	22.1	22.1
0	+20	20.2	21.6	21.0	20.3
	Average	**19.6**	**19.4**	**20.7**	**20.2**
	Closing Values	9.2	9.4	12.2	13.3

Table E6: Averaged GPS Displacements, Dynamic Test 9, STA 1 (mm)

Actual Displacements (mm)		Averaging Durations				
N+/S-	W+/E-	5 min	10 min	20 min	30 min	1 hr
+40	0	39.8	37.0	36.8	37.9	39.4
0	-40	36.2	41.1	41.8	41.2	39.8
-40	0	34.0	41.8	42.0	42.6	41.0
0	+40	39.6	42.3	42.2	40.6	41.1
	Average	**37.4**	**40.5**	**40.7**	**40.6**	**40.3**
	Closing Values	3.4	2.6	4.8	1.5	0.6

Table E7: Averaged GPS Displacements, Dynamic Test 10, STA 1 (mm)

Actual Displacements (mm)		Averaging Durations									
N+/S-	W+/E-	1 min	2 min	3 min	4 min	5 min	10 min	20 min	30 min	1 hr	2 hr
+40	0	36.3	38.6	39.4	40.1	41.0	42.5	39.4	40.8	41.0	41.3
0	-40	37.6	38.7	39.7	39.8	38.9	38.3	41.0	41.8	39.6	40.7
-40	0	40.5	42.0	42.7	43.3	43.4	42.1	41.3	42.6	42.2	40.2
0	+40	40.5	41.3	41.1	41.9	42.2	41.0	39.8	40.5	40.2	40.6
	Average	**38.7**	**40.2**	**40.7**	**41.2**	**41.4**	**40.9**	**40.4**	**41.4**	**40.7**	**40.7**
	Closing Values	9.1	8.4	8.9	9.8	9.5	8.8	5.2	3.9	0.8	2.8

E.2 DYNAMIC TEST RESULTS – STATION 2

Tables E8 – E14 contain the results of the seven dynamic tests performed on Station 2. These figures pertain to the discussion found in Section 3.3.1.

Table E8: Averaged GPS Displacements, Dynamic Test 4, STA 2 (mm)

Actual Displacements (mm)		Averaging Durations							
N+/S-	W+/E-	5 min	10 min	20 min	30 min	1 hr	2 hr	12 hr	24 hr
0	+20	7.7	19.0	17.0	18.0	18.6	19.5	21.4	23.2
0	+10	4.6	11.3	11.0	9.9	9.9	10.4	14.1	13.6
0	+5	7.9	12.9	9.1	7.3	5.0	5.5	13.6	6.1
0	+4	8.9	5.8	5.4	4.1	5.4	5.0	9.9	4.4
0	+3	11.6	4.8	4.6	3.6	2.2	3.0	11.6	6.8
0	+2	4.3	7.9	6.2	2.6	1.5	2.5	5.6	1.8
0	+1	6.1	5.4	2.5	1.2	2.7	1.2	4.1	6.9

Table E9: Averaged GPS Displacements, Dynamic Test 5, STA 2 (mm)

Actual Displacements (mm)		Averaging Durations							
N+/S-	W+/E-	1 min	2 min	3 min	4 min	5 min	10 min	20 min	30 min
0	+10	6.8	7.6	8.9	11.6	12.8	11.1	10.6	12.3
0	+10	5.9	9.9	9.9	10.0	10.0	12.1	16.1	13.9
0	+10	9.7	11.4	10.3	10.2	10.0	9.7	7.5	9.1
0	+10	11.4	11.7	12.4	12.4	12.5	13.2	13.1	13.8
0	+10	10.7	9.9	9.0	8.3	8.0	9.0	11.3	12.6
0	+10	10.0	10.6	12.0	12.9	13.9	13.6	16.1	13.8
0	+10	11.2	11.7	12.7	13.3	13.7	14.1	16.2	13.8
0	+10	11.5	13.3	15.2	16.1	15.1	7.7	10.1	9.9
	Average	**9.7**	**10.8**	**11.3**	**11.8**	**12.0**	**11.3**	**12.6**	**12.4**

Table E10: Averaged GPS Displacements, Dynamic Test 6, STA 2 (mm)

Actual Displacements (mm)		Averaging Durations				
N+/S-	W+/E-	5 min	10 min	20 min	30 min	1 hr
0	+10	12.8	10.4	9.7	11.7	9.3
+10	0	10.9	8.9	9.0	10.4	12.6
0	+10	7.9	9.3	12.3	12.9	12.0
+10	0	14.3	10.7	13.7	13.8	11.0
	Average	**11.5**	**9.8**	**11.2**	**12.2**	**11.2**

Table E11: Averaged GPS Displacements, Dynamic Test 7, STA 2 (mm)

Actual Displacements (mm)		Averaging Durations					
N+/S-	W+/E-	5 min	10 min	20 min	30 min	1 hr	2 hr
0	-20	19.4	17.6	17.4	18.1	20.0	21.6
0	-20	12.7	14.7	19.9	21.4	18.6	22.2
0	-20	18.6	21.1	22.8	22.8	19.8	19.8
0	-20	20.5	19.5	22.3	22.3	22.2	21.2
	Average	**17.8**	**18.2**	**20.6**	**20.6**	**20.2**	**21.2**

Table E12: Averaged GPS Displacements, Dynamic Test 8, STA 2 (mm)

Actual Displacements (mm)		Averaging Durations			
N+/S-	W+/E-	5 min	10 min	20 min	30 min
+20	0	20.1	21.6	20.9	21.9
0	-20	18.7	17.7	17.7	18.6
-20	0	19.1	18.8	18.7	18.7
0	+20	20.0	21.9	21.9	20.8
	Average	**19.5**	**20.0**	**19.8**	**19.8**
	Closing Values	2.7	3.8	5.6	9.2

Table E13: Averaged GPS Displacements, Dynamic Test 9, STA 2 (mm)

Actual Displacements (mm)		Averaging Durations				
N+/S-	W+/E-	5 min	10 min	20 min	30 min	1 hr
+40	0	40.1	39.1	39.5	39.4	39.2
0	-40	37.1	40.3	41.0	41.4	40.4
-40	0	36.3	35.1	34.9	34.8	37.0
0	+40	39.2	44.1	41.8	40.7	41.7
	Average	**38.2**	**39.6**	**39.3**	**39.1**	**39.6**
	Closing Values	1.9	0.8	3.3	1.3	0.9

Table E14: Averaged GPS Displacements, Dynamic Test 10, STA 2 (mm)

Actual Displacements (mm)		Averaging Durations									
N+/S-	W+/E-	1 min	2 min	3 min	4 min	5 min	10 min	20 min	30 min	1 hr	2 hr
+40	0	38.0	38.0	37.1	36.4	35.9	35.6	39.2	38.8	39.0	39.0
0	-40	39.2	38.1	38.5	39.4	40.0	40.0	40.2	40.4	38.4	40.2
-40	0	37.7	37.4	37.6	37.6	37.9	39.8	38.5	36.8	36.1	37.7
0	+40	39.9	40.2	40.6	40.0	39.9	38.9	39.6	42.2	41.5	41.0
	Average	**38.7**	**38.4**	**38.4**	**38.4**	**38.4**	**38.6**	**39.4**	**39.6**	**38.8**	**39.5**
Closing Values		13.0	12.2	11.6	11.0	10.7	9.2	6.9	3.4	2.3	3.2

APPENDIX F

Additional MicroSAFE Information

F.1 SYSTEM UPDATES

This section discusses updates made to the MicroSAFE system. These updates include the Graphical User Interface (GUI) and the battery. Costs, applications, and advantages to the MicroSAFE system will also be presented.

F.1.1 Current GUI

Although the GUI has undergone many small changes over the last 2 years, the overall form and function have remained the same. Figure F1 shows the *Inquire* screen of the current GUI. Once a unit is connected to the computer, a user will press the *Inquire* button to verify connection to the unit and begin communication. The GUI will report back the serial number of the MicroSAFE unit along with system parameters pertaining to the last acquisition stored on the device. The user has the option to *Download* this acquisition data and save them to the computer or *Program* the unit for another acquisition, thereby deleting all data stored on the unit.

To program the unit for data acquisition, the user will press the *Program* button. A small dialogue box will open, giving the user the option of loading a previous configuration file (used for programming many MicroSAFE devices to perform identical acquisitions) or starting with a new programming configuration. Once this selection is made, three screens will then appear, one after the other, allowing the user to select the type of data acquisition (raw data, rainflow data, or both), select the acquisition mode (scheduled or event-detection), select the data

151

rate (8, 16, or 32 Hz), input the bin size, and input the amount of time that MicroSAFE will use to record strains that will zero the strain gage before each acquisition.
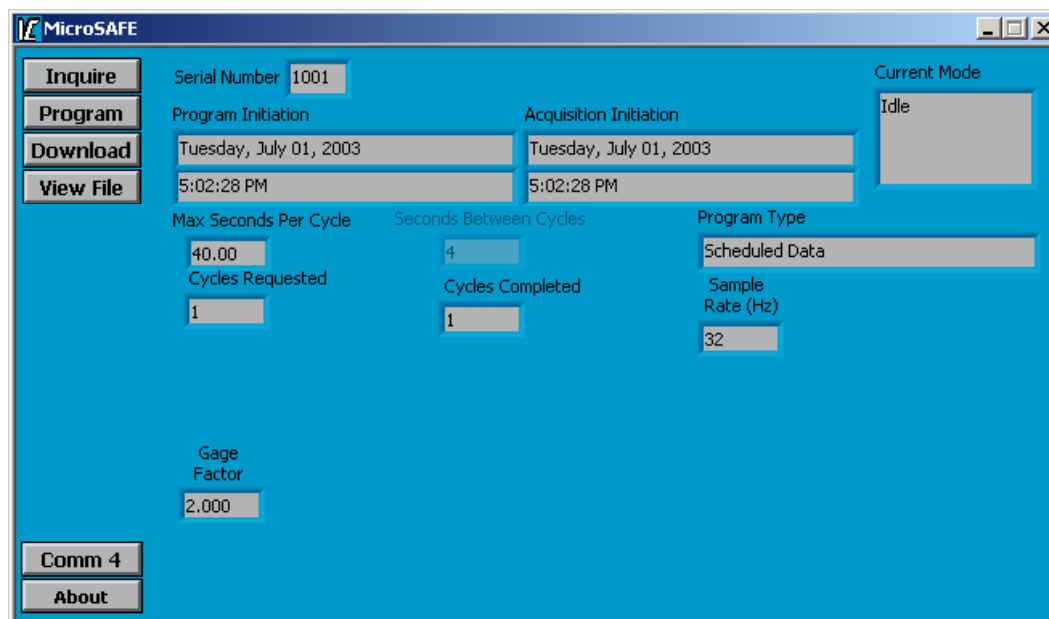
Figure F1: MicroSAFE Inquire Screen

Figure F2 shows the MicroSAFE Program Setup screen, where the user will then select the start time of the acquisition, seconds of sleep between acquisitions (a minimum value is specified by the GUI), maximum seconds of acquisition per cycle (2047 seconds is the maximum value allowed by the current GUI), and the requested number of acquisition cycles before termination. Once these values are specified, the GUI gives the percentage of memory used for this program setup. If there is not enough memory to perform the requested acquisitions, the *percentage of memory used* box will blink red. Programming

cannot continue until one or more of the values are changed to lower the memory usage below 100%. The time plot at the bottom of the screen will update as values are altered to give the user a timeline representation of the acquisition sequence(s) requested.
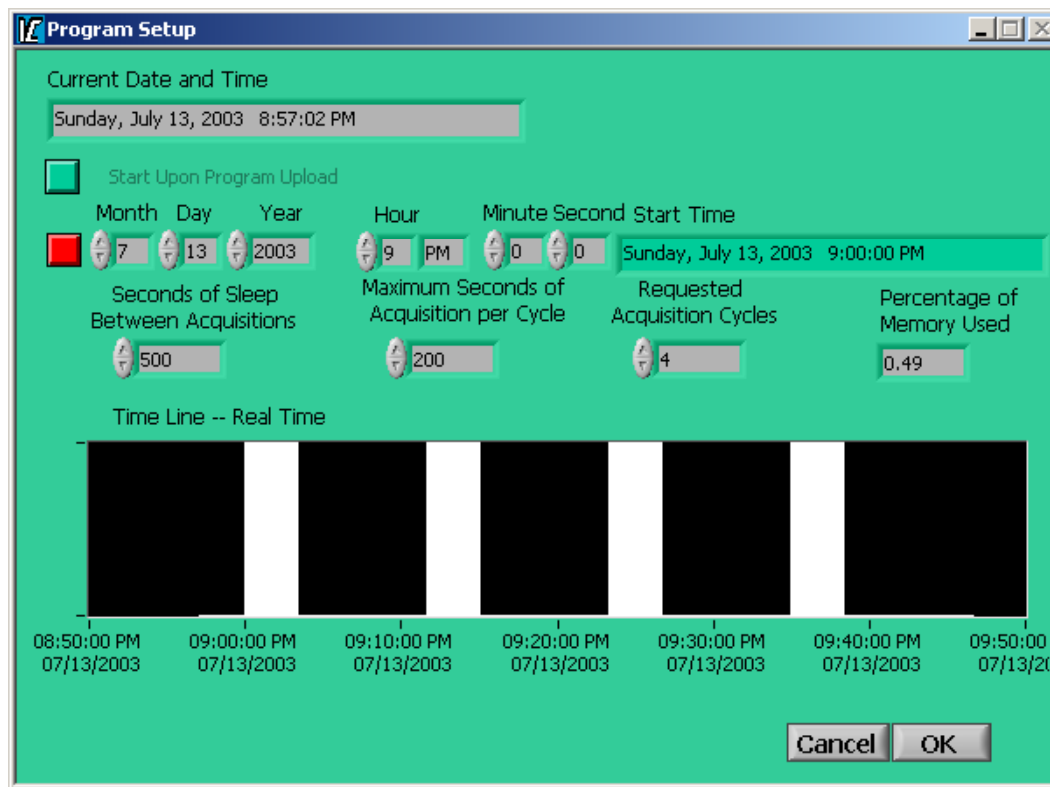
Figure F2: MicroSAFE Program Setup Screen

Section F.1.2 discusses the new GUI and changes to a few of these input parameters. Even considering these changes, programming of the MicroSAFE units will be conducted in a manner similar to that mentioned above.

From the home screen (not shown) and the *Inquire* screen, the user also has the option to *View File*. This will open another window where any MicroSAFE data file, stored on the computer as a *.MSD file, can be viewed graphically. If raw strain data are contained within the file, they can be viewed by pressing the *Graph Data* button. Various zooming options are available to navigate the plot of strain versus time, shown in Figure F3. If rainflow data are contained within the file, the frequency plot of cycle counts versus bin size can be viewed by pressing the *Graph Rain* button, as shown in Figure F4.
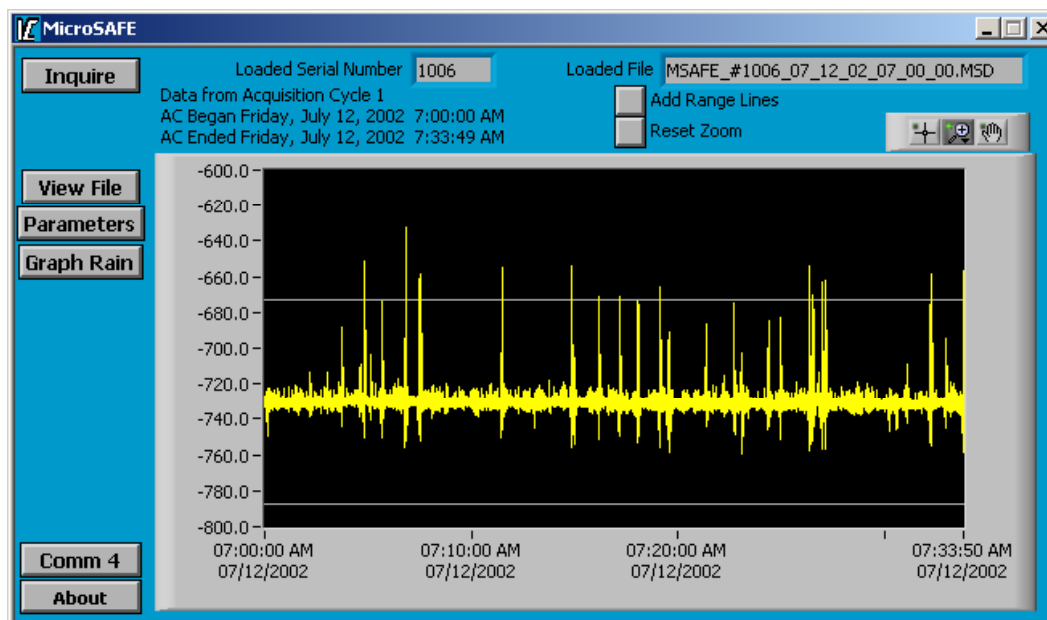
Figure F3: MicroSAFE Strain Plot
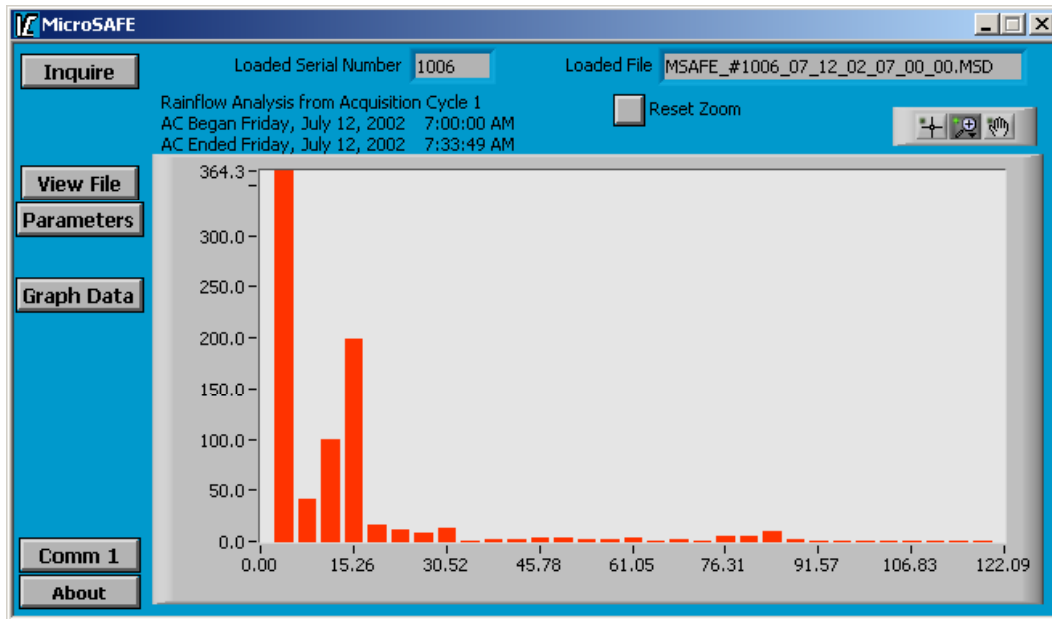
Figure F4: MicroSAFE Rainflow Plot

F.1.2   New GUI

A new GUI will accompany the reprogrammed units, scheduled for delivery in August 2003. Through exhaustive testing of the MicroSAFE devices in both the laboratory and in the field, the requirements of the MicroSAFE system were narrowed further and better defined for creation of the new GUI. The explicit needs and the corresponding changes to the GUI will be covered in this section.

The first change to the GUI was the elimination of multiple sampling rates. All data will be taken at 32 Hz in the new version of the GUI. This change was decided based on the excitation frequencies of structures that would most likely be examined by TxDOT using the MicroSAFE system. According to the Nyquist Theorem, the sampling rate must be twice the rate of the highest frequency component of the signal to be able to reproduce that signal frequency.

155

This theorem only guarantees the capture of the signal frequency, and not necessarily the peaks and valleys of the signal itself. To effectively capture these peaks and valleys in a dynamic test, as would be the case on a bridge, the sample rate should be at least 10 times higher than the sampling frequency (Frank, 2003). The effects of data aliasing are depicted in Figure F5. The upper figure shows a sine wave that is sampled adequately, while the lower figure shows the same sine wave that would be aliased, or misrepresented, due to the lower sampling rate. Because some bridge structures can vibrate or be excited at up to 3 Hz, 32 Hz was selected as the frequency for all data sampling using the MicroSAFE system.
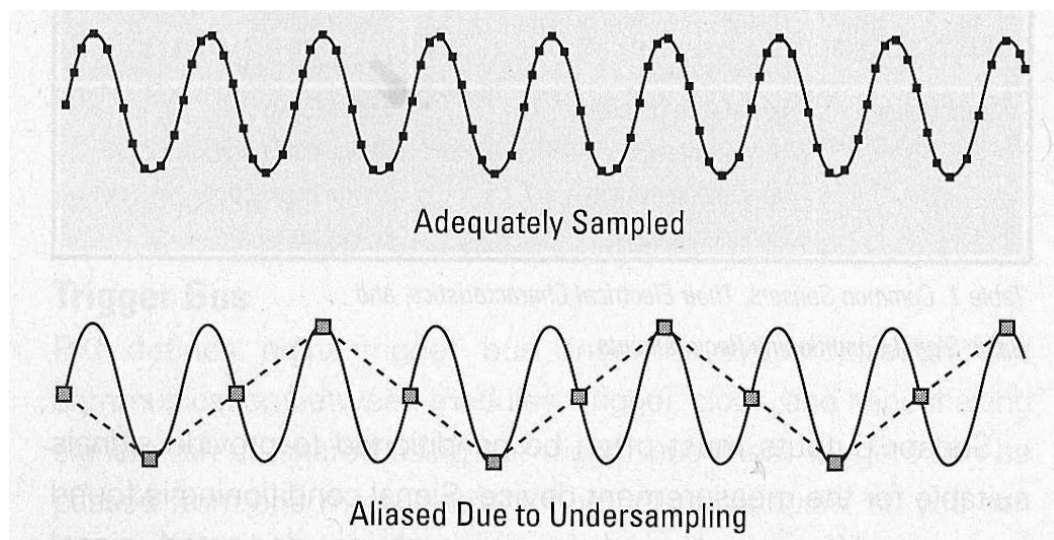

Figure F5: Data Aliasing (National Instruments, 2003)

Raw data storage capabilities will be removed from the MicroSAFE devices when the new GUI is released. Additional random access memory (RAM) is needed for the new rainflow algorithm because of its increased computational requirements. To keep the devices small in size and inexpensive in

156

price, there is a finite amount of memory available in each MicroSAFE device. Memory previously allocated for raw data storage will now be allocated for processor use during rainflow calculation.

The ability for real-time transfer of raw data to the personal computer will be added to the new GUI. This will allow raw data to be logged and stored on a personal computer (PC). These acquisitions will be limited in time because the unit will be connected to a PC for the duration of acquisition. Users will most likely use this function before beginning rainflow acquisition on a new site, to get an idea of actual strains experienced before setting the bin sizes for the rainflow acquisition.

Maximum acquisition time for each cycle will be extended to 24 hours. This will involve 23 hours and 59 minutes for rainflow acquisition. One minute will be allowed for sleep between cycles (if more than one is requested), unit power-on and wake-up, and auto-zeroing of the strain gage before the start of acquisition. Because rainflow data will be taken for extended periods of time, the event-detection mode can be considered obsolete and will therefore be removed. All acquisitions will begin according to a date and time inputted by the user.

Previous versions of the MicroSAFE GUI used 31 bins during rainflow counting. The user would select the width of the bins (10 microstrain, for example) and the GUI would program the widths of each bin (0-10 aY, 10-20 aY, 20-30 aY and so on, up to 300-310 aY). The new GUI will use 32 bins, rather than 31. The use of more bins will allow the user to capture more ranges of strain during an acquisition. This also allows the MicroSAFE output to resemble that of most commercially available rainflow counting programs that use even numbers of range bins.

The new GUI will also allow the option of splitting the first bin at a user-defined threshold strain range value. During programming, the user will declare a

threshold value of the strain range that best represents the level of background noise present at that installation site. Some sites may have a small background noise component (2-3 aɣ), while other sites may have a larger background noise component (6-8 aɣ). Any observed strain range below this threshold value will be logged in a special sub-bin of the first bin. Observed strain ranges above the threshold value, but below the minimum value of the next full-width bin, will be logged in the remaining portion of the first bin as in previous versions of the GUI. This function will help to remove large numbers of cycle counts that will appear in the first bin due to background noise in the system. This will make the first bin more meaningful in data analysis. Background noise effects are further explained in Section 4.3.1.

Another change to the new GUI will be the manner in which ambient temperature is logged. Previous versions of the GUI logged ambient temperatures at the start and finish of every data acquisition, which would be a maximum of 34 minutes apart. Between cycles, the unit was allowed time to rezero the strain gage and account for temperature fluctuations. Since cycles may last up to 24 hours, temperature values must be logged with regularity for data correction during analysis. The new GUI will program the units to record the ambient temperature every hour and will use these temperature measurements to correct strain data hourly for accurate measurements over a 24-hour period.

Finally, the new GUI will allow downloads of data from current and previous cycles during the acquisition. The user will not have to stop the acquisition to download previously logged data, as with previous versions of the GUI. Data download during acquisition may be slower than if the unit was idle. The exact amount of delay will not be known until the new GUI is delivered and tested.

F.1.3 Battery Updates

As stated in Section 4.2.3, power is provided by non-rechargeable, epoxy-potted battery packs specifically made by Invocon for the MicroSAFE system. The battery depicted in Figure 4.4 is rated for 3 months of continuous service. This battery pack and 10 others like it have been in non-continuous service (approximately 20% duty) for over 1 year without need for replacement. This level of service would be representative of probable TxDOT usage.

Other battery packs are currently available from Invocon for use with the MicroSAFE system. If necessary, battery packs rated for 1 year of continuous service can be purchased. Also, Invocon has announced plans for a replaceable battery pack. In this model, a new type of weatherproof enclosure would be constructed that would allow replacement of the individual battery cells without discarding the entire battery structure. Precluding replacement of the entire battery pack (housing, wires, and battery cells) would reduce the overall cost of replacing batteries on this system. It is likely that replacement cells will be available locally, rather than exclusively from Invocon, further reducing replacement costs.

In addition to updates to the power supply itself, the new GUI will utilize a low-voltage detection circuit present on the second-generation MicroSAFE hardware. This circuit will evaluate battery life between acquisitions and terminate the acquisition sequence if the battery voltage is below a predetermined threshold value. In the event of a deficient power supply, the full sequence of requested acquisitions may not be completed. However, because of the low-voltage detection circuit, all previously recorded data will be saved on the MicroSAFE device previous to a total loss of battery power.

F.1.4   Cost

A single MicroSAFE device as described above would cost $1,500 (as reported by Invocon in early 2002). This would include the most current version of the GUI, a user's manual for the product, and technical support should it be needed.

Batteries for the MicroSAFE system must be purchased separately. Costs (as of early 2002) were $150 for the 3-month non-rechargeable battery pack and $300 for the 1-year non-rechargeable battery pack. As stated in Section F.1.3, these batteries are likely to last longer than the manufacturer's rating, but currently require complete replacement when necessary. As of July 2003, prices for the new battery packs where individual cells can be replaced have not been released.

F.1.5   Applications

The MicroSAFE system can be used to collect strain data at any location. Although the raw data capture mode requires full-time connection to a PC, the MicroSAFE system can record actual strains anywhere a strain gage can be affixed. The system can be positioned and set up with ease, data can be taken quickly, and the system dismantled with minimal disruption to the bridge structure or the environment of its users. The system is non-invasive because of its size and can perform in almost any environment with reliable results.

Though the MicroSAFE system can be employed to take raw strain data with relative ease, most users will choose to use the rainflow counting capabilities of this system. Any structure where fatigue is an issue (bridges, buildings, aircraft, etc.) can benefit from the MicroSAFE system. The entire system (hardware and power source) can be placed nearly anywhere on any type of structure and perform autonomously during data acquisition before needing

attention from an outside user. Data download requires connection to a laptop computer for a maximum of 5 minutes, while programming of a new data acquisition scheme takes only a few seconds given the knowledge of a few simple parameters beforehand.

F.1.6   Advantages

In comparison to other single- or multi-channel data acquisition systems, the MicroSAFE system has many advantages. System startup costs are low at only $1650 for a complete, ready to use single-channel system. The system is small and weatherproof, allowing it to be placed in any location and in any environment. Because of its size, the MicroSAFE system can be hidden or disguised on a structure. Users can program the system and leave the site until acquisition is complete, allowing them to make more efficient use of their time. In addition, rainflow counts are done on-board, making data ready for interpretation immediately upon download and without additional effort or calculation by the user.

Ultimately, this system allows any user to affordably obtain all necessary hardware in a single package, install that package on a structure with speed and ease, obtain meaningful data immediately, and interpret that data quickly and easily.

Bibliography

1. Alampalli, Sreenivas. <u>Measuring Bridge Vibration for Detection of Structural Damage</u>. New York Department of Transportation, 1995.

2. Alampalli, Sreenivas. <u>Significance of Operating Environment in Condition Monitoring of Large Civil Structures</u>. *Shock and Vibration*, v 6, n 5, 1999. p. 247-251.

3. American Institute of Steel Construction. <u>Manual of Steel Construction: Load & Resistance Factor Design</u>. AISC, Inc. 1998.

4. Angus, Mike. *E-mail conversation with Mezure staff regarding Florida DOT participation.* January 2001.

5. Angus, Mike. *E-mail conversation with Mezure staff.* October 2, 2002.

6. ASTM E 1049 – 85 <u>Standard Practices for Cycle Counting in Fatigue Analysis.</u> American Society for Testing and Materials. 1997.

7. Bilich, Andria L. *Matlab script for generating plots of number of satellites over a specific location.* April, 2003

8. Bilich, Andria L., et. al. <u>SNR-based Multipath Corrections to GPS Phase Measurements</u>. Power-point presentation. University of Colorado – Boulder. 2002.

9. Buhl, Marshall. <u>Crunch – A batch-oriented Postprocessor for Wind Turbine Data Analysis</u>. http://wind.nrel.gov/designcodes/crunch/, National Wind Technology Center, 2003.

10. Conner, George and Conway, Fred. *E-mail conversation with Alabama DOT personnel.* January, 2001.

11. Downing, S. D., and Socie, D. F., <u>Simplified Rainflow Counting Algorithms</u>, International Journal of Fatigue, Vol 4, No. 1, January 1982, pp. 31-40.

12. Duff, Keith and Hyzak, Michael. <u>Structural Monitoring with GPS</u>. *Public Roads*, 1997. http://www.tfhrc.gov/pubrds/spring97/gps.htm

13. Frank, Karl H. CE 397 – Experimental Techniques. Class Notes. Spring, 2003.

14. Givan, Glenn. *E-mail conversation with Kentucky DOT personnel*. January, 2001.

15. Haigood, Alan. *E-mail conversation with Invocon staff*. September, 2002.

16. Hofmann-Wellenhof, B., Lichtenegger, H., and Collins J. Global Positioning System: Theory and Practice Fourth Ed. Springer Wien, New York. 1997

17. Palmgren Steel Products manual for Milling Table (PN 49181).

18. Misra, Pratap and Enge, Per. Global Positioning System: Signals, Measurements, and Performance Ganga-Jamuna Press. Lincoln, Massachusetts. 2001.

19. National Academy of Sciences. The Global Positioning System. National Academy Press. Washington, D.C. 1995.

20. National Instruments. Document on Data Aliasing. National Instruments, 2003.

21. Neislony, Adam. Rainflow Counting Method. (Matlab computer program), http://www.mathworks.com, 2003.

22. O'Shea, Dennis. *E-mail conversation with Delaware DOT personnel*. January, 2001.

23. Scott, John S. The Penguin Dictionary of Civil Engineering. Penguin Books, Ltd., 1984.

24. Sime, James and D'Attilio, Paul. *E-mail conversation with Connecticut DOT personnel*. January, 2001.

25. TexasFreeway.com Website. http://www.texasfreeway.com, 2003.

26. Vishay, Inc. http://www.vishay.com, 2003.

27. Wood, Sharon L. Evaluation and Monitoring of Texas Major and Unique Bridges. Project Proposal. August, 2001.

Vita

Christopher Thomas Bilich was born in Dallas, Texas on March 17, 1979, the son of Thomas and Georgeann Bilich. He graduated from Plano Senior High School in Plano, Texas, in August of 1997 and entered the University of Texas at Austin to pursue his undergraduate degree in Mechanical Engineering. In 1998, after realizing a tremendous interest in large, magnificent structures, he changed engineering disciplines to become a Civil Engineer. Chris graduated with Honors in 2001 from the University of Texas at Austin with a Bachelor of Science in Civil Engineering. He immediately entered the graduate school at the University of Texas at Austin in the Department of Civil Engineering to pursue his Master of Science in Engineering. In May of 2003, he accepted a position as a Construction Inspector with Figg Bridge Engineers in Tampa, Florida.

Permanent Address: 4632 Versailles Ln.
                                     Plano, TX 75093

This thesis was typed by the author.